esa

DOCUMENT

document title/ titre du document

MARCO POLO

PAYLOAD DEFINITION DOCUMENT

prepared by/*préparé par*	Marco Polo Study Team
reference/*réference*	**SCI-PA/2008.002/Marco-Polo**
issue/*édition*	3
revision/*révision*	0
date of issue/*date d'édition*	
status/*état*	
Document type/*type de document*	TN
Distribution/*distribution*	

European Space Agency
Agence spatiale européenne

ESTEC
European Space Research and Technology Centre - Keplerlaan 1 - 2201 AZ Noordwijk - The Netherlands
Tel. (31) 71 5656565 - Fax (31) 71 5656040 www.esa.int

APPROVAL

Title *Titre*	issue *issue* 3	revision *revision* 0
author *auteur* Marco Polo Study Team	date *date*	
approved by *approuvé par*	date *date*	

CHANGE LOG

reason for change */raison du changement*	issue/*issue*	revision/*revision*	date/*date*
major revision on resource budgets on most instruments definition of interfaces to S/C	3	0	30.01.09

CHANGE RECORD

Issue: 3 Revision: 0

reason for change/*raison du changement*	page(s)/*page(s)*	paragraph(s)/*paragraph(s)*

Table Of Contents

1 INTRODUCTION

The MarcoPolo NEO sample return mission has been selected for assessment study within the ESA Cosmic Vision 2015-2025 programme. This mission is considered as an M-class mission (RD6). Among other selected candidates the MarcoPolo mission has been studied by ESA's Concurrent Design Facility and is subsequently assessed by competitive industrial teams. The first selection milestone will be met in the end of the year 2009. Only 2 out of the 5 M-class missions will be continued by a consolidation phase until the final selection in the years 2011.

This document is a compilation of the model payload of MarcoPolo. Besides its primary goal to return a sample to Earth, a suite of scientifically important instruments has been selected by the MarcoPolo Science Study Team (SST). The payload elements are selected as such that they serve and accomplish the scientific goals as identified in the Science Requirements Document (AD1). The definition of the instrumentation was fully supported by individual members of the SST. Further information was obtained through the instrument DOI studies

This document will guide the spacecraft design and mission architecture throughout the assessment study.

Throughout this document **no** margins have been applied to the resource budgets of the instruments.

The Technology Readiness Level (TRL) estimate of the instruments is according the information provided by the respective institution.

2 ACRONYMS

AD	Applicable Document
APS	Active Pixel Sensor
APXS	Alpha Particle X-ray Spectrometer
BELA	BepiColombo Laser Altimeter
CPEM	Charged Particle Environment Monitor
ESA	European Space Agency
FM	Flight Model
FOV	Field of View
MRD	Mission Requirement Document
N/A	Not Applicable
NAC	Narrow Angle Camera
NAHRIC	Narrow Angle – High Resolution Camera
NEO	Near Earth Object
N/K	not known
NPA	Neutral Particle Analyser
QE	Quantum Efficiency
RD	Reference Document
RSE	Radio Science Experiment
SRD	Science Requirements Document
SST	Study Science Team
TBC	To Be Confirmed
TBD	To Be Determined
TRL	Technology Readiness Level
WAC	Wide Angle Camera
XRF	X-Ray Fluorescence

3 LIST OF FIGURES AND TABLES

3.1 Figures

3.2 Tables

4 APPLICABLE AND REFERENCE DOCUMENTS

Applicable

[AD1] **Marco Polo Science Requirements Document**, [MP-RSSD-RS-001], issue 1c, Document providing Science objectives and science requirements, including measurement specifications

[AD2] **Marco Polo Mission Requirements Document**, [SCI-PA/2008.001/Marco-Polo], issue 2.0., Document providing the mission/system requirements.

[AD3] **Marco Polo – Assessment of Planetary Protection issues**, [SCI-PA/2008.013/Marco-Polo], issue 1.0., Document providing recommendations on Planetary Protection issues

relating to the potential NEO targets. Note: will be provided by ESA at the negotiation meeting

[AD4] **Marco Polo Environmental Document**, [SCI-PA/2008.014/Marco-Polo], issue 1.0, Note: will be provided by ESA at the negotiation meeting

[AD5] **Marco Polo Consolidated Report on Mission Analysis to Candidate Target NEOs**, [Ref TBD], issue 1.0, ESOC, document describing the NEO reference trajectory as well as mission operations and ground segment to be used in Phase 2. Note: will be provided by ESA at the beginning of the Phase 2 of this study

[AD6] **Marco Polo Payload Definition Document**, [SCI-PA/2008.002/Marco-Polo], issue 2.0, Document providing preliminary resources for a possible science payload suite

[AD7] **CDF Model Input Specification**, [CDF-IFS-001], issue 3.1, and associated Excel workbooks 'Mission Input Issue 3 rev 1.xls' and 'data exchange.xls'

[AD8] **Margin Philosophy for SCI-PA Assessment Studies**, [SCI-PA/2007.022], issue 1.0

[AD9] **Soyuz-Fregat 2-1b from the Guiana Space Centre User's Manual,** issue 1.0, June 06. Note: The launch vehicle performances to be used in this study are defined in [RD3]

[AD10] **ECSS-E-10 series**, available from http://www.ecss.nl

[AD11] **ECSS-E-20 series**, available from http://www.ecss.nl

[AD12] **ECSS-E-30 series**, available from http://www.ecss.nl

[AD13] **ECSS-E-40 series**, available from http://www.ecss.nl

[AD14] **ECSS-E-50 series**, available from http://www.ecss.nl

[AD15] **ECSS-E-60A**, available from http://www.ecss.nl

The above documents are subject to updates; [AD1] through [AD6] are expected to be matured by the Agency during the contract throughout Phase 1. ESA may provide a final version of each document to the Contractor at the start of Phase 2.

Reference

[RD1] **Marco Polo CDF IFP material**, Final presentation material of the internal ESA assessment study (Summary of the CDF study report [RD2])

[RD2] **Marco Polo CDF study report**, CDF-72(A), Final report of the internal ESA assessment study. Note: will provided by ESA at the negotiation meeting

[RD3] **Mission Analysis guidelines for Marco Polo**, [SCI-PA/2008.027/Marco-Polo], issue 1.0, ESOC, document providing reference transfer trajectories for Phase 1 of this study

[RD4] **Study overview of the Near-Earth Asteroid Sample Return**, [SCI-PA/2007.004/DA], ESA Technology Reference Study Summary

[RD5] **Deimos Sample Return Technology Reference Study**, [SCI-A/2006.010/DSR], ESA Technology Reference Study Summary

[RD6] **Comic Vision Presentation to Industry**

[RD7] **Marco-Polo: NEO sample return mission proposal**, M.A. Barucci and M. Yoshikawa on behalf of the European and Japanese NEO science community, June 2007

[RD8] **http://www.esa.int/techresources/ESTEC-Article-fullArticle_par-50_1151301926473.html**, TRL definition (also available in Annex 2)

5 CONTACT PERSONS

The Science Study Team of the Marco Polo mission has defined a model payload that achieves the scientific goals of this mission.

6 PAYLOAD OVERVIEW AND SUMMARY TABLES

6.1 Core Payload Complement

The main scientific goal of this mission is to return a sample from a primitive Near Earth Object (NEO) to Earth. However, a dedicated suite of scientific instruments is required to identify the best landing sites, collect context information and for an overall description of the NEO and its environment.

The proposed model payload consists of the following elements,

- **Wide Angle Camera**
- **Narrow Angle Camera**
- **Close-up Camera**
- **Laser Altimeter**
- **Visible/Near Infrared Spectrometer**
- **Mid Infrared Spectrometer**
- **Radio Science Experiment**
- **Neutral Particle Analyzer**

These were defined by the Science Team in order to meet the science requirements defined in [AD1]. It is important to note that the primary set of instruments (core payload complement) helps fulfil the science requirements defined in [AD1] as “shall” requirements while the additional

scientific objectives (defined as “should” in [AD1]) are being addressed by a set of additional instruments defined in 6.2;

In addition to this remote sensing payload a small number of in-situ instruments are proposed if the required resources are vailable. They will take an additional data set on surface properties during touch down while sampling the surface. This suite of touch-down instruments consists of:

- **Alpha Particle X-ray spectrometer**
- **Attenuated Total Reflection Infrared Spectrometer (Volatile Sensor) and microscope**
- **Temperature Sensor**
- **Electric Field Sensor**

In a classical configuration the proposed **Electric Field Sensor** is deployed by an antenna system. Due to the mechanical and operational complexity a new design proposes to exploit the lander legs to accommodate the sensors. This design is currently under study.

A similar accommodation scenario is applicable for the X-ray spectrometer and Volatile Sensor/microscope. In the given baseline mission scenario it appears unlikely that a dedicated deployment device is feasible. Since a direct or close contact to the surface is required it may be a possibility to use the landing gear especially feet for accommodation. This can be either a shared or individual compartment.

Table 1 provides an overview on all payload elements and their resource budgets.

Table 1 Summary of resource budgets per instrument of the selected model payload complement

	WAC	**NAC**	**Laser Altimeter**	**VisNIR**	**MidIR**	**RSE[##]**	**NPA**	**Σ[#]**
Overall TRL[#]	N/K	N/K	N/K	6-8	4-5	9	5 (6 in fall 2008)	
Units	1 (+2 shared with NAC)	3	1	2	1	1	1	
Interface to S/C								
accommodation	observ. platform	observ. platform	observ. platform	observ. platform	observ. platform	communication system	observ. platform	
mechanical	flat mounted	flat mounted	flat mounted	flat mounted	flat mounted	-	flat mounted	
electrical	28 V regulated	28 V regulated	28 V regulated	28 V regulated	28 Vregulated	-	28 V regulated	
data	Spacewire	Spacewire	Spacewire	Spacewire	CAN bus	-	CAN bus	
thermal	radiator	radiator	radiator	radiator	radiator	-	-	
Weight [kg]	1.0	6	4.0	4.2	2.0	-	2.2	**19.4**
Volume [mm]	150x120x95	170x170x145 150x150x150 300x300x500	150x100x100	310x170x123 150x180x82	160x220x370	-	200x200x100	
Power [W]								
peak	N/K	N/K	N/K	21	3.5	-	11	
observation	18.5	18.5	22	18	2	-	11	**90**
standby	N/K	N/K	N/K	7	1	-	7	
Temperature ops /non-ops	-5 to -25 / -60 to -40 (detector)	-5 to -25 / -60 to -40 (detector)	tbd	-90°C (detector)	tbd	tbd	tbd	
Data product								
single	59 Mbit	59 Mbit	80 bit/shot	0.45 Mbit	12 Mbit	-	6.25 kbit	
total	(680 Gbit[*]) 300 Gbit**	(912 Gbit*) 336 Gbit**	919 Mbit[***]	54 Gbit[****]	8.7 Gbit[5*]	-	7 Gbit	**706.6**
rate			80 bit/s	2.3 Mbit/s	24 kbit/s	-	0.06 kbs	
Compression	1.8	1.8	N/K	3-10	2-5	n/a	is included	
Orbit	Table 3	Table 3	Table 3	Table 3	Table 3	Table 3	Table 3	
Pointing	nadir	nadir	nadir	+ ,nadir	nadir	-	nadir	
absolute error	7.5	1.25 mrad				better than 0.1 x 3dB beam width	10 mRad	
relative error (stability)	0.15 mrad/s	0.025 mrad/s	0.1 mrad (tbc)		0.1 mrad (over 7 seconds)	see instrument description	object within field of view	

[#]The TRL estimate is based on the information provided by external institution. More detailed TRL assessment can be found in some of the individual instrument chapters.
[##]The resources of the RSE are allocated in the communication system of the spacecraft
[*]radius 910 m, distance 2000 m, for calculation see instrument Table 4, Table 5
[**]radius 550 m, distance 2000 m, for calculation see instrument Table 4, Table 5
[***]2001 SK 162 with 1820 m diameter and an orbital distance of centre of mass of 5000m (4090 m from surface) . Laser spot diameter of 10 m. 19 weeks (from SOA doc) and 100% duty cycle achieves full coverage with 5 m of cross-talk spacing at a circular body.
[****]1100 m diameter, 2000 m distance
[5*] 1100 m diameter, 2000 m distance, calculation in Table 13
[+] aligned with NAC within an accuracy of 0.12 mrad
[#] **no system margin of 20% applied**

Table 2 Summary of resource budgets per instrument of the payload suite located close to the sample mechanism.

	Close up imager (option b)	Electric field sensor (Ace)	APXS	Thermal Sensor	Volatile Sensor / Microscope	Σ^{+}
TRL	N/K	3 in a boom-less configuration	4 (9, previous FM)	9	4	
Units	1 (2 shared with WAC/NAC)	2 pairs of electrodes on legs, 1 plate detector 1 CPEM, 1 electronics box	1	3+2+2+2#	2	
Interface to S/C						
accommodation	surface pointing after landing	undeflected FOV plane +/-45° of both asteroid and sunward direction	contact to regolith	contact to regolith	contact to regolith	
mechanical	S/C body, or arm	lander legs	feet or depl. device	feet, sampler	feet	
electrical	28 V regulated	28 V regulated	28V regulated	28V regulated	28 V regulated	
data	SpaceWire	SpaceWire	CAN bus	CAN bus	Spacewire	
thermal	radiator	no	no	no	no	
Weight [kg]	0.65	1.7	0.35	0.24	0.18	**3.12**
Volume [mm]	60x60x250	E field sensors: Volume: 7.7x104 mm3 Surface Area:2 electrodes 1.4x104 mm2 Displacement current unit: 136 x 70 x 15mm (lwh) CPEM 116mm high x 137mm diam. electronics 110x95x115mm	52(∅) x84 160x80x10	20x20x40 (e-box)	26 (∅) x 158	
Power [W]						
peak	24	1.7	1.5	0.5	1.2	
observation	21	1.5	1.5	0.5	1.2	**25.7**
standby				0.5	-	
Temperature ops – non-ops [°C]	-70/+30 -150/+125	-20 +25 -20 +50	-150/+50 -150/+100	tbd	-143/+47 -143/+47	
Data volume						
single measurement	59 Mbit/image		192 kbit	100 bit	21 Mbits	
total	7.6 Gbit***	1.5-5.5 Mbit	960 kbit*	0.1 Mbit	105 Mbit*	**7.7**
rate	200 kbit/s	170 bit/s	3.2 kbit/s**	0.1 kbit/s	0.35 Mbits/s**	
Requirement for measurement		mounted on lander leg	deployment device		deployment device	

* the data volume refers to 5 images/spectra during one sampling approaches, **5 minutes for data transmission, ***calculation based on 4 filters, one landing site

3 sensors in the sampling head, 2 sensors per foot

+ **no system margin of 20% applied**

7 MISSION PROFILE & SCIENCE OPERATIONS – SUMMARY

The main goal of this mission is to return a sample from a primitive Near Earth Asteroid to the Earth. The collected sample material will be curated in dedicated facilities for further distribution to international scientific community.

It is vitally important that the target asteroid as such and the sampling site(s) specifically are well characterized by other methods. A suite of remote sensing instruments will analyse the asteroid and its environment, and delivers a sound description of all accessible surface regions.

The remote sensing instrument actively participates in the decision from which location the sample will be collected.

A typical mission includes a Soyuz-Fregat 2-1B launch from Kourou, French Guyana. The launch is envisaged for the time frame 2017-2018.

Table 3 provides an overview of the science operation after arrival at the target asteroid.

At arrival and during initial fly-by manoeuvres a first observation campaign of the asteroid determines key parameters like the shape, surface properties and a first approximation of the mass.

From further distance at a fixed position relative to the centre of the body a first complete observation campaign describes further parameter like spin axis and rotation period. A first map of the whole surface will be obtained as well. The rotation period and axis might be determined during approach phase already.

Subsequently a detailed description of the gravity field provides a mandatory data set for proximity operations and landing.

During an extended phase of global characterisation all payload elements will carefully describe the body and its environment. After this phase a pre-selection of the landing sites will be made.

The next phase is dominated by close approach manoeuvres for a detailed investigation of the landing sites and rehearsals for the landing procedure.

The sample will be collected during a short period during which the spacecraft is kept in contact with the surface through the use of push-down thrusters or simply performs a short (~few seconds) touchdown manoeuvre. The suite of touch-down instruments obtains context data of the sampling spot.

The spacecraft returns into a safe orbit and verifies via an internal monitoring system if a sample has been collected and transferred into the Earth return capsule.

In case of a negative result the procedure has to be repeated. In total a collection of three samples from three different landing sits is envisaged.

The sample mass will be in the order of up to 100 g with a required minimum of 10 g.

After a successful sample collection the spacecraft returns to Earth and the re-entry capsule safely delivers the asteroid material. After initial inspection in a dedicated curatorial facility the material will be distributed to laboratories for detailed research.

Table 3 Science operation scheme

Activity	Instruments	Resolution @ surface [mm]	Orbit	Distance [km]	Duration [weeks]	Comment
Initial Fly bys	WAC*	tbd	Fly by	TBD	2	Initial estimation of the mass of the Asteroid
	NAC**	tbd				
	RSE	n/a				
	Laser Al	tbd				
Far Global Characterisation	WAC	1278	5 km formation flying	5	2	Spin axis and rotational period
	NAC	128				
	RSE	n/a				
	Laser Alt	tbd				
	Vis IR	1248				
	Mid IR	3750				
	NPA	n/a				
Detailed Gravity Field	RSE	n/a	Uncontrolled orbit which allows determination of the gravity field as indicated in AD 1.	3	4	Detailed gravity field
	WAC	767				
	Laser Altimeter	tbd				
Global Characterisation	WAC	332	1.25 km 09:00-21:00 orbit	1.25	8	Low resolution mapping of the Asteroid
	NAC	33				
	RSE	n/a				
	Laser Altimeter	tbd				
	Vis IR	312				
	Mid IR	980				
	NPA	10^5				

*FOV 30°, pixel size 10 µm **FOV 3°, pixel size 10µm

Table 3 continued

Activity	Instruments	Resolution @ surface [mm]	Orbit	Distance [km]	Duration [weeks]	Comment
Local Characterisation	WAC	25	Descent to 100 m	0.1	5	High resolution characterisation of potential landing sites
	NAC	2.6				
	RSE	n/a				
	Laser Altimeter	tbd				
	Vis IR	25				
	Mid IR	80				
	NPA	10^4				
Landing	Close-up imager	15 µm	Landing	0	10	Sample collection
	APXS*	n/a				
	Volatile Sensor/ microscope*	n/a / 8 µm				
	Temperature sensor*	n/a				

* these are additional payload elements if resource budget allows accommodation

8 DESCRIPTION OF BASELINE INSTRUMENTS - ORBITER

1.1 Marco Polo Camera System MPCS – Wide Angle Camera WAC

1.1.1 INTRODUCTION

This section describes a wide angle camera WAC compatible with the Marco Polo mission requirements. Scientific issues that can be addressed with this experiment are also identified.

1.1.2 SCIENTIFIC GOALS AND PERFORMANCE REQUIREMENTS

The main scientific objective of the WAC can be summarized in the following sentence (taken from the science requirements document):

GR-030: A shape model of the NEO shall be obtained with an accuracy of typically 1 m in height and spatial resolution with respect to the centre of mass.

The shape can be obtained if the entire asteroid is included in one WAC image while the spacecraft in a distant orbit for global characterisation of the target. The shape and mass provide information on the bulk density of the body. WAC images are also used for the determination of the rotation motion of the body (period, axis, state), to provide the larger surface context for NAC fields and to find the asteroid in the stellar field when the payload will be switched on. Its wide field is suitable for search of satellites around the main target and its f ratio brings advantages for the identification of low surface brightness structures, for instance during limb sounding for activity. Last, but not least, the WAC may also be utilized for navigation purposes, in particular during the approach phase to the NEO.

1.1.3 DESCRIPTION

The WAC is a small aperture camera for the visible wavelength range providing wide angle low resolution images of the target (or other fields). Single bandpass imaging is sufficient for the WAC applications.

1.1.3.1 Instrument concept

The WAC is a compact dioptric design with a 65 mm focal length, the f/# will be kept as slow as possible, compatible with the scientific and the mechanical constraints, in order to have a large field of view and high sensitivity. The lenses for this camera have to be small, simple, and

effective. The fewest number of lens elements is used, all optical surfaces are spherical or flat. A modified double Gauss design can be adopted paying attention to lateral and axial color balancing and to keep distortion as low as possible.

The field of view will be of 18° in order to include an object of diameter of 1400 m fully in the field of view at 5 km from the center of mass in order to support the task for shape reconstruction of the body.

The same detector system and filter concept as used for the NAC is also used for the WAC. Refocusing of the camera is not foreseen.

The baseline for the command and data management is an integrated approach for the NAC and WAC into a single Command and Data Processing Unit (CDPU). The instrument is complemented by a general electronics equipment (for voltage, power, harness) that serves both the NAC and the WAC.

1.1.3.2 Operation requirements

The WAC will be used
- nadir pointing for body shape imaging and rotation monitoring
- limb pointing for special applications like shape model details and activity search
- any pointing direction for in-flight calibrations and special applications at the target (satellite search) and for navigation purposes

WAC operations is done in quasi-continuous mode and snapshot mode at the target. Full orbit operations must be possible.

Default operations is by timeline; in exceptional cases (commissioning, in-flight problems, special science and navigation applications) commanding and data transmission in interactive mode may be required.

1.1.3.3 Interfaces and physical resource requirements

The NAC optomechanics plus detector is fixed mounted pointing into nadir direction. The front end electronics is to be placed close to the detector system. The whole camera equipment should have a compact arrangement. Proper temperature range of detector system and optomechanics is critical for camera operations and performance quality. Active control may be required (including DPU and general electronics).

1.1.3.4 Calibration

The ground calibration activity shall provide the characterisation of the spectral, geometric, radiometric and linearity properties of the camera. The measurements have to be realized on each subsystem (h/w units to be integrated in the WAC).

The WAC in-flight calibration will be based on the observation of selected star fields in order to verify:

- PSF
- Optical axis pointing direction
- Image distortion
- Spectral and radiometric calibration

Furthermore, the WAC and the NAC have to follow common activities as:

- Co-alignment of the bore-sights of each camera with respect to the nadir pointing axis
- Cross spatial registration (relative spatial offsets for each camera)
- Radiometric cross-calibration

The relative boresight alingment of the WAC may also of interest with respect to other instruments (spectrometer).

1.1.3.5 Cleanliness, planetary protection and pre-launch activities

Normal requirements for cleanliness and pre-launch activities as typical for visible cameras used for space exploration will be applied. Since the instrument is not meant to reach the surface, planetary protection issues are not applicable (except the whole spacecraft crashes or remains in an unintended way on the surface of the NEO).

1.1.3.6 Critical points

The WAC may not deliver properly focused images of the body surface during the close approach phase to the NEO.

1.1.3.7 Heritage

SIMBIOSYS in the BepiColombo mission.

Table 4 Summary table of WAC instrument

Parameter	Unit	Value/Description	Remarks
Reference P/L	N/A	SIMBIOSYS	
Type of optics	NA	Dioptric	
Type of camera	NA	Wide angle camera	

OPTICS			
Pupil diameter	mm	10	
Focal length	mm	65	
F#	NA	6.5	Diffraction limited at 600 nm
FoV	°	18 x18	Global FOV for all filters
Pixel scale	‘’/px	31.6	
Spectral range	nm	400-950	
Filters		1	Panchromatic
DETECTOR			
Type of detector	n/a	Si PIN-CMOS	Hybrid
Pixel size	µm	10 x 10	
Pixel number		2048x2048	
Exposure time	ms	2	
Read out time	µsec	0.2	
Full well capacity	el.	120000	
A/D conversion	bit/px	14	
Operating T		-5°C -- 25°C	
CONFIGURATION/ LAYOUT			
Units	#	5	Camera optomechanics + Detector + Front end electronics + CPDU[2] + General electronics[3]
Preferred location for sensor	n/a	Focal plane	
Preferred location for electr.	n/a	compact arrangement	
Excitation sources	#	n/a	
Strength of sources	mCi	n/a	
PHYSICAL			
Mass, total	g	500 500 1000 1500	Optomechanics Detector + Front end electronics CDPU[2] General electronics[3]
Dimensions (detector + electronics)	mm	110x50x50 100x60x20 150x120x25 150x150x50 300x300x500	Optomechanics Detector Front end electronics CDPU[2] General electronics[3]
Sample area	mm	n/a	
POWER			
Average	W	2.5 6 10	Detector+front end electronics DPU[2] General electronics[3]
Peak	W	TBD	

DATA RATE/VOLUME			
Average tm rate	kbits	TBD	
Data volume per image	Mbit	59	(excl. header infos)
Data volume total (Raw data volume per basic shape characterisation and filter,uncompressed)[1]	Mbit	6.8*E5 3.0*E5 6.8*E5 3.0*E5 3.0*E5 7.6*E4 6.8*E5 3.0*E5	R = body radius Δ = distance to surface R=190m, Δ =500m R=190m, Δ =1000m R=220m, Δ =500m R=220m, Δ =1000m R=550m, Δ =2000m R=550m, Δ =5000m R=910m, Δ =2000m R=910m, Δ =5000m
POINTING			
Pointing	mrad	7.5	
Pointing accuracy	µrad/s	150	
THERMAL			
Temperature ranges op. Sensor Head and electronics board	°C	-5°C -- 25°C	
Temp. ranges op. Deployment-device		n/a	
Temperature ranges Non-op	°C	-60°C -- 40°C	
Sensor Head / electronics board		TBD	
Temp. ranges Non-op. Deployment-device		n/a	
Temperature stability	°C	1	
CONTAMINATION			
EMC requirements	power supply	TBD	
DC magnetic	n/a	n/a	
Chemical requirements	n/a	n/a	
SUPPORT ITEMS			
Deployment system	n/a	n/a	
Covers, Shutters	n/a	TBD	also used for in-flight calibration

Notes to Table

1 For the basic shape characterisation it is assumed that the full silouette of spherical target body is imaged every 10 deg in longitude and latitude while rotating through the camera field of view. Data volume is for a single filter and assuming uncompressed data. A repetition margin of 2 assumed.
2 The CDPU is foreseen to operate both, the NAC and the WAC.
3 The General electronics supports both, the NAC and the WAC and has built-in redundancy.

tbd

1.2 Marco Polo Camera System MPCS – Narrow Angle Camera NC

1.2.1 INTRODUCTION

This section describes a narrow angle camera compatible with the Marco Polo mission requirements. Scientific issues that can be addressed with this experiment are also identified.

1.2.2 SCIENTIFIC GOALS AND PERFORMANCE REQUIREMENTS

The following requirements are cited from the Science Requirements Document as reference for the expected scientific performance of this instrument:

LR-010: An area of the size of the expected landing accuracy around the potential sampling sites shall be imaged in the visible in at least three colour filters, with a spatial resolution of the order of millimetres.
GR-010: The complete surface of the NEO shall be imaged in at least 3 different colours, in the visible range with a spatial resolution of the order of decimetres, and with local solar elevation angle between 30 and 60° elevation.
GR-030: A shape model of the NEO shall be obtained with an accuracy of typically 1 m in height and spatial resolution with respect to the centre of mass, in both illuminated and unilluminated regions.

High spatial resolution images will be necessary to carefully analyze the morphology and topography of the NEO surface. Thanks to the high spatial resolution observations it will be possible to identify landing site which are suitable (from the scientific and operations points of view).for sample acquisitions.

High spatial resolution images will be of paramount importance for the overall target body characterization in terms of:
• surface topography and distribution of morphological features (e.g., boulders, craters, fractures)
• generation of a Digital Terrain Model (DTM) of some regions
• analysis about NEO fragmentation/accretion history and evolution
• bulk composition of the body (size, shape, rotational properties)
• overall characteristics orbit, rotation, size, shape, mass, gravity and density

NAC imaging may also be needed for complementary details of the shape model obtained mostly through WAC imaging and for a close characterisation of any satellite body that might known to exist or that might be discovered by the mission around the main target.

Furthermore, high spatial resolution images shall be also important:
• to support the s/c navigation
• to help (by broad-band filter images) exploration of mineralogical and chemical compositions.

1.2.3 DESCRIPTION

The asteroid is intrinsically a dark object, and in the determination of the performances of the instrument an average albedo of 0.06 is assumed. It implies that the surface features have typically a low contrast. The low albedo makes it difficult to obtain high contrast images that are necessary to well study the regolith properties. An high contrast image can be obtained only if the optical contrast performance of the camera, including the residual diffraction contribution, is very high.

Optical designs with central obscuration are well known for their loss of contrast in extended object images and for their straylight problems. Therefore, for the NAC, an unobstructed and unvignetted optical design concept is very much preferred. Moreover, one of the main scientific objectives of the NAC is the generation of the Digital Terrain Model (DTM) of specific regions, which is based on the matching of the windows obtained in different images of the same areas. The central obstruction reduces the matching capabilities and consequently the vertical accuracy, since it degrades the point spread function (PSF) sharpness and decreases the modulation transfer function (MTF).

1.2.4 INSTRUMENT CONCEPT

The NAC optical design is based on an off-axis TMA (three mirror anastigmatic) configuration which follows the heritage of the OSIRIS cameras for the Rosetta mission, that are working in-flight, very well satisfying the original specifications.

The NAC design is based on a focal ratio of 8 and a focal length of 400 mm, in order to provide the spatial resolution set in the scientific requirements. The diffraction limit has been calculated at 650 nm which is the middle of the spectral range coverage requested, in order to have an encircled energy greater than 70% all over the FoV and in the entire spectral range of interest for the camera. The NAC layout guarantees good aberration balancing over the full FoV of the instrument, an MTF greater than 52% and distortion less than 1.5%.

According to preliminary calculations the optical design allows to estimate a good S/N ratio and it is not necessary to have a panchromatic filter covering the entire spectral range. Following the scientific requirements one may think of one filter with a broad band coverage of 100 nm, and three filters with bandwidth of 10 nm, which central wavelengths will be selected according to

specific scientific simulations. The filters will be directly and permanently applied in front of the detector.

The requirement to observe very close to the surface, i.e. at 100 m, is very demanding in terms of focus depth, which is not possible to satisfy without introducing a mechanism moving – at least - one optical element in the camera. Furthermore, the focal plane position is sensitive to very small variation of the distance of surface elements which requires the usage of autofocusing through an appropriate sensing device.

The NAC is designed around a detector of 2048 x 2048 pixels with pixel size of 10 μm to guarantee a pixel scale of 0.05 m over the field of view of 3°x3° when imaging the surface at 2 km distance. An array solution is preferred over linear detectors in order to allow snapshot image acquisition, which appears less critical with respect to requirements on pointing and stability, and reducing the number of images for a surface mosaic.

The image sensor is based on a Hybrid Active Pixel Sensor (APS) that uses CMOS readout technology. Its characteristics/capabilities of low power consumption, high radiation tolerance and very high Quantum Efficiency (QE) ensure a high performance of the camera system, even for short exposure times of the order of milliseconds, as it may be required in the Marco Polo mission.

The baseline for the command and data management is an integrated approach for the NAC and WAC into a single Command and Data Processing Unit (CDPU). The instrument is complemented by a general electronics equipment (for voltage, power, harness) that serves both the NAC and the WAC.

1.2.4.1 Operation requirements

The NAC will be used
- nadir pointing during global mapping of the target
- nadir and off-nadir pointing (0-60 deg) for the TDM application of the target
- limb pointing for special applications like shape model details and activity search
- any pointing direction for in-flight calibrations and special applications at the target (satellite imaging)

NAC operations is done in quasi-continuous mode and snapshot mode at the target. Full orbit operations must be possible.

Default operations is by timeline; in exceptional cases (commissioning, in-flight problems, special science applications) commanding and data transmission in interactive mode may be required.

1.2.4.2 Interfaces and physical resource requirements

The NAC optomechanics plus detector is fixed mounted pointing into nadir direction. The front end electronics is to be placed close to the detector system. The whole camera equipment should have a compact arrangement. Proper temperature range of detector system and optomechanics is

critical for camera operations and performance quality. Active control may be required (including DPU and general electronics).

1.2.4.3 Calibration

The ground calibration activity shall provide the characterisation of the spectral, geometric, radiometric and linearity properties of the camera. The measurements have to be realized on each subsystem (h/w units to be integrated in the NAC).

The NAC in-flight calibration will be based on the observation of selected star fields in order to verify:

- PSF
- Optical axis pointing direction
- Image distortion
- Spectral and radiometric calibration

Furthermore the NAC and the WAC have to follow common activities as:

- Co-alignment of the bore-sights of each camera with respect to the nadir pointing axis
- Cross spatial registration (relative spatial offsets for each camera)
- Radiometric cross-calibration

The relative boresight alingment of the NAC may also of interest with respect to other instruments (spectrometer).

1.2.4.4 Cleanliness, planetary protection and pre-launch activities

Normal requirements for cleanliness and pre-launch activities as typical for visible cameras used for space exploration will be applied. Since the instrument is not meant to reach the surface, planetary protection issues are not applicable (except the whole spacecraft crashes or remains in an unintended way on the surface of the NEO).

1.2.4.5 Critical points

The NAC has to focus the surface from different distances ranging from about 5 km, where the global mapping is performed, to 100 m, where the imaging of the potential sampling sites is done. This implies that it will have to work at large focus depth which is not considered possible that without moving one or more optical elements of the camera. The most likely solution is to apply an autofocus mechanism using a dedicated autofocusing device and acting on one optical element of the camera optics.

1.2.4.6 Heritage

OSIRIS in the Rosetta mission and SIMBIOSYS in the BepiColombo mission.

Table 5 Summary table of NAC instrument

Parameter	Unit	Value/Description	Remarks
Reference P/L	n/a	OSIRIS on Rosetta SIMBIOSYS on BepiColombo	
Type of optics	NA	TMA (tri-mirror anastigmatic design)	Unobstructed all-reflective
Type of camera	NA	Narrow angle camera	
OPTICS			
Pupil diameter	mm	50	
Focal length	mm	400	
F#	NA	8	Diffraction limited at 650 nm
FoV	°	3 x3	Global FoV for all the filters
Pixel scale	‘’/px	5.2	
Spectral range	nm	400-950	
Filters		4	
DETECTOR			
Type of detector	n/a	Si PIN-CMOS	Hybrid
Pixel size	μm	10 x 10	
Pixel number		2048x2048	
Exposure time	ms	250	
Read out time	μsec	0.2	
Full well capacity	El.	120000	
A/D conversion	bit/px	14	
Operating T		-5°C -- 25°C	
CONFIGURATION/ LAYOUT			
Units	#	5	Camera optomechanics + Detector + Front end electronics + CDPU[2] + General electronics[3]
Preferred location for sensor	n/a	Focal plane	It's a must (not only preferred)
Preferred location for electr.	n/a	campact arrangement	
Excitation sources	#	n/a	
Strength of sources	mCi	n/a	
PHYSICAL			
Mass, total	g	2500 500 500	Optomechanics Detector Front end electronics

		1000 1500	CDPU[2] General electronics[3]
Dimensions (detector + electronics)	mm	170x170x100 100x60x20 150x120x25 150x150x50 300x300x500	Optomechanics Detector Front end electronics CDPU[2] General electronics[3]
Sample area	mm	n/a	
POWER			
Average	W	2.5 6 10	Detector+front end electronics DPU[2] General electronics[3]
Peak	W	TBD	
DATA RATE/VOLUME			
Average tm rate	kbits	TBD	
Data volume per image	Mbit	59	(excl. header infos)
Data volume total (Raw data volume per panorama; panorama = one full surface coverage per filter,uncompressed)[1]	Mbit	4.0*E4 1.0*E4 5.4*E4 1.3*E4 2.1*E4 0.3*E4 5.7*E4 0.9*E4	R = body radius Δ = distance to surface R=190m, Δ =500m R=190m, Δ =1000m R=220m, Δ =500m R=220m, Δ =1000m R=550m, Δ =2000m R=550m, Δ =5000m R=910m, Δ =2000m R=910m, Δ =5000m
POINTING			
Pointing	mrad	1.25	
Pointing accuracy	µrad/s	25	
THERMAL			
Temperature ranges op. Sensor Head and electronics board	°C	-5°C -- 25°C	
Temp. ranges op. Deployment-device		n/a	
Temperature ranges Non-op	°C	-60°C -- 40°C	
Sensor Head / electronics board		TBD	
Temp. ranges Non-op. Deployment-device		n/a	

Temperature stability	°C	1	
CONTAMINATION			
EMC requirements	power supply	TBD	
DC magnetic	n/a	n/a	
Chemical requirements	n/a	n/a	
SUPPORT ITEMS			
Deployment system	n/a	n/a	
Covers, Shutters	n/a	TBD	also used for in-flight calibration

Notes to Table

1 The listed data volume compares to the coverage of the complete surface of a spherical body of the given radius in a single filter, assuming no data compression. Swath overlaps are not included. The actual data volume depends on the science objectives and their implementation for the mission. A very rough estimate for the global mapping may be (filters = 4, swath overlap factor = 2, replication margin = 2) results in a factor of 16 high data volume. Local characterization data may be of the same amount.

2 The CDPU is foreseen to operate both, the NAC and the WAC.

3 The General electronics supports both, the NAC and the WAC and has built-in redundancy.

1.3 Marco Polo Camera System MPCS – Close-up Camera CUC

1.3.1 INTRODUCTION

This section describes a close-up camera (CUC) compatible with the Marco Polo mission requirements. Scientific issues that can be addressed with this experiment are also identified.

1.3.2 SCIENTIFIC GOALS AND PERFORMANCE REQUIREMENTS

The main scientific objectives of the CUC can be summarized in the following items (taken from the science requirements document):

SC-010: The regolith size distribution of the actual sampling site shall be measured before sampling to sizes as small as 20μ m in an area about 5 times larger than the area sampled by the sampling device.

SC-020: The texture and organisation of the regolith surface in the sample shall be measured before sampling to an accuracy of 15μ m.

SC-040: An additional " local characterisation" shall be performed after the sample collection

The Close-up camera will help to determine physical key properties of the target surface, in order to provide context to the sample analysis. It will determine the grain size distribution of the regolith, and the composition and aggregation state of loose near-surface materials. Through multi-color imaging, the CUC will establish the degree of spectral heterogeneity of the surface at small scales. The measurements will bear on quantifying weathering processes operating on the asteroid, in terms of local erosion, sedimentation, deposition and precipitation rates close to the landing site. It will also explore the pre- and post-sampling constitution of the surface location where the regolith sample will be taken.

1.3.3 DESCRIPTION

The CUC is a compact imaging device for the 450-900 μ m wavelength range designed for microscopic resolution (down to ~15 μm) at close object distances. The technical characteristics of CUC depend strongly on the lowest possible (object) distance between CUC and the observation target, which in turn depends on the instrument accommodation.

Two possible options are considered:
- A microscope design, with a typical object distance of 15 mm
- A tele-microscope design, with a nominal object distance of 150 mm.

Option a) would be realized by accommodating the CUC on the sampling & deployment device of the mother spacecraft, or on a dedicated movable arm attached to the S/C. Option b) would be realized by accommodating the CUC directly on the spacecraft panel facing the asteroid.

For operation the CUC uses the CDPU and general electronics devices foreseen for the WAC/NAC camera system (the latter is assumed not to be in operation while the S/C is on the surface for sample collection).

1.3.3.1 Instrument concept

The instrument consists essentially of three key components, i.e. (1) optics, (2) a multi-color illumination device and (3) a CMOS APS detector with readout electronics (similar to the ones used with the WAC and NAC). Furthermore, due to the intrinsically small depth of field of microscopic designs, a focusing device is needed. Depending on the accommodation and on the chosen optical design, focusing could be implemented either by moving the lens wrt the focal plane, or by moving the whole CUC instrument wrt the target.

The illumination device consists of 4 arrays of light emitting diodes covering the R, G, B and near IR bands. In addition to enabling the characterization of heterogeneity of the asteroid surface, these colors will allow near true-color reconstruction to be performed.

1.3.3.2 Operation requirements

The CUC will operate before and after each sampling operation. Depending on the actual accommodation, deployment may be required before image acquisition. Prior to the acquisition sequence, the camera will be focused. This will be achieved automatically by acquiring several images at different focus distances, and using an algorithm that determines the best focus position based on image contrast. Alternatively, compatibly with the available data volume, the whole set of images taken at different focus positions could be relayed to Earth, so that a 3D reconstruction of the sampling site could be performed. Each data set will consist of 5 images, one for each LED channel, and one without illumination, in order to subtract the background scattered contribution. WAC and NAC are assumed to be out of operation while the CUC images are taken at the surface of the asteroid.

Depending on the option and hardware implemented (see section 1.1.3) coverage of the surface area for sampling by CUC imaging has to be achieved by adequate maneuvering of the mother S/C or by proper pointing of the dedicated deployment device.

Default operations is by timeline; in exceptional cases (commissioning, in-flight problems, special science and focussing applications) commanding and data transmission in interactive mode may be required.

1.3.3.3 Interfaces and physical resource requirements

The mechanical dimension of the CUC depends strongly on the accommodation options:

a) typical object distance is about 15 mm
b) object distance is about 150 mm

In option a) the mechanical design is more compact (in z-direction) than option b) (see spreadsheets below).

1.3.3.4 Calibration

Calibration target for color and radiometric calibration on the lander deck or at lander legs will serve as CUC calibration purposes.

1.3.3.5 Cleanliness, planetary protection and pre-launch activities

Normal requirements for cleanliness and pre-launch activities as typical for visible cameras used for space exploration will be applied. Since the actual camera is not meant to reach the surface, planetary protection issues are not applicable (except the whole spacecraft crashes or remains in an unintended way on the surface of the NEO). However, it is noted that distance holder and/or light protection curtains may get in contact with the NEO surface and may thus be subject to planetary protection measures applicable for the mission.

1.3.3.6 Critical points

It is generally difficult to acquire images with microscopic resolution at large object distance. It might be advisable to reconsider the 15 µm resolution requirement.

Depth of field is extremely reduced at these magnification levels. In order to image a sample with a considerable 3-d structure, it might be needed to perform a series of images at different focusing positions.

Direct solar illumination of the sample has to be prevented for color imaging to be successful.

Temperatures above 125°C are critical for the camera head which is located outside the spacecraft.

1.3.3.7 Heritage

- Rosetta Lander Imaging System.
- ROKVISS imaging system (on ISS)
- ExoMars-PanCam-HRC (in development)
- GIPF- MIROCAM (ESA technology programme)

In the two tables below the summaries for the two CUC options a) and b) listed above are given.

Table 6 Summary table of CUC instrument (option a)

Parameter	Unit	Value/Description	Remarks
Reference P/L	n/a	Rolis	
CHARACTERISTICS			
Type of detector	n/a	CMOS-APS	same as NAC/WAC
Spectrum range	nm	450 - 900	
Focal Length	mm	10	TBC
FOV (angular)	°	90x90	in x and y- direction (partial vignetting)
IFOV	mrad	1	
Pixel scale	µm/pix	15	With an object distance of 15mm
Measuring time	min.	3	
Energy Resolution	nm	40	with LED illumination
Number of samples	#	n/a	

CONFIGURATION/ LAYOUT			
Units	#	1	one unit (includes: Optics, detector, detector electronics, illumination device, and focusing mechanism)[1]
Preferred location for sensor	n/a	Lander deployment arm or sampling device	downward looking to surface
Preferred location for electr.	n/a	inside CUC electronics box	
Excitation sources	#	n/a	
Strength of sources	mCi	n/a	
PHYSICAL			
Mass, total	g	350	Optomechanics and Detector (incl. FEE+box); without CDPU and general electronics[1,2].
Dimensions (detector + electronics)	mm^3	60x60x100	Optomechanics and Detector (incl. FEE+box); without CDPU and general electronics[1,2].
Sample area	mm	50x50	With an object distance of 15mm, unvignetted
POWER			
Average	W	3 6 10	TBC; Sensor and illumination CDPU[1,2] General electronics[1,2]
Peak	W	6 TBD	TBC; Sensor and illumination and focus drive in operation CPDU+General electronics[1,2]
DATA RATE/VOLUME			
Average tm rate	kbits	TBD	
Data volume per sample	Mbit	59	Per color channel, uncompressed
Data volume total	Mbit	3.8*E4	4 filters+clear; 5 sampling sites[3] of 125cm^2; pre- and post-sampling; single focus setting[4]; uncompressed
POINTING			
Pointing	n/a		
Pointing accuracy	°		
THERMAL			
Temperature ranges op. Sensor Head and electronics board	°C	-70C to +40°C	
Temp. ranges op. Deployment-device		n/a	
Temperature ranges Non-op	°C	-150°C to +125°C	
Sensor Head / electronics board			clarification needed
Temp. ranges Non-op. Deployment-device		n/a	
Temperature stability	°C/h	10	
CONTAMINATION			
EMC requirements	power supply	TBD	
DC magnetic	n/a	n/a	
Chemical requirements	n/a	n/a	
SUPPORT ITEMS			
Deployment system	n/a	n/a	

Covers, Shutters	n/a	TBD	also used for in-flight calibration

Table 2 Summary table of CUC instrument (option b)

Parameter	Unit	Value/Description	Remarks
Reference P/L	n/a	Pan-Cam Exomars	
CHARACTERISTICS			
Type of detector	n/a	CMOS-APS	same as NAC/WAC
Spectrum range	nm	450 - 900	
Focal Length	mm	100	As an example; TBC
FOV (degrees)	°	12	in x and y- direction
IFOV	mrad	0.1	
Pixel scale	µm/pix	15	With an object distance of 150mm
Measuring time	min.	5	Per sample
Energy Resolution	nm	40	with LED illumination
Number of samples	#	n/a	
CONFIGURATION/ LAYOUT			
Units	#	1	One unit (includes: optics, detector, detector electronics, illumination device and focusing mechanism)
Preferred location for sensor	n/a	Lander deployment arm or spacecraft bottom panel	downward looking to surface
Preferred location for electr.	n/a	inside CUC FEE- box	
Excitation sources	#	n/a	
Strength of sources	mCi	n/a	
PHYSICAL			
Mass, total	g	650	Optomechanics and dDetector (incl. FEE+box): Stefano+DLR without DPU and harness
Dimensions (detector + electronics)	mm^3	60x60x250	Optomechanics and Detector (incl. FEE+box):
Sample area	mm	50x50	
POWER			
Average	W	5 6 10	TBC; Sensor and illumination CDPU[1,2] General electronics[1,2]
Peak	W	8 TBD	TBC; Sensor and illumination and focus drive in operation CPDU+General electronics[1,2]
DATA RATE/VOLUME			
Average tm rate	kbits	TBD	
Data volume per sample	Mbit	59	Per color channel, uncompressed
Data volume total	Mbit	3.8*E4	4 filters+clear; 5 sampling sites[3] of 125cm[2]; pre- and post-sampling; single focus setting[4]; uncompressed
POINTING			
Pointing	n/a	n/a	
Pointing accuracy	°	n/a	
THERMAL			

Temperature ranges op. Sensor Head and electronics board	°C	-70C to +30°C		
Temp. ranges op. Deployment-device		n/a		
Temperature ranges Non-op	°C	-150°C to +125°C		
Sensor Head / electronics board		TBD		clarification needed
Temp. ranges Non-op. Deployment-device		n/a		
Temperature stability	°C/h	10		
CONTAMINATION				
EMC requirements	power supply	TBD		
DC magnetic	n/a	n/a		
Chemical requirements	n/a	n/a		
SUPPORT ITEMS				
Deployment system	n/a	n/a		
Covers, Shutters	n/a	TBD		also used for in-flight calibration

Notes to Tables

1 It is foreseen to use the CDPU and general electronics (power device) of the WAC/NAC camera also while operating the CUC at the sampling site. Here, it is assumed that WAC and NAC will not be in operation while the S/C is at the sampling site.
2 Mass, dimension and power for dedicated deployment arm (if any) are not included in the table.
3 The actual area where the surface sample is taken is assumed to be 5x 5 cm^2.
4 The estimation of the data volume assumes just a single focus setting for surface imaging. Given the narrow focussing depth of the camera and the possible uneven surface constitution, it is well possible that more than one focus setting will be required for the full characterization of the sampling sites.

8.1 Laser altimeter

8.1.1 INTRODUCTION

A Laser altimeter will contribute to the characterization of the target asteroid in the areas of geodesy and geophysics, and will also be crucial for the navigation of the spacecraft in the gravity field of the asteroid by providing accurate range data to the asteroid.

8.1.2 SCIENTIFIC GOALS AND PERFORMANCE REQUIREMENTS

The following requirements are cited from the Science Requirements Document as reference for the expected scientific performance of this instrument;

GR-030: A shape model of the NEO shall be obtained with an accuracy of typically 1 m in height and spatial resolution with respect to the centre of mass, in both illuminated and unilluminated regions.

GR-040: The mass of the NEO shall be determined to an accuracy of about 1 % (may need to be rediscussed for small objects).

AS-020: The J1 and J2 terms of the gravitational field should be determined with tbc accuracy.

The following list describes the expected output values and contributions to other complex scientific and engineering aspects:

- Derive topographic profiles
- Derive a global shape model of the target asteroid
- Assist in studies of asteroid geodetic parameters (e.g., coordinate system, rotation)
- Assist in orbit determination and gravity data modeling
- Assist in spacecraft manoeuvring
- Measure surface roughness and albedo (at the laser wavelength)

Performance;

- High signal-to-noise for reliable pulse detection (>95%) during night and day from a typical range of 5 km. Minimum range: 100 m.
- Range accuracy: < 0.5 m
- Laser footprint from 5 km: 1 m (tbd.). Divergence (full cone): 20 mrad
- Pulse repetition rate shall allow for a seamless along-track ground pattern
- Allow for pulse shape modeling
- Lifetime: 1 year; total no of shots: 5 Mio (classical system, tbc.)

(see performance spread sheet in Table 7)

8.1.3 DESCRIPTION

The instrument will consist essentially of 3 components, a Laser transmitter, a Laser receiver with a receiver optics of approx. 2 cm, as well as a data processing unit.

8.1.3.1 Instrument concept

The instrument will measure the two-way travel time of a Laser pulse travelling from the instrument to the surface and back. A topographic profile along the ground track of the spacecraft will be produced. By interpolation, a global shape model will be derived. By measurements of pulse amplitude and shape, the reflectivity of the surface, as well as slope and surface roughness (within the footprint of the Laser) can be modelled.

Two design options can be considered (chapter 8.1.3.7)

A topographic profile along the ground track of the spacecraft will be produced. As an option, we envisage a mechanical scanning mechanism to increase the instrument field-of-view perpendicular the spacecraft track.

The scanner is a rotating circular wedge prism, which sits in front of a combined Tx-Rx optics. The free aperture of this scanner is 4 cm resp 2.5 cm (see Table 1), the rotation speed is low.

In Figure 1, the ground pattern of such a scanner is depicted in principle. The labelling of the axes in terms of scale is not representative for a potential Marco Polo scanner. The rotating speed of the scanner will be adapted to the range and speed over ground of the Marco Polo spacecraft. The blue squares represent the positions of the FOV of the detector and the laser spot for each laser pulse.

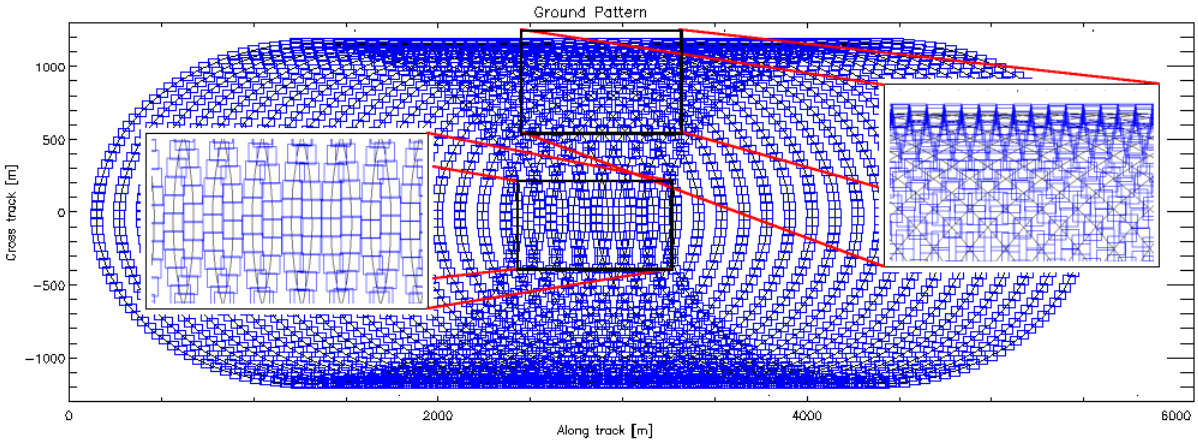

Figure 1: Ground pattern of scanner consisting of one rotating wedge prism (scale not representative for Marco Polo)

Figure 2 explains the working principle and optical path of a combined Tx-Rx optics including scanner. The laser beam is depicted in red, the path of the light reflected from the surface in blue. The laser beam becomes expanded by two lenses and deviated by the wedge prism. The path of reflected light is the same as for the laser beam expect for a mirror which feds the reflected light to the detector.

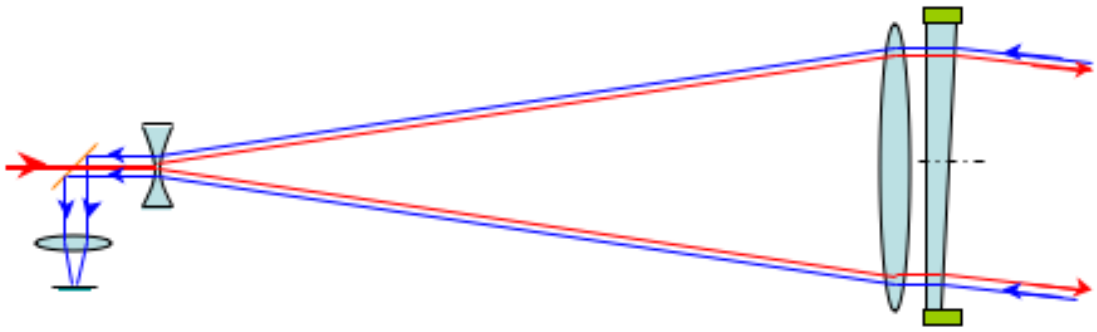

Figure 2 Optical path of a combined Tx-Rx optics. The wedge prims is depicted at the right.

The operational and technical details of the scanner are under investigation.

8.1.3.2 Orbit, operations and pointing requirements

The instrument will operate during approach to the asteroid and during the spacecraft orbit phase. It will typically fire at a rate of 1 Hz, which ensures a seamless ground pattern in along-track direction.

Nighttime observations and daytime observations (which have to overcome the solar background noise) are equally possible. The pointing shall be accurate to within the size of the Laser footprint. The instrument should also be capable for 2-way (offline) ranging measurements to terrestrial Laser stations for instrument alignment calibration, performance tests, and also, to support the tracking of the spacecraft.

The divergence of the laser beam is 200 µrad, which results in a laser spot diameter of 1 m at a range of 5 km. At lower ranges, the footprint decreases below 1 m and the pulse repetition rate will be increased in order to obtain the seamless along-track spacing, which results in a finer grid spacing, e. g. 0.1 m from 1 km range.

8.1.3.3 Interfaces and physical resource requirements

- Instrument size of 23 x 16 x 14 cm
- Total mass not exceeding 5 kg (incl. DPU)
- Thermal control interface (e. g. heat pipe to radiator or direct radiation to space)
- Temperature ranges:
  Operational:
  Electronic boxes: -20°C to +50°C
  Laser head, Detector: -10°C to +45°C
  Non-Operational:
  Electronic boxes: -40°C to +60°C
  Laser head, Detector: -40°C to +60°C

8.1.3.4 Calibration

- Verification of the alignment of transmitter and receiver using Earth ranging, which requires an unobstructed FOV during the cruise phase to the asteroid (no aperture covers, no masking by other s/c components)
- Measurements of instrument alignment wrt the spacecraft coordinate system, in particular the camera using star observations
- Radiometric calibration of the Laser receiver using star observations

8.1.3.5 Cleanliness, planetary protection and pre-launch activities

Cleanliness and Contamination Control during instrument and spacecraft AIV according to the very strict rules for space-laser applications. A contamination budget of level 500A/2 until end of mission for optical surfaces exposed to space or the asteroids surface is required. The amount of contamination caused by landing and sampling (raised dust) shall be estimated by the S/C and the potential impact on the laser altimeter optics considered.

Planetary Protection: no special requirements from the laser altimeter

8.1.3.6 TRL and development plan

The following TRLs (NASA Technology Readiness Levels) are mainly derived from the current BELA development for BepiColombo mission. Once the BELA development is finished, the TRL is 9.

- Laser Optics/Optomechanic/BEX: TRL 6
- Laser Electronics: TRL 6
- Laser Pump diodes: TRL 6

Thermal-vacuum, vibration and EMC tests were conducted with all laser subsystems.
The pump diode qualification program was directly contracted with ESA. A comprehensive test program is ongoing. For BELA, the laser pump diodes are not seen as the most vulnerable point.

- Baffles: TRL 6

A reflective Stavroudis-Baffle is used for the Receiver (20 cm diameter) and for the transmitter (9 cm diameter). Other baffle types were studied at DLR and ESA contracted two Baffle studies for the BepiColombo program.
In the frame of the development of a transmitter baffle for BELA, DLR studied, modelled and designed several baffle types. Only minor problem for the adaption of the baffles for the requirements of the MarcoPolo mission.

- Rx Telescope: TRL 6

Prototype fabricated, several tests for performance verification

- Detector and Focal Plane Assembly: TRL 6

Start/Rangefinder Electronics incl. Algorithm (Filter, Pulse shape analysis etc): TRL 4
Bread Board of a fast start electronic tested at DLR
Bread Board of a rangefinder electronic tested at UBE
Rangefinder combined with start electronic under development (detailed design phase)

Schematic BELA hardware configuration (see Figure 3):
The laser electronic boxes (Laser Electronics, Electronic Unit) are separated from the optical bench of the instrument. The Electronic Unit holds the power converter, the digital processing unit and the rangefinder electronic.
The Laser Electronics controls the laser operation and drives the pump diodes inside the laser head in which the laser beam is generated. The laser beam becomes collimated and expanded by the beam expander, exits the instrument through the transmitter baffle and hits the asteroid surface.
The reflected signal is received and focussed on the detector assembly. The rangefinder inside the Electronics Unit analyzes the return signal.
The baffles protect the transmitter and receiver optics against environmental fluxes (mostly Sun).
Electrical and optical harness is not shown in the Figure 3.

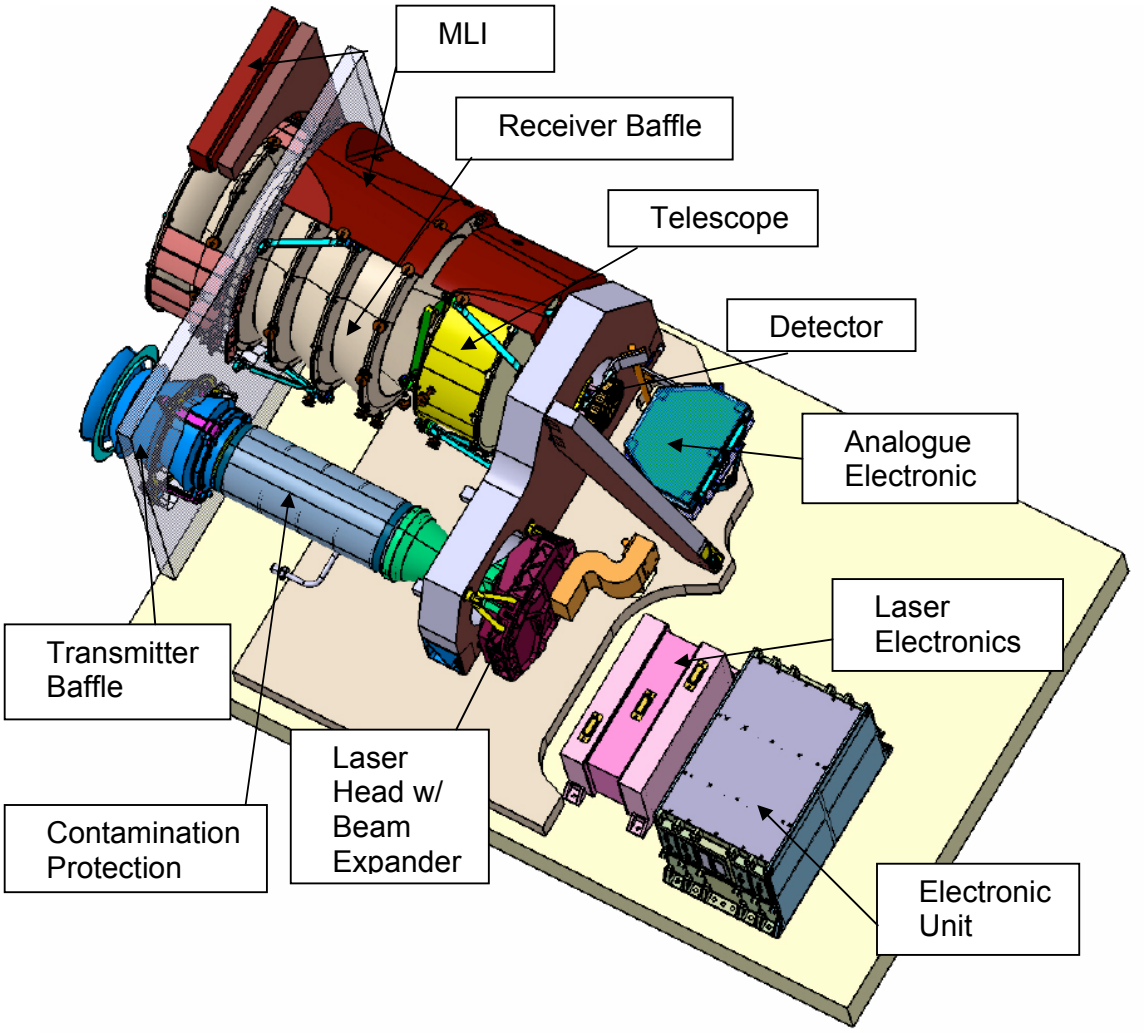

Figure 3 Sketchmap of the BELA laser altimeter

The laser box comprises of two laser lines in cold-redundancy configuration. The same applies to the laser electronics, the digital processing unit and the power converters.

8.1.3.7 Critical points and heritage

As optical receiver systems are standard for space applications, the proper choice of the optical system is not critical. In contrast, the choice of an appropriate laser drives the complexity of the instrument.

The Marco Polo Laser Altimeter bases on the BELA (BepiColombo Laser Altimeter) wherever possible. On the one side, experiences and knowledge gathered during the BELA programme will

be available for the Marco Polo Laser Altimeter. On the other side, hardware used for BELA will be widely used for the Marco Polo Laser Altimeter. This is mostly relevant for parts, which are dedicated laser altimeter parts like optical elements, optical coatings, laser pump diode technology, laser driver electronics, detector electronic & algorithms and much more. All these parts and sub-assemblies are successfully space-qualified during the BELA program. Of course, BELA differs much from the Marco Polo Laser Altimeter in terms of performance and operation requirements, but the basic principle is the same and requires the same laser hardware parts, laboratories, procedures, ground support equipment etc. which all is established and used during the BELA program. Therefore, the difference between BELA and the Marco Polo Laser Altimeter is not a drawback.

Two different instrument configurations are considered:
"MARCO I" is a classical laser altimeter like BELA with performance parameters specifically designed for the mission. This would reduce size, total mass, and required power compared to BELA. We therefore do not anticipate any major changes to the detector and onboard-software etc.

"MARCO II" is al laser altimeter based on single-photon counting. The detector is a silicon APD, operated as photon-counting device, which requires only a few (< 10) signal photons for a detection event and consequently a very small laser. Such Laser systems now become operational in terrestrial airborne applications, and have been studied by a DLR-lead consortium under ESA contract in 2002: LAPE: Laser Altimeter for Planetary Exploration. Such a new system would have dramatically reduced size, mass, and power requirements. However, besides the development and space-qualification of the detector, a new pulse detection and processing scheme must be developed.

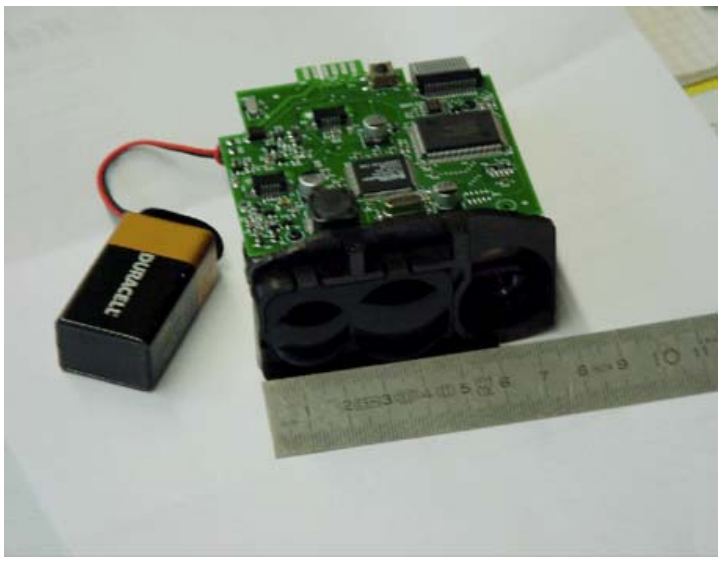

Figure 4 Microchip laser

8.1.3.8 Summary table

Table 7 Summary of laser altimeter parameters and instrument performance

	MARCO I Classical Laser Altimeter	**MARCO II Single-Photon Counting Laser Altimeter**
Performance Parameter		
Laser	4 mJ	0.1 mJ
Laser Wavelength	1064 nm	1064 nm
Laser Pulse Length	3-8 ns	1-10 fs
Pulse Repetition Rate **)	1 Hz	1 Hz
Laser Beam Divergence	200 μrad (tbc.)	200 μrad (tbc.)
Laser Spot on surface (at 5 km range)	1m	1m
Receiver Optics Diameter	4 cm	2.5 cm
Detector Quantum Efficiency	0.25	0.25
Max. range to surface ***)	5 km	5 km
Optical system transmission	0.8	0.8
Albedo	0.05	0.05
Length of Range Gate	200 ns	200 ns
Bandwith of Rx optical filter	1.0 nm	1.0 nm
Signal Photo Electrons	1100	10
Instrument Parameter		
Operation Power *)	22 W	22 W
Data rate	800 bit/s (80 per shot)*	tbd
Dimensions	15 x 10 x 10 cm (tbc)	10 x 5 x 5 cm (tbc)
Nominal Lifetime	1 year or 5 Mio pulses	1 year or 5 pulses
Total Mass	4 kg (tbc.)	3.5 kg (tbc.)

*) Primary power from S/C. The instrument provides its own power converters with 75% efficiency. The difference in pulse energy has no remarkable impact on the overall instrument power.

**) The given value is the nominal value. The pulse repetition rate can be adjusted in order to fulfil scientific requirements

***) The maximum range results from the MarcoPolo CDF study. A larger range is possible.

8.2 MAPIS Visible/Near infrared spectrometer

8.2.1 INTRODUCTION

Spectroscopy is an important tool to characterize the composition of planetary bodies.

A V-IR imaging spectrometer is an important instrument to characterize NEOs in order to derive their surface mineralogy, to connect the mineralogical composition with the surface morphology and to map the complete surface of the body. Spectra at different spatial resolution are needed to identify mineralogical provinces on the asteroid surface.

8.2.2 SCIENTIFIC GOALS AND PERFORMANCE REQUIREMENTS

The following requirement is cited from the Science Requirements Document as reference for the expected scientific performance of this instrument;

GR-020: The complete illuminated surface of the NEO shall be imaged in the near-IR wavelength range to characterise the mineral properties of the surface with a spectral resolution of at least $\lambda/\Delta\lambda$ in the order of 200 and a spatial resolution of the order of meter to characterize the mineral properties of the surface.

An imaging spectrometer is required in order to obtain a detailed description of the mineralogical composition of the different geologic units (crater walls and bottoms, ejecta, etc…).

Surface mineralogy and petrology investigation is possible mainly by visible and near-infrared wavelength spectroscopy. Compositional characterizations of asteroids involve analysis of spectra parameters that are diagnostic of the presence and composition of particular mineral species and various materials expected on the target body. Most of the interesting minerals have electronic and vibration absorption features in their NIR reflectance spectra. An identification of the related mineral phases requires a moderate spectral resolution. Organic materials expected on primitive type may be more difficult to evidence and require slightly higher resolution.

Beside that, information about the primary silicates such olivine and pyroxene and their chemistry (abundance of Fe in olivine and of Ca in pyroxene) can be achieved. The relation between ortophyroxene (low Ca) and clinopyroxene (high Ca) can be studied from the analysis of the band position and band strength ratios. Secondary minerals, such as phyllosilicates, have water and OH absorption features at 1.4, 1.9 μm and in the 2.9-3.3 μm range. The presence of the 1.4 and 1.9 μm bands is indicative of undissociated water in the mineral, while the presence of the 1.4 μm band alone suggests OH groups like hydroxyls. The exact position of the bands should be diagnostic of the mineralogy. Similarly, information on the mineralogy of clays and other phyllosilicates can be obtained from the position and relatively intensity of the bands (at 1.4, 1.9, 2.16-2.23 and 2.3 + 2.7 μm) while carbonates have other features in 2.0-3.3 μm range.

In particular asteroid of C taxonomic type (tentatively associated to carbonaceous chondrites) can show in their surface the presence of hydrated silicates, while D types are expected to including organic materials. In the follow table the position and the width of the detected bands on asteroids are listed:

Table 8 Observed absorption features associated with hydrated minerals on asteroids

Wavelength (μm)	Width (μm)	Transition	Reference
<0.4	>0.1	$Fe^{2+} \rightarrow Fe^{3+}$ intervalence charge	e.g., *Gaffey and McCord* (1979)
0.43	0.02	6A1 → 4A1,4E(G) Fe^{3+} spin-forbidden as in jarosite	*Vilas et al.* (1993)
0.60–0.65	0.12	6A1 → 4T2(G) Fe^{3+} in Fe alteration minerals	*Vilas et al.* (1994)
0.7	0.3	$Fe^{2+} \rightarrow Fe^{3+}$ in phyllosilicates	*Vilas and Gaffey* (1989)
0.80–0.90	0.08	6A1 → 4T1(G) Fe^{3+} in Fe alteration minerals	*Vilas et al.* (1994)
3.0	>0.7	structural hydroxyl (OH) interlayer and adsorbed H_2O	*Lebofsky* (1978, 1980)
3.07	0.2	H_2O ice NH_4-bearing saponite	*Lebofsky et al.* (1981) *King et al.* (1992)

8.2.3 INTRUMENT DESCRIPTION

8.2.3.1 Instrument concept

The instrument concept is based on a push broom imaging spectrometer in the spectral band [0.4-3.3] μm using a matrix array detector. Each recorded image gives a full spectrum of one spatial dimension. The second spatial dimension is obtained using the moving of the orbiter with respect to the asteroid. In case that the push broom concept could not be used due to "uncontrolled" orbit, the overall mapping could be done by software reconstruction of the spectral images acquired during the complete mission.

Note: due to the absence of scanning device, during the descend, if the instrument boresight points the same direction, MAPIS will only be able to record spectra in one spatial direction at different scales vs the altitude.

Apart from a possible shutter, the instrument optical head has no moving part which increases its stability. Different instrument concepts will be studied in order to identify the best arbitration between science requirements and instrument constraints. At this stage of the design a classical slit spectro-imaging concept is considered. **This kind of design gives a maximum envelop mass budget. Some other designs are under investigation and could potentially reduce mass and volume budgets.**

It is assumed that DCDC convertor is provided by the instrument main electronics. A main electronics concept is evaluated in terms of mass, volume and power later in this document.

The proximity electronic is based on an ASIC and a FPGA minimizing its mass and volume (see Figure 5).

The instrument and the detector shall be cooled by means of radiator and Peltier elements (TBC). The typical detector temperature will be 160K (TBC)

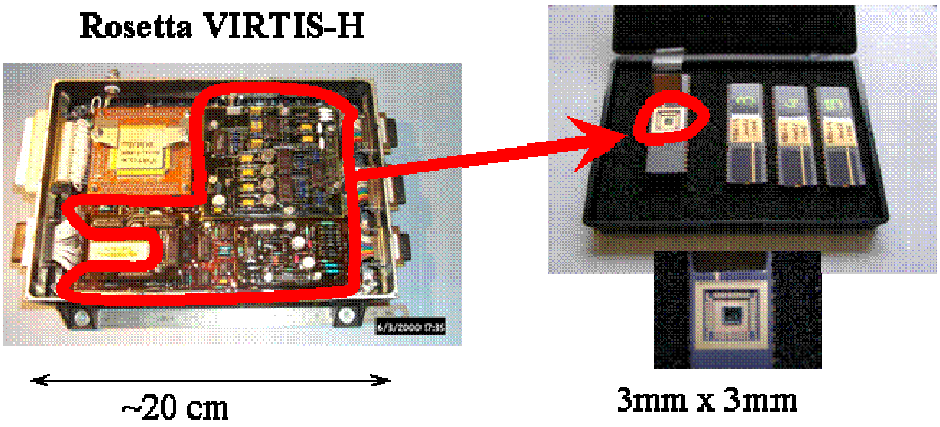

Figure 5 Electronic miniaturisation (ASIC + FPGA)

In Figure 6 a sketchmap shows the key components of the proposed design of the instrument.

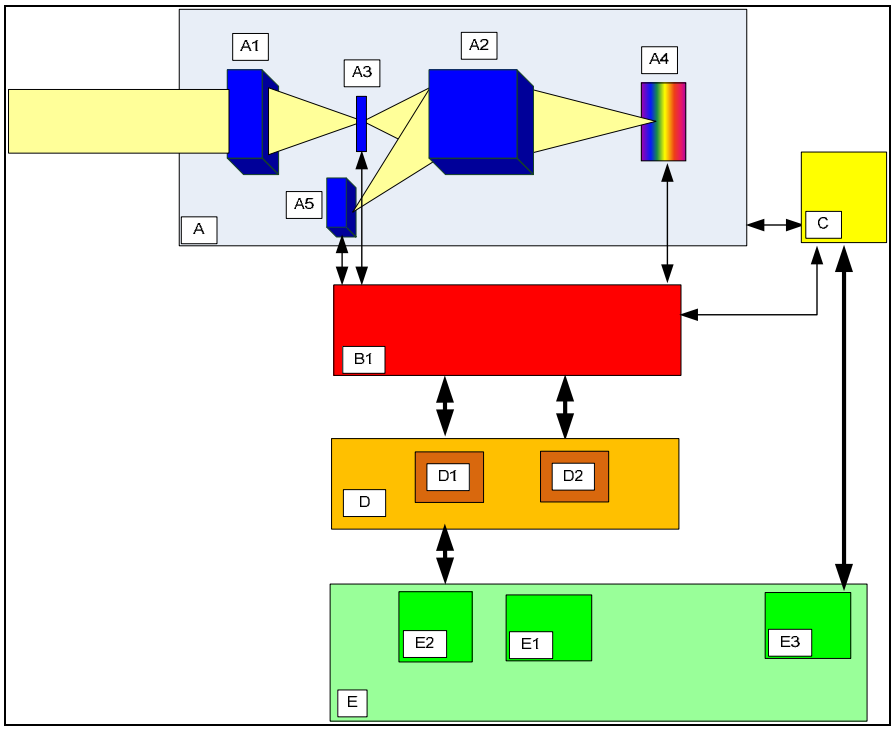

Figure 6 Sketchmap of the Vis NIR spectrometer

A) Optical head
A1) Collecting sub-system – A2) Dispersing and imaging sub-system – A3) spatial filtering and shutter sub-system – A4) Spectral image and detector – A5) radiometric calibration sub-system
B) Proximity electronics
C) Cooling system
D) Main electronics
D1) DCDC converter – D2) DPU board
E) Spacecraft resources
E1) 28V – E2) TM – E3) Thermal well

8.2.3.2 Orbit, operations and pointing requirements

Table 9 Operating modes versus power consumption of the VisNIR spectrometer

	Operating modes		
		Calibration	*operations*
	Goal	Relative radiometric using an internal lamp	Close or far mapping
	Duration	30 sec	8 weeks
	Power average	18W (1)	18W (1)
	Additional peak power	3W (2)	1W (3)
	Operational constraints	N/A	N/A
	Number of occurrence of the operation	every 500 spectral images	

(1) Average power: 15W + 25% efficiency of DC/DC converter = 18W
3W for 3.3V devices
7W for cooler
5W for ME (including DC/DC convertor)

(2) Peak power: 3W
2W for calibration
1W for shutter (3)

8.2.3.3 Interfaces and physical resource requirements

The instrument alignment with the NAC/WAC shall be known within an accuracy of 0.12 mrad corresponding to half a pixel field of view.
The radiator should stay in the shadow during operations

8.2.3.4 Calibration

The in-flight spectral calibration shall be performed by pointing external sources such as stars or planets. This pointing will also be used to cross check instruments co-alignments. The conception of the instrument shall be done to minimize the number of occurrences of this operation.

The in-flight radiometric calibration shall be done using internal sources lighting the pupil. This calibration will be used to monitor the variation of the instrument radiometric response. This operation shall be done at the beginning and the end of each session.

If possible, ideally, a radiometric calibration could be done by pointing a spectrally flat external source such as the moon when it is close enough to fill the instrument FOV.

8.2.3.5 Cleanliness, planetary protection and pre-launch activities

No specific requirements

8.2.3.6 Critical points

At this point of the study, the main critical point is the mass of the instrument. We estimate a margin of 30% of the nominal value.

8.2.3.7 Heritage and TRL assessment

The heritage comes from:

- development of the overall optical head and proximity electronics of IR imaging spectrometers for MarsExpress, Rosetta and VenusExpress.

It has to be emphasized that such imaging spectrometers are mass consuming but for higher performances.

- strong contribution in mission payloads for BepiColombo, Hayabusa, ExoMars.

The assessment of the technology readiness level provides the following result;

- Mirrors & mountings: TRL=6
- Grating and mounting: TRL=5
- In flight calibration devices: TRL=8
- Shutter systems: TRL=8
- Detector: TRL=8
- Proximity electronics (ASIC like): TRL=5
- cooler system: TRL=8

8.2.3.8 Summary table

Table 10 Description summary of the VisNIR spectrometer

Parameter	Units	Value/Description	Remarks
Heritage P/L	n/a	Rosetta / BepiColombo/ Hayabusa	
Type of instrument	n/a	imaging IR spectrometer	
Type of optics	n/a	Mirrors and grating	
Type of detectors	n/a	MCT	Mercury-Cadmium-Telluride
OPTICS			
Spectral Range	μm	0.4-3.3 μm	
FOV	mrad	32	
Pixel IFOV	mrad	0.25	
Aperture	mm	40	
Focal length	mm	120	
Focal number	#	3	
Spectral Channels	#	1	
spectral resolution	$\lambda/\Delta\lambda$	>100	
Signal to noise ratio	n/a	>100	
Detector			
Type of detector		MCT	
Pixel lines in array	#	128	
Pixels per array line	#	256	
Pixel size	μm	30	
Exposure time	msec	80	Typical
Repeat time	msec	200	
Operating temperature	K	160	
A/D conversion	bit/pix	14	
Full well capacity	ke-	2000	
Readout time	msec	20	
SWATH and RESOLUTION			
Swath width @ 5km	km	0.16	
Swath length @ 5km	M	1.25	
Spectral sampling	nm	20	
Angular resolution	mrad	0.25	
Spatial (pixel) resolution @ 5km	m	1.25	
PHYSICAL			
Optical head mass,	g	1700 (2200g including 30% margin)	Including proximity electronics (300g), optical head (1000g), thermal device (400g)
Main electronic mass	g	1536 (2000g including 30%	Including DCDC boards (500g), DPU boards (300g), box (586g),

		margin)	harness (150g)
Optical head dimension	mm	210x110x90	
Proximity electronics dimension	Mm	100x60x33mm	
Main electronics dimension	mm	150x180x82mm	
Optical head footprint	mm	270x110	Includes proximity electronics
Main electronics footprint	mm	180x150	
POWER			
Total average power	W	18	
Additional peak power	W	3	
ELECTRICAL			DCDC convertor is provided by instrument main electronics.
Low	V	3.3	To operate ASIC and detectors
High	V	Between 10V and 15V	To operate power devices (lamps, coolers)
Data			
Data rate		2.3Mbit/s	
Cube volume		0.45 Mbit	
Data volume (whole body)		See table below (4)	
Data volume (descend)		1.3Gbit	Assuming 10' descend No compression
Compression factor		None	In case of data volume limitation a compression could be used (10 max – 7 nominal - 3 lossless)

(4) Data volume is calculated to cover the overall surface of 3 typical objects using the following assumptions:

- 256x128 pixels
- 14 bits,
- no compression
- no redundancy

Object 2001 SG286

Orbit distance (m)	Object diameter (m)	Data volume (Gbit)	Calibration data volume (Gbit) (5)
500	440	139	0.55
1000	440	35	0.14
500	280	56	0.22

1000	280	14	0.05

Object 2001 SK162

Orbit distance (m)	Object diameter (m)	Data volume (Gbit)	Calibration data volume (Gbit) (5)
2000	1100	54	0.21
5000	1100	8	0.03
2000	1820	150	0.6
5000	1820	23	0.09

Object 1989 UQ

Orbit distance (m)	Object diameter (m)	Data volume (Gbit)	Calibration data volume (Gbit) (5)
3000	900	17	0.07
5000	900	6	0.02

(5) 1 calibration - including 2 images - every 500 acquisitions ➔ ratio data volume 0.004. Could be adjusted depending on environment stability.

8.3 Mid IR spectrometer

8.3.1 INTRODUCTION

Mid-infrared spectroscopy provides information on the surface mineralogy (silicates and organics), the surface temperature, thermal inertia and presence and properties of regolith. The compositional information complements the data obtained form UV-Vis-NIR spectrosocopy and provides global context for the returned samples. Spectroscopic maps are used to determine the surface temperature distribution which, with the use of thermal models, can constrain the surface thermal inertia and dominant regolith particle size. These properties will be used to inform the sample site selection. In addition, they provide valuable information for determination of sizes and albedos from optical and IR observations of unresolved NEOs using the radiometric method and study of the Yarkovsky effect.

8.3.2 SCIENTIFIC GOALS AND PERFORMANCE REQUIREMENTS

The following requirements are cited from the Science Requirements Document as reference for the expected scientific performance of this instrument;

GR-050: The surface temperature shall be derived to an accuracy of at least 5 K (goal 1 K) at a spatial resolution of the order of 10 m at a number (tbc) of rotational phases from which the thermal inertia can be determined to a precision of better than 10 % .

GR-060: The complete surface of the NEO shall be imaged in the mid-IR with a spatial resolution of the order of 10 m or better to identify silicate spectral features in the 9 – 11 μm (and optionally in the 5-8 μm and 18-22 μm bands) with a spectral resolution of at least $\lambda/\Delta\lambda$ in the order of 200.

LR-020: An area of the size of the expected landing accuracy around any of the potential sampling sites shall be imaged in the wavelength range of 9 – 11 μm (and optionally in the 5-8 μm and 18-22 μm bands) with a spectral resolution of at least $\lambda/\Delta\lambda$ in the order of 200 and with a spatial resolution of the order of decimetres.

8.3.2.1 Objectives

The objectives of a mid-IR spectrometer are to

- Derive the surface temperature to an accuracy of at least 5 K (goal 1 K) at a spatial resolution of the order of 10 m at a number (*tbc*) of rotational phases from which the thermal inertia can be determined to a precision of better than 10 % .
- Map the complete surface of the NEO with a spatial resolution of the order of 10 m or better to identify silicate spectral features in the 9 – 11 μm (and optionally in the 5-8 μm and 18-22 μm bands) with a spectral resolution of at least $\lambda/\Delta\lambda$ in the order of 200.

8.3.2.2 Thermophysical properties

Typical surface temperatures for an NEO at a heliocentric distance of 1 AU range from as low as 100 K in unilluminated areas to almost 400 K near the subsolar point for a slow rotating low thermal inertia object. Diurnal cycles in the asteroid surface temperature are strongly dependent on the thermal and physical properties of the top several centimetres of the surface. Many factors have an effect on temperature, including albedo, but thermal inertia is the key parameter. Thermal inertia is defined as a combination of thermal conductivity K, density ρ, and specific heat capacity CP: $\Gamma = \sqrt{K\rho C_P}$, and represents the ability of the subsurface to store and conduct heat energy away from the surface during the day and to return that heat energy to the surface through the night. Deriving and understanding the thermal inertia of a surface can help to identify the small-scale characteristics of that surface. Fine grained and loosely packed material typically exhibits a low value of thermal inertia, while higher values are common for rocks and exposed bedrock.

The surface and subsurface temperature of a surface element of an NEO can be calculated using a thermophysical model, where the thermal diffusion equation is solved for subsurface temperatures by a forward-time finite-difference method, with the appropriate boundary conditions. Synthetic spectra are then derived and fitted to observed IR spectra to constrain the thermophysical properties. Recently, sophisticated thermophysical models have been applied to NEOs, modelling their known shapes and pole orientations, in order to determine their surface thermal inertia Γ. Mueller et al. (2007) found Γ = 150 J m-2 K-1 s-1/2 (all subsequent values are in these units) for (433) Eros and Γ = 350 for (25143) Itokawa. Harris et al. (2005) measured Γ = 180 for (1580) Betulia and Mueller et al. (2007) determined Γ = 150 for (33342) 1998 WT24. Thus, the average NEO surface inertia appears to be considerably greater than that of (large) main belt asteroids (MBAs): Müller and Lagerros (1998) obtained Γ = 5-25 for five MBAs using the Infrared Space Observatory. Delbó et al. (2007) have found the average thermal inertia to be 200 ± 40. All these values lie between the expected extremes of 40 (fine particulate dominated surface such as the lunar regolith) and 2200 (solid rock, e.g. granite).

These data have been obtained from disk integrated models observed at one geometry (solar phase angle) and are therefore an average of the overall surface visible at that time. Spatially resolved data obtained at a range of rotational phases and local phase angles will allow the influence of local topography, (shadowing and beaming) and regolith properties (composition, size distribution) to be studied and provide more powerful constraints on the surface conditions.

Kieffer et al. (1977) discuss what may be inferred about Martian surfaces from measurements of Γ, which can also be applied to asteroid surfaces. The principal thermophysical property determining inertia is the conductivity (k) which is closely related to particle size [e.g., Kieffer et al. (1973), Palluconi and Kieffer (1981), Jakosky (1986)]. Assuming a uniform particle size and a smooth, homogeneous surface, the thermal conductivity of the bulk material is strongly affected by the particle diameter [e.g., Wechsler and Glaser (1965), Presley and Christensen (1997)], varying by several orders of magnitude, while density and heat capacity change little. Therefore, thermal inertia will also vary significantly with particle size. Lower thermal inertias (about $\Gamma \leq 170$) may indicate a surface covered with fine particles with diameters less than about 0.1 mm. $\Gamma \geq 170$ may be due to: particle distributions with mean particle diameter greater than 0.1 mm; distributions of small particles, larger blocks and exposed bare rock, or surfaces consisting of bonded fine particles.

In addition to the derivation of near-surface properties, the thermal inertia is a key parameter in determination of the Yarkovsky effect, caused by anisotropic emission of thermal photons, which is the dominant long term perturbing force for km sized bodies and provides the key for dynamical transfer from the main belt.

It can be seen that it is difficult to interpret values of thermal inertia because a great variety of surface types can result in the same area average thermal inertia. The spatial and rotational phase resolution of in-situ data, and the further constraints on surface properties from other instruments (particularly if a separate lander is included) will allow major advances to be made.

8.3.2.3 Composition from Mid-IR spectra

Emission spectra in the thermal infrared are well suited to addressing silicate mineralogies. This spectral region contains the Si-O stretch and bend fundamental molecular vibration bands (typically in the ranges 9-12 and 14-25 μm, respectively). Interplay between surface and volume scattering around these bands creates complex patterns of emissivity highs and lows which are very sensitive to, and therefore diagnostic of, mineralogy as well as grain size and texture. The three main types of feature observed in mid-IR spectra are:

Christiansen features are due to rapid changes in the refractive index are responsible for an anomalous dispersion that makes the particulate sample transparent. This phenomenon produces the appearance of the Christiansen features at shorter wavelength with respect to the reststrahlen features. The Christiansen feature, which is directly related to the mineralogy and the grain size, appears in the spectra between 8 and 9.4 μm.

Reststrahlen features are due to the vibrational modes of molecular complexes. The absorption coefficient at resonance wavelengths is very strong producing the most intense bands in the infrared spectrum by surface scattering. They are strongly depended on grain sizes; for smaller grain sizes, the main reststrahlen features decrease their spectral contrast. These features are visible between 9 and 12 μm and at wavelength larger than 20 μm.

Transparency features. In the spectral region where the absorption coefficient decreases, grains become more transparent. Usually, this occurs at 11-13 μm between main restrahlen bands and at longer wavelengths (> 30 μm) where the absorption coefficient decreases. If the grain size is small, volume scattering occurs and transparency features are observable due to a loss of photons crossing many grains.

Many of the major rock-forming elements and their complexes have fundamental vibration frequencies corresponding to mid- and thermal-IR wavelengths, 5–50 μm. Nearly all silicates, carbonates, sulfates, phosphates, oxides, and hydroxides show mid-IR and thermal IR spectral signatures [e.g., Lyon (1962); Hunt and Salisbury (1974), (1975), (1976); Farmer (1974)] Bands in the 4–7-μm region are mostly over-tones and combination tones of the stretching and bending of SiO and AlO fundamentals with some lattice modes present in minerals. Also, carbonates have strong absorptions from CO_3 internal vibrations in the 6–8-μm region; these bands are easily distinguished from silicate absorptions [Adler and Kerr (1963); Hunt and Salisbury (1975)]. Hydroxide-bearing minerals (clays) also have characteristic mid-IR spectra [Van der Marel and Beutelspacher (1976)], with spectral features from the fundamental bending modes of OH attached to various metal ions, such as an H-O-Al bending mode near 11 μm in kaolinite [Hunt (1980)]. Phosphates and sulfates also have diagnostic absorption bands associated with their anion

complexes (PO 3–4 and SO 4–4), as do oxides, nitrites, and nitrates. Sulfides and halogenide salts are also readily distinguished [Hunt and Salisbury (1975)].

The interpretation of the continuum of reflectance or thermal emissivity of an asteroid surface is difficult and not unique, since asteroid surfaces are composed of mixtures of minerals whose spectral properties are non-linearly combined. Asteroid spectra are affected not only by the chemical composition of the surfaces, but also by several physical parameters, such as particle size, porosity, packing, and thermal gradients [Logan et al. (1973); Salisbury and Estes (1985); Salisbury and Walter (1989), Arnold (1991); Ruff et al. (1997); Lane and Christensen (1998); Lane (1999); Harloff and Arnold (2001)]. These effects only become significant as the particle size becomes small (<~100 μm) and are most important as the size approaches the wavelength being observed (e.g. Salisbury and Walter (1989)).

Because of their spectral similarity in the visible and near-infrared regions, C-type asteroids have always been associated with CI and CM meteorites especially due to their matching weak absorption features in the shortest wavelength regions. Mid-infrared spectroscopic (2-25 microns) analysis will give further stronger constraints on this subject. Cohen *et al.* (1998) and Witteborn *et al.* (2000) interpreted emissivity features in spectra of (1) Ceres obtained on board the Kuiper Airborne Observatory (KAO) as indicative of fine-grained olivine. Barucci *et al.* (2002) and Dotto *et al.* (2004) report Infrared Space Observatory (ISO) spectra of two low albedo asteroids: 10 Hygiea (C-type) and 308 Polyxo (T-type). The spectra of both objects exhibit an emission plateau near 10 μm. The Hygiea spectrum rises somewhat slowly longward of this to a peak near 20 μm, whereas the Polyxo spectrum has a narrower transparency minimum centered near 12.5 μm, similar to CO3 meteorite and crystalline olivine spectra. These authors also note similarities to carbonaceous meteorites and that small grain sizes are required to reproduce the 10-μm plateau.

Theoretical approaches, developed by Hapke (1981, 1993) and Shkuratov *et al.* (1999), can be used to model the thermal emission of the asteroid particulate surface using the optical constants of the suitable materials.

8.3.2.4 Requirements of Mid-IR spectrometer

We require an instrument capable of measuring the surface temperature to a precision of a few K from which the thermal inertia and other surface properties can be constrained.

The instrument should operate between 5 and 25 microns to sample the wide range of mineralogical features in the mid-IR and ensure good sampling of the thermal emission for temperatures from 100 to 400 K.

A spectral resolution of at least 100 is required to provide good sampling of emission features and continuum.

A spatial resolution of order 10m is required to sample approximately isothermal regions, separate different factors influencing the thermal inertia and derive local properties required for potential landing site definition.

Observations of each surface element at a range of rotational phases provide much greater constraints on the properties by reducing thermal model redundancies.

8.3.3 DESCRIPTION

8.3.3.1 Instrument concept

The instrument is a Fourier transform mapping spectrometer utilising a set of coated KBr prisms and germanium lens to produce an interferogram on a linear detector array, allowing spectral image cubes of the target body to be measured. The instrument covers the key spectral range of 5 to 25 μm with a maximum programmable resolution of 1 cm^{-1}. (0.01 μm at λ = 10μm) This extended spectral range is vital, as it includes important diagnostic mineral absorption bands as well as the thermal continuum due to the full diurnal temperature range of the object.

Using beam-shearing prisms to image the interferogram on to a detector array rather than a traditional moving mirror arrangement leads to a highly reliable, compact, low mass and low power instrument with no moving parts except a scan/calibration mirror assembly. The instrument also incorporates a low power miniature black body target to maintain radiometric calibration during operation. Current versions of the instrument use a radiator to passively cool a stepped 512x2 detector array, however, due to the relatively low spectral resolution (≈100nm) requirement and high signal levels expected an uncooled 2D array (e.g. 512x512) could also be used in imaging mode.

The interferogram can either be Fourier transformed by the on board data processing unit for low spectral resolution operation (e.g. thermal mapping) or off line by returning the complete interferogram to Earth to produce 3D image cubes.

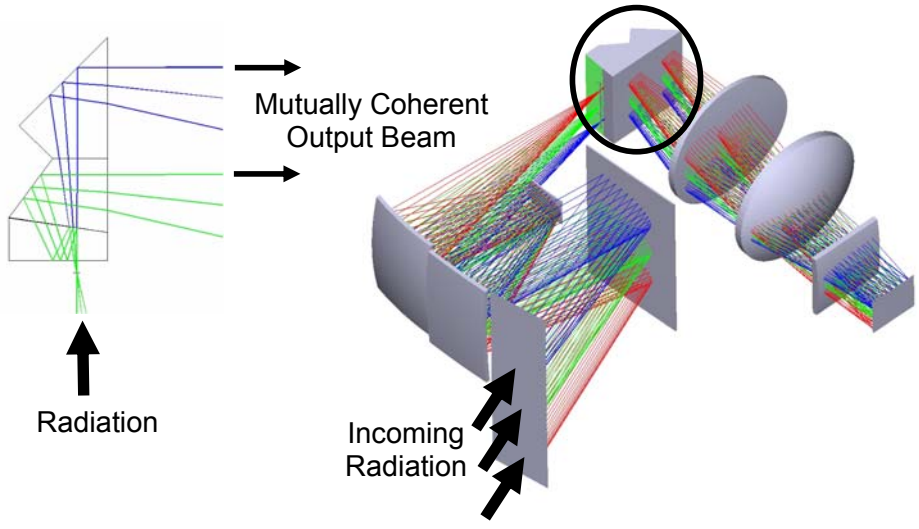

Figure 7. The Spatially modulated Inteferometer concept.

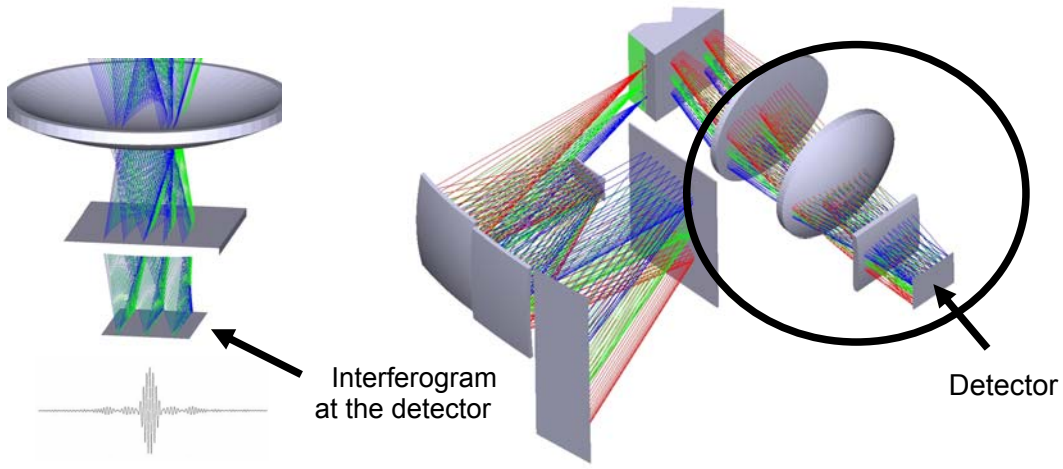

Figure 8. The Spatial modulated interferometer (SMI) instrument measurement technique

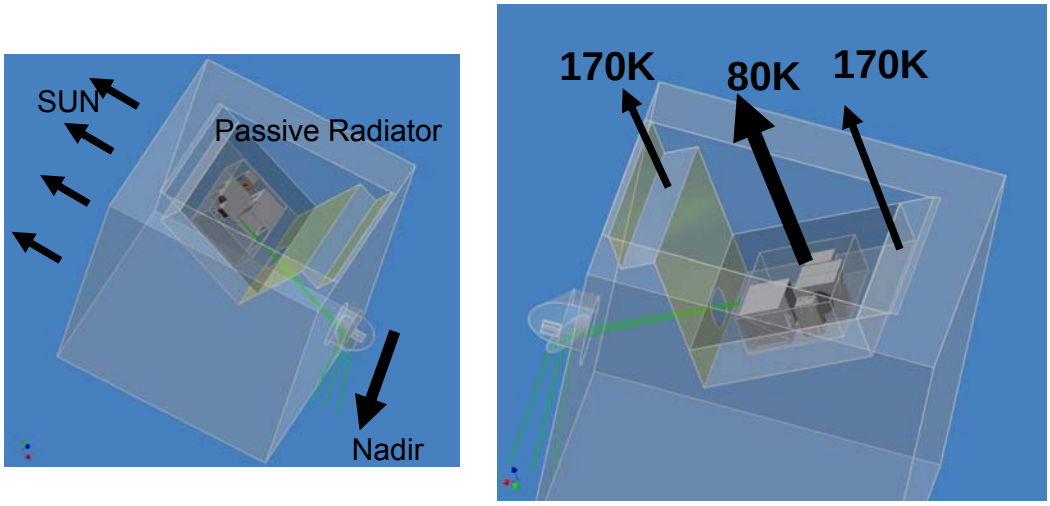

Figure 9. Instrument radiator requirements for a cooled array option, should higher spectral resolution or a shorter integration time be required.

8.3.3.2 Orbit, operations and pointing requirements

	operations
Goal	Surface mapping
Duration	7 Seconds per scan/calibration cycle
Power (peak and mean)	3.5 Watts (pk), 2 Watts (ave)
Pointing requirements	<0.1mrad over 7 seconds to allow spatial oversampling during 7 second scan/calibration cycle. Common bore sight with imaging experiment.
Telemetry (Data Rate & Volume)	1.5Mbytes per image (assuming no compression)
Operational constraints	If cooled detectors used, radiator orientation constraints must be pointed away from the Sun and target object.
Number of occurrences of the operation	Dependent on mission phase, continuous day/night operation during survey and mapping phases.

Since accurate surface temperature measurement (±0.2K) is a primary requirement for robust determination of surface properties due to variations in their thermal signature, a scan pattern that includes interleaved views of calibration targets and space is essential. For the SMI, a possible scan sequence that allows for spatial oversampling of the field of view is:

- Nadir position 1
- Nadir position 2
- Nadir position 3
- Space view
- Nadir position 1
- Nadir position 2
- Nadir position 3
- Calibration target

The integration time for each nadir position is automatically adjusted to maintain uniform spatial sampling. Based on previous instrument studies the total time expected for this scan pattern is approximately 7 seconds. In order to maintain good co-registration of the array during and between scans a pointing of accuracy of at least 0.1mrad over 7 seconds is required.

The most likely operational mode would involve step-scanning the FOV over the surface and using (e.g.) a 10x10 macro pixel to improve signal to noise. Given the relatively slow average orbital speed and good signal through put of the revised instrument design, it is possible to imagine a scan pattern along the following lines:

1. View space and calibration target for 1 second.
2. Slew onto NEO and step scan the array in 5 pixel steps (to guarantee 10 pixel spatial resolution). This builds up the scene multiple times to sample different parts of the spatial

interferogram at each macro pixel. This also improves s/n, integrate at each position for (e.g.) 1 second. This will take approximately 96 seconds, assuming no adjustment for integration time.

3. Back to space view and calibration target.

The complete scan pattern would take 98 seconds, equivalent to 38.9m of worst case orbital velocity. However, the spatial resolution would be approximately 5m resolution for ten 250µm pixels, assuming no smear. This technique will improve the signal to noise significantly, but may not be necessary for daytime observations.

The power estimates in the statement of interest do not include the overhead of a DC/DC convertor, or make assumptions on the use of a specific data bus (e.g. SpaceWire/CAN-bus etc).

The power estimates are necessarily crude. For example, the detector read out, housekeeping were assumed to be managed by a representative FPGA (e.g. radiation tolerant RT54SX32S). Given the inevitable use of local storage in the instrument, a CAN bus should be OK.

Table 11 Power consumption

	Power [W]	**remark**
Total average	2	
Peak	3.5	e.g. Hot calibration target warming and scan/calibration assembly moving simultaneously.
Detector + electronics	2	

8.3.3.3 Interfaces and physical resource requirements

Four fixation points. Power connection 0-28V data and commands serial interface.
The volume estimates from current optical design is: 160 x 220 x 370 mm3 – but the instrument is not box shaped: Instrument now occupies a volume approximately 6400cm3; however, the actual optics only occupies a volume of 460 cm^3. Mass of the optics is approximately 1.3kg, with out light weighting. This does not include the scan/calibration mirror assembly or the calibration target, therefore a reasonable estimate of 2kg including low mass calibration target and scan mirror could be used.

8.3.3.4 Calibration

Internal blackbody calibration target and deep space view.

8.3.3.5 Cleanliness, planetary protection and pre-launch activities

At the level of the ExoMars AEP experiment.

8.3.3.6 Critical points

Detector array (cooled/un-cooled) to be evaluated. Dwell time and operation mode e.g. sit and stare versus push-broom.

8.3.3.7 Heritage

The instrument design has been extensively studied for Earth and Mars remote sensing applications. Two breadboard instruments have been assembled and tested, a demonstration system with cooled detectors (Reininger 2001) and a compact flight-like breadboard (Mortimer et al 2007).

Current status and further development activities

- Fully functioning breadboard exists and is completing testing.
- Instrument is currently between TRL 4 and 5.
- To June 2008
  - Complete functional testing of existing breadboard instrument
  - Improve basic asteroid/Moon thermophysical model for instrument characterisation (Lunar Diviner project)
- Development of the instrument to 2010:
  - New generation of flight compatible optics, based on the experience gained with the current generation breadboard.
  - Evaluate lower spectral resolution options (~10 cm-1) using un-cooled detector arrays specifically for mineralogy applications.
- Bring the breadboard to TRL 6 using the flight instrument qualification facilities already in place at Oxford:
  - Thermal vacuum testing.
  - Radiometric and field of view calibration
  - Vibration testing.

8.3.3.8 References

Adler, H. H.; Kerr, P. F. (1963) Infrared spectra, symmetry and structure relations of some carbonate minerale. *Am. Mineral.*, 48, 839-853.

Arnold, G., (1991). Measurements of the spectral emittance of particulate minerals and some remote sensing implications, *Vibrational Spectroscopy*, 2, 245-249.

Barucci, M.A., Dotto, E., Brucato, J.R., Muller, T.G., Morris, P., Doressoundiram, A., Fulchignoni, M., De Sanctis, M.C., Owen, T., Crovisier, J., Le Bras, A., Colangeli, L. and Mennella, V. (2002). 10 Hygiea: ISO infrared observations. *Icarus* 156, 202-210.

Cohen, M., Witteborn, F.C., Roush, T., Bregman, J. and Wooden, D. (1998). Spectral irradiance calibration in the infrared. VIII. 5-14 micron spectroscopy of the asteroids Ceres, Vesta, and Pallas. *Astron. J.,* 115, 1671-1679.

Delbó, M. (2004). The nature of near-Earth asteroids from the study of their thermal infrared emission. PhD thesis, Freie Universität, Berlin.

Delbó, M., dell'Oro, A., Harris, A.W., Mottola, S. and Mueller, M. (2007). Thermal inertia of near-Earth asteroids and implications for the magnitude of the Yarkovsky effect. *Icarus* 190. 236-249.

Dotto, E., Barucci, M.A., Brucato, J.R., Muller, T.G. and Carvano, J. (2004). 308 Polyxo: ISO-SWS spectrum up to 26 micron. *Astron. Astrophys*. 427, 1081-U1130.

Farmer, V.C. (1974). Infrared spectra of Minerals, *Mineral Society*, London,

Hapke, B. (1981). Bidirectional reflectance spectroscopy. I – Theory. *J. Geophys. Res.*, 86, 3039-3054.

Hapke (1993) *Theory of Reflectance and Emittance Spectroscopy*, edited byR. E. Arvidson and M. J. Rycroft, Cambridge Univ. Press, New York

Harloff, J. and Arnold, G. (2001). Near-infrared reflectance spectroscopy of bulk analog materials for planetary crust. *Planet. Space Sci.* 49, 191-211.

Harris, A.W., Mueller, M., Delbò, M. and Bus, S.J. (2005). The surface properties of small asteroids: Peculiar Betulia - A case study. *Icarus* 179, 95-108.

Hunt, G. R., (1980). Electromsgnetic radiation: The communication link in remote sensing, in Remote Sensing in Geology, B. S. Siegal and A. R. Gillespie eds, Wiley, New York, pp. 4-45.

Hunt, G. R., and Salisbury, J. W. (1974). Mid-Infrared spectral behavior of ignous rocks, *Environ. Res. Paper*, 496-AFCRL-TR-74-0625, p. 142.

Hunt, G. R., and Salisbury, J. W., (1975). Mid-Infrared spectral behavior of sedimentary rocks, *Environ. Res. Paper*, 520-AFCRL-TR-750356, p. 49.

Hunt, G. R., and Salisbury, J. W., (1976). Mid-Infrared spectral behavior of metamorphic rocks, *Environ. Res. Paper*, 543-AFCRL-TR-76-0003, p. 67

Jakosky, B.M. (1986). On the Thermal Properties of Martian Fines. *Icarus* 66, 117-124.

Kieffer, H.H., Chase, S.C., Miner, E., Munch, G. and Neugebau.G (1973). Preliminary Report on Infrared Radiometric Measurements from Mariner-9 Spacecraft. *J. Geophys. Res*. 78, 4291-4312.

Kieffer, H.H., Martin, T.Z., Peterfreund, A.R., Jakosky, B.M., Miner, E.D. and Palluconi, F.D. (1977). Thermal and Albedo Mapping of Mars During the Viking Primary Mission. *J. Geophys. Res.* 82, 4249-4291.

Lane, M. D., (1999). Mid infrared optical constants of calcite and their relationship to particle size effects in thermal emission spectra of granular calcite, *J. Geophys. Res.*, 104, 14099-14108 .

Lane, M. D., and Christensen, P. R., (1998). Thermal Infrared Emission Spectroscopy of Salt Minerals Predicted for Mars, *Icarus*, 135, 528-536.

Logan, L. M., et al., (1973). Compositional implication of Christiansen frequency maximum for infrared remote sensing applications, *J. Geophys. Res*., 78, 4983-5003.

Lyon, R. J. P., (1962). Evalutation of infrared spectrophotometry for compositional analysis of lunar and planetary soils, Stanford Res. Inst. Final Rep. Contract, NASA, 49-04

Mortimer et al. (2007). Development of a miniaturised remote sensing interferometer American Astronomical Society, DPS meeting #39, #34.09

Mueller, M., Delbó, M., Kaasalainen, M., Di Martino, M., Bus, S. and Harris, A.W. Indications for regolith on Itokowa from thermal-infrared observations. PASP Conference Series. (2007) in press.

Müller, T.G. and Lagerros, J.S.V. (1998). Asteroids as far-infrared photometric standards for ISOPHOT. *Astron. Astrophys.* 338, 340-352.

Palluconi, F.D. and Kieffer, H.H. (1981). Thermal Inertia Mapping of Mars from 60-Degrees-S to 60-Degrees-N. Icarus 45, 415-426.

Presley, M.A. and Christensen, P.R. (1997). Thermal conductivity measurements of particulate materials .2. Results. *J. Geophys. Res.-Planets* 102, 6551-6566.

Reininger (2001) A Spatially Modulated Interferometer for mapping Maritain water vapour Sources. D.Phil Thesis Univ. Oxford 2001.

Ruff, S. W., Christensen, P. R., Barbera, P. W., Anderson, D. L. (1997). Quantitative thermal emission spectroscopy of minerals: A laboratory technique for measurement and calibration, *J. Geophys. Res*., 102, 14899-14913.

Salisbury, J. W., and Estes, J. W. (1985). The effect of particle size and porosity on the spectral contrast in the midinfrared, *Icarus*, 71, 586-588.

Salisbury, J. W., Walter, L. S., and D'Aria, D. (1988). Mid-infrared (2.5 to 13.5 μm) spectra of igneous rock, *U. S. Geol. Surv. Open File Report*, Reston, Virginia

Salisbury, J. W., and Walter, L. S., (1989). Thermal infrared (2.5-14.5 μm) spectroscopic remote sensing of ignieous rock types on particulate planetary surface, *J. Geophys. Res*., 94, 9192-9202.

Shkuratov, Y., Starukhina, L., Hoffmann, H., Arnold, G. (1999). A Model of Spectral Albedo of Particulate Surfaces: Implications for Optical Properties of the Moon, *Icarus*, 137, 235-246.

Van der Marel H. W. and Beeutelspacher H., (1976). Atlas of Infrared Spectroscopy of Clay Mineral and their Admixtures, Elsevier, Amsterdam

Wechsler, A.E. and Glaser, P.E. (1965). Pressure Effects on Postulated Lunar Materials. *Icarus* 4, 335-&.

Witteborn, F.C., Roush, T.L. and Cohen, M. (2000). Thermal Emission Spectroscopy of 1 Ceres: Evidence for olivine. In: M.L. Sitko, A.L. Sprague and D.K. Lynch (Eds.), Thermal Emission Spectroscopy and Analysis of Dust, Disks, and Regoliths (ASP Conf. Ser., vol. 196), Univ. of Chicago Press, Chicago, pp. 197-203.

8.3.3.9 Summary table

Table 12 Summary table of the mid-IR spectrometer

Parameter	Units	Value/Description	Remarks
Reference P/L	N/A	SMI	Spatially Modulated Interferometer
Type of optics	N/A	Aspheric Al Mirrors, Aspheric Germanium Lenses	
Type of detectors	N/A	Cooled MCT array/Uncooled thermopile array	Options depend on spacecraft radiator constraints, spectral resolution and integration time
OPTICS			
FOV	mrad	64	
Pixel IFOV	μrad	750	
Aperture	mm	40x50	
Focal length	mm	200	
Focal number	#	4	
Spectral Range	μm	5-25 micron	
Spectral Channels	#	N/A	Interferogram is returned
Signal to noise ratio	N/A	Thermopile≈100, cooled array >1000	Dependent on detector array selected
Spectral resolution		resolving power 1000 (max)	@ 10 μm, software programmable

FOCAL PLANE ARRAYS			
Pixel lines in array	#	640	
Pixels per array line	#	480	
Pixel size	μm	25	tbc
Exposure time	sec	0.1-1	Minimum integration time for un-cooled array is 100ms
Repeat time	sec	7	Includes calibration target and space view scans.
Operating temperature	°C	30/–196	Controlled by a TEC, dependent on detector type used
A/D conversion	bit/pix	16	
SWATH and RESOLUTION			
Swath width	m	320	@ 5 km distance
Swath length	#	50	Pixels
Spectral sampling	nm	100nm	On average, programmable
Angular resolution	μrad	750	
Spatial (pixel) resolution	m	0.27	@ 1.09 km distance
PHYSICAL			
Mass, total	kg	2.0 Kg	Including radiator
Dimension	mm	160x220x370	instrument not box shaped actual volume is 6400 cm^3.
Volume	cm^3	525	
Footprint			
POWER			
Total average power	W	2	
Peak power	W	3.5	Hot calibration target
Detector + electronics	W	2	
cooler	W	n/a	Passive radiator
Data			
Data rate		≈3kbytes/second	At maximum spectral resolution
Data volume	KB	see Table 13	
Data volume (whole body		see Table 13	
Compression factor		TBD	2 – 5 expected

Table 13 Absolute basic data volumes for 16 bit resolution 640x480, without compression. Final column is the basic data estimate

Target	Diameter (m)	Orbit radius from CoM (Assume	Single Cover (MB)	Global Coverage for	2xFOV Overlap (MB)

		spherical)		**e.g. 10 local times (MB)**	
2001 SG286	280	500	57.39	573.93	1147.86
2001 SG286	280	1000	10.06	100.57	201.14
2001 SG286	440	500	234.28	2342.82	4685.64
2001 SG286	440	1000	30.19	301.90	603.80
2001 SK162	1100	2000	54.60	546.01	1092.02
2001 SK162	1100	5000	5.80	57.97	115.94
2001 SK162	1820	2000	264.51	2645.08	5290.17
2001 SK162	1820	5000	18.79	187.86	375.73

Table 13 gives rough estimates of mapping volume, assuming:
1. 16 bit per pixel resolution.
2. 640x480 array, no macro-pixels.
3. Simple, spherical target, calculation based on the number of FOVs required to give global coverage using a simple push-broom scan.
4. No data compression (could be of order a factor of 5 based on our experience with CIRS).
5. No space view or calibration views (ideally there should one space view and one calibration view per scene).
6. No spatial oversampling. For basic Nyquist spatial sampling we'd need at least two overlapping FOV's, so this would double the total values (last column).
7. These should be considered a minimum, complete coverage over a greater range of local times improves the accuracy of the surface property measurements.

8.4 Radio science experiment

8.4.1 INTRODUCTION

The determination of asteroid masses is usually done by the observation of close approaches of nearby asteroids or for binary asteroids, by measuring the influence of the primary over the secondary. However, such situations are not common and this is why masses are not known for a great number of bodies. Knowing the mass is scientifically important because, accompanied with an accurate shape model, it allows the determination of the body's bulk density, which in turn gives some indication of its internal structure, such as the amount of porosity. Thus the accurate determination of the mass of the target is always considered as a high priority of space missions aimed at visiting a small body, even if it is not the ultimate mission objective.

Radio Science (RS) is the general study of phenomena affecting the propagation, scattering and reception of electromagnetic transmissions with wavelengths longer than roughly 0.1 mm. In the context of planetary science, this term has come to indicate a focus on the use of radio signals travelling between the spacecraft and an Earth terminal. It then includes the scientific application of radio tracking data for the precise determination of spacecraft's orbit and the scientific information that can be derived from such determination. Radio signals provide an extremely precise measurement of the radio path between the ground station and the spacecraft. When the radio path is well-clear of occulting material, the spacecraft can be treated as a "test particle" falling in the gravity field of the planetary system with the component of its velocity along the line-of-sight to the tracking station measured by the Doppler effect. Gravity experiments are based on determining the motion of the satellite in response to the variations in mass distribution within a planet, and this method has been extended to small bodies. The NASA Near probe used RSE to determine the mass of the asteroid Mathilde (Yemonans et al. 1997) and the gravity field of Eros (Yeomans et al., 2000). The mass of the asteroid Itokawa was also measured by the Hayabusa spacecraft – which did not go into orbit around the object - but in this case, another method was chosen using a combination of the LIDAR instrument and the camera (see Abe et al. 2006), allowing a mass determination with a 5% uncertainty (new analysis of the data is under way and may reduce the error bars). RS was also used with an X-band link.

The Radio Science Experiment (combined with data from the satellite's camera and possibly a Laser Altimeter) can thus determine the mass, centre of mass (as opposed to centre of figure), gravity field, shape, rotation axis and moments of inertia of the object. The motion of the satellite is monitored using Doppler shifts in the frequencies of some band (Ka/Ka and/or X/X) transponder system and solving for the gravitational field of the object, with knowledge of the relative position of the object and the satellite and the object's rotation state. If the duration is long enough, it can also allow the determination of the high orders of the body's gravity field which is a key science objective to gain a first order understanding of the internal structure of the body and the mass distribution relating to the surface shape. Indeed, the harmonic coefficients of the gravity field can be determined and compared with those expected from an object with the same shape but a uniform density distribution. Any differences would indicate some degree of large-scale inhomogeneity. All the retrieved parameters from the RSE will necessarily be solved for simultaneously based on data from a set of radio science passes. These passes will need to have

ground tracks well-distributed across the body's surface in order to sample the gravity field effectively. However, measuring anything more than J2 remains very challenging.

RSE was one of the primary objectives of the ESA phase-A study of the Don Quijotte mission aimed at deflecting an asteroid from its trajectory. However in this case, RSE was also used to determine the change of semimajor axis of the asteroid, and the required performances were thus very ambitious. However, most of the indications below are inspired from those studies.

8.4.2 SCIENTIFIC GOALS AND PERFORMANCE REQUIREMENTS

The following requirements are cited from the Science Requirements Document as reference for the expected scientific performance of this instrument;

GR-040: The mass of the NEO shall be determined to an accuracy of about 1 % (may need to be rediscussed for small objects).

AS-010: The inner structure of the NEO should be constrained, with the goal of doing this to a depth of about 100 m and a spatial resolution of about 10 m.

AS-020: The J1 and J2 terms of the gravitational field should be determined with tbc accuracy.

Science requirement:

The accuracy of the mass determination increases obviously with the proximity of the object to the satellite. For a same accuracy, the level of required proximity depends on the mass of the object (less massive object need a closer approach). In the current concept, the satellite should fly closely to the asteroid and even land on it. Having an accurate knowledge of the mass is extremely important because, accompanied with an accurate shape model (volume) via imaging and laser altimetry, it can allow an accurate determination of the bulk density of the object. From experience, the mass determination is much more precise than the volume determination therefore the error of the volume determination is the driver for the error in the mean bulk density. A mass determination with accuracy of 1% or less should nevertheless be considered.

Instrument requirements:

Radio Science instrumentation combines equipment on the ground with on-board spacecraft hardware required to create and maintain a highly stable and precise radio link. Two-way radio signals are generated on the ground and transmitted "uplink" through some large antennas. These transmissions are received by the spacecraft transponder, shifted in frequency, and then retransmitted "downlink" to the Earth where they are received either at the original site or at a second site, possibly located on another continent. Transponder design is such that the frequency of the downlink signal is coherently related to the received uplink frequency by a known integer ratio. The downlink signal frequency being derived precisely from that of the uplink, it is possible to measure changes in the radio path length by comparison of the received downlink signal with the ground oscillator that originally generated the uplink signal. An increase in the radio path length decreases the phase of the received downlink signal relative to the ground oscillator, and vice-versa. Hydrogen maser clocks are used for the fundamental frequency reference on the ground, hence measurement of the downlink phase provides an extremely precise method for determining changes in the round trip propagation time to the spacecraft. For instance, a 1-Hertz difference between the frequencies of the uplink and downlink signals means that the total radio path length is changing at the rate of 1 wavelength per second. Overall the short-term accuracy of

the measurement procedure depends on the signal-to-noise ratio achieved and, ultimately, on the stability of the ground station oscillator over the round trip flight time of the radio signals to the spacecraft and back.

In general, the RSE experiment needs accurate study of the following parameters:

- Relative motion between Earth and asteroid
- Earth rotation
- Earth solid tides
- Propagation effects of the electromagnetic waves
- Non gravitational forces
- Spacecraft motions
- High Gain Atnenna (HGA) pointing motion
- Mechanical deformation of the onboard and ground antennas.

In effect, the total Doppler received by the ground station is the addition of a Doppler noise due to phenomena such as solar radiation pressure, thrusters operations, … and the actual Doppler resulting from the acceleration caused by the object. For the RSE measurements to be successful, all perturbing forces on the spacecraft must be modelled accurately as the Doppler noise is the limiting factor for mass determination. It is caused by a number of sub-factors which can be quantified by the so-called Allan variation. Among these factors are the instrumental noise sources (e.g. thermal, transponder quantisation, ground station), which account for a large part of the error. However, these errors can be greatly reduced by integrating over a long time.

In addition, an estimate of non-gravitational perturbations is necessary. The dynamics of a spacecraft orbit around a small asteroid is indeed quite different from that involved around planets, moons or very large asteroids. The orbital radii are very small, of the order of a few km or less. The attracting mass is small too, so the orbital period is typically large and the orbital velocity is reduced to a few cm per second. In such a situation, the angular momentum contained in the orbital motion becomes very small, and the perturbing forces, especially those induced by the Solar Radiation Pressure (SRP) can have a very strong effect. In addition to changes in angular momentum, the SRP forces quickly build up eccentricity and thus, within just a few days, lead to an impact or an escape from orbit. Numerical analysis has shown that the SRP helps maintain a sun-synchronous orbit. For a wide range of cross-section-to-mass ratios, the effect of continuous SRP forces on an orbit that is initially perpendicular to the Sun direction results in a rotation of the orbit plane, such that the near-terminator conditions are maintained, even for prolonged period. Thus, for the RSE to be successful, the SRP must be modelled accurately, and several studies have already developed such models. Non-gravitational forces can be difficult to characterize a priori because they require detailed modeling of the spacecraft geometry and surface properties, the attitude behaviour, the spatial and temporal variations of the incident radiation and particle fluxes and the interaction of these fluxes with the surfaces. The limitations on the accuracy are likely to be a result of varying SRP over the spacecraft surface. But the emission and absorption properties of the spacecraft surface materials must definitely be known with good accuracy (1% uncertainty at most).

Then, thrusters operation must be avoided during the RSE because of the great uncertainty in the associated forces and attitude changes. Attitude changes that do not use thrusters (i.e. using wheels) are permissible but will result in small changes that can be modelled in the perturbations due to the different geometry with respect to the Sun.

Solar plasma noise has also to be determined if signals go through regions of high-solar plasma density. The latter effect can be eliminated by using two radio links, for instance S and X-band or X and Ka-band. The use of two bands or VLBI techniques (Delta-DOR) may also be considered to eliminate the Doppler noise generated by ionospheric/tropospheric effects. Finally, it shall not be necessary to use an ultra-stable oscillator as we do not expect any great presence of gas on a non-active primitive body and thus, one-way non-coherent link is not necessary.

Based on experience and simulations, an observation campaign of 4 to 6 weeks after entering in the Hill's sphere of RSE tracking should allow a complete mapping of the gravity field of the object. However, this largely depends on the asteroid properties (mass, rotation rate, diameter). Moreover, all indications above depend on the chosen orbit (orbit plane angle with respect to Earth LOS, eclipse/no eclipse, etc …). Therefore, the precise definition of the RS requirements should be done once the orbital parameters are done.

8.4.3 DESCRIPTION

8.4.3.1 Instrument concept

In a full multifrequency configuration three radio links are established between the ground station and the spacecraft: a X/X link, a X/Ka link (with the Ka downlink coherent with the X-band downlink) and an independent Ka/Ka link (only required for a very high level of accuracy). This configuration was extensively studied and tested in the past years. It guarantees a measurement accuracy independent from the solar elongation angle (Sun-earth-probe angle), as it cancels out the noise from the solar corona and interplanetary plasma. Plasma noise has been the main limitation of X-band Doppler and ranging system in interplanetary radio tracking.

For the required accuracy, the operational radio link of RSE can be a two-way coherent radio X/X and X/S or X/Ka link band. Hydrogen maser is used as a frequency standard for generation/reception of the uplink/downlink signal. For instance, studies of the Don Quijotte concept proposed the use of a transponder system for the following bands:

- Ka/Ka band RSE
- X/X for spacescraft operations and communications, including emergency

The following receiving and transmitting frequencies shall then be used:

- X-band uplink (at approx. 7100 MHz)
- X-band downlink (at approx. 8400 MHz)

- Ka-band downlink (at approx. 32000 MHz)
- Ka-band uplink (at approx. 34000 MHz)

The satellite radio subsystem shall then be capable of using a transponder for the X/Ka-band for both RSE and spacecraft operations and communications. This requirement is particularly important if plasma effect cannot be neglected. Indeed, the use of Ka-band downlinks will not enhance the accuracy on the Doppler instrument noise but will allow decreasing the uncertainty on the dispersive errors.

The transponder ratios of the coherent radio links shall be constant with the following numerical values:

- X-band transponder ratio: $k_X = 880/749$
- Ka-band transponder ratio: $k_{Ka} = 3344/749$

if there is an X-band uplink in the 7100 MHz frequency band.

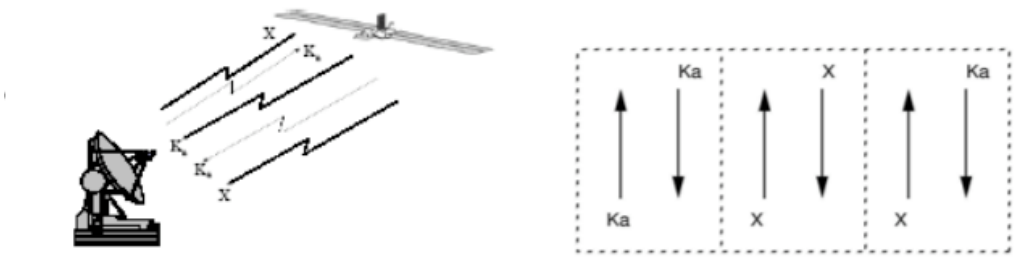

Figure 10 E**xample of a multi-frequency configuration ensuring a nearly complete cancellation of the plasma noise both in range and range rate measurements.**

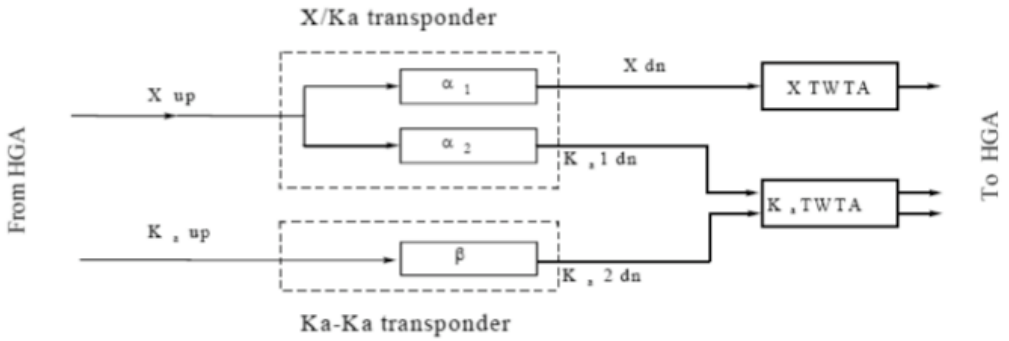

Figure 11 Example of a schematic of RS links used for the RSE (from Bepi Colombo). The independent Ka-Ka transponder must be considered only if a high level of accuracy is required. Here, $\alpha_1=k_{X/X}$= 880/749, $\alpha_2=k_{X/Ka}$= 3344/749 and $\beta=k_{Ka/Ka}$= 3344/3599.

The radio link shall be capable of guaranteeing the required Doppler and range errors for worst case conditions (rain attenuation) assuming 95% availability. The ranging tone frequency of 25 MHz should be the baseline. Although not a scientific requirement, a separate coherent Ka/Ka-band translator can be used for high precision measurements of the gravity field (in order to ensure a safe landing on the asteroid) and shall provide the possibility for a wide band ranging system. The uplink/downlink Ka-band translator ratio shall be constant at the numerical value: $k_{Ka/Ka}$ = 3344/3599 if the Ka-band uplink is the 34200 MHz frequency band. Other advanced techniques (Delta DOR measurement via VLBI technique) may also be considered as an option.

Note that we only consider here the use of Ka-band, but a trade-off shall be performed so as to employ either S or Ka band as a second downlink band taking into transponder mass, antenna size, and so on, and also telecommunication system parameters such as data rate, ground station visibility etc … However, because it is less sensitive to plasma effects than S-band and due to its use in other missions, Ka-band shall be favoured.

The radiofrequency subsystem shall be able to operate all links simultaneously via the High Gain Antenna (HGA). Depending on the mission design and in particular the geometry between the Sun, Satellite, the Earth and the object, a steering antenna or some agile capability (3-axis active control) may be required.

8.4.3.2 Orbit, operations and pointing requirements

Orbit

The RSE orbit must be chosen so that it can achieve the requirements defined in previous sections. The length of the observation campaign depends on many factors concerning the asteroid properties (e.g. true rotation period of the object) and both the length of a tracking pass and the number of tracking passes per day.

Operations

The satellite shall not perform AOCS (Attitude and Orbit Control System) operations during four consecutive operation windows. Possible operation constraints shall be clearly identified. The High

Gain Atenna (HGA) shall be pointed toward the Earth and the spacecraft shall have a permanent communication link with the ground segment during RSE operations. The satellite radio subsystem shall then be capable of using a transponder for the X/Ka-band for both RSE and spacecraft operations and communications. It shall then be able to operate all links simultaneously via the High Gain Antenna (HGA).

The preferred location in space best suited for the conduction of RSE shall be at a minimum geocentric distance from the Earth to provide the best radio link margins, and to keep the solar plasma noise contribution to the Doppler and range values at minimum. It shall also be located at large distance to the Sun to minimize the solar gravity and solar radiation disturbance on the satellite.

The ground-segment operations are not described here, but should also be address elsewhere for completeness.

Pointing

The HGA pointing accuracy (or spacecraft if no antenna pointing system) shall be greater or equal to 0.1 times the 3dB beam width during the whole time of RSE operations. The pointing stability of the system shall be such that the residual velocity error is smaller than 0.1 μm/s at all times during RSE operations.

8.4.3.3 Interfaces and physical resource requirements

Thermal control

The RF system is sensitive to temperature variations. It should then be located in a thermally stable environment of the spacecraft in order to avoid thermal insulation. The heat dissipated by the RF signal generation is about 5 W so no active thermal control system is required.

Electronics, radiation shielding

No particular radiation shielding is required. Most needed components of RSE equipment are or will be flight proven in a near future (Smart-1 and Bepi Colombo).

Data processing and transfer

The basic amount of data from an RSE is very low and is limited to house keeping data. However, f the RSE is combined with camera and laser altimeter measurements to determine the 3D-shape model of the object, advanced algorithm shall be necessary and the data processing loads shall likely be needed.

Mechanical structure and hardness

No particular stability requirements are needed.

Power

The KaTe experiment on Smart-1 had a power consumption of 18 W. Deep Space 1 carried a similar transponder having a peak consumption of 13 W. Thus, 15 W seems a reasonable value, taking into account technology improvements in the frame of Bepi Colombo.

Mass

Most of the equipments are part of the telecommunication subsystem and are therefore not considered as payload equipment. However, the upgrade of the telecommunication X/X transponder to also be able to use X/Ka downlink band implies additional mass and power (with subsequent modification of the antenna). This capability is likely to be necessary only for RSE operations and shall then be considered in the payload budget as it will be interpreted as additional science-driven mass to the telecommunication system. As an indication, the mass of the experiment KaTe onboard SMART-1 was 4.7 kg, for a 18 W X/Ka band transponder. The mass of a classical X/X band transponder (see, e.g., Hershel) is about 3 kg. Therefore, the additional mass may be about 1.5 kg, assuming some technology improvements.

8.4.3.4 Calibration

The estimate of the accelerations due to SRP relies on the knowledge of the optical properties of the spacecraft surfaces (emissivity, absortivity and reflectivity). To achieve the required accuracy, these properties shall be known to an accuracy of 1% at the beginning of the gravity campaign and 10% at EOL.

8.4.3.5 Cleanliness, ground activity and other requirements

A complete error budget of the measurements will necessarily include the ground system and ancillary instrumentation. This is especially important as the mechanical noise of the antenna and tropospheric noise will be the leasing sources of measurement errors in range rate. While little can be done to limit the antenna mechanical noise (gravity and wind loading), tropospheric noise, mostly due to water vapour, can be successfully calibrated by means of advanced water vapour radiometers. The need for these calibration instruments shall be carefully evaluated.

The ground segment shall be selected to be adapted to the requirements described in previous sections. In particular, it shall be capable of:

- Transmitting an X-band uplink carrier signal modulated with TC and range signals.
- Transmitting a Ka-band uplink carrier signal modulated with range signals.
- Receiving X-band and Ka-band downlinks simultaneously.
- Receiving dual frequency ranging signals.

The timing error of the maser clock, NCO phase readout accuracy and path delay instabilities shall then be limited to reduce the resulting error contribution to the 1-sigma Doppler and Ranging noises. The use of a second station may also be considered to reduce the time needed for the determination of the gravity field.

8.4.3.6 Critical points

As indicated, many aspects of the RSE need some crucial mission parameters to be evaluated against the achievement of the scientific goals. The most important ones are the mass of the target asteroid, the orbital distance and the measurement time. The mass and the orbital distance affect

the determination of the gravity field, the asteroid centre of mass and the spacecraft position from the asteroid. A larger mass would be desirable in order to increase the determination of these parameters. However, potential targets for a space mission are generally small (below a few km in size) so the RSE will be necessarily done in a low-gravity environment. A smaller orbital distance from the asteroid would be desirable in order to help the positioning of the spacecraft with respect to the center of mass. A trade off evaluation of these parameters is surely needed. The same holds true to concerning the parameters which will help size the system. These concern the requirements on Allan variance (propagation media, thermal and mechanical deformation, station location, uncertainty of the HGA motion about the spacecraft center of mass, thermo-mechanical stability of the HGA etc …), the radio link budget to reach the required SNR (atmospheric loss, rain attenuation link, antenna gains, downlink/uplink power, noise temperature, etc …).

Finally it has to be noted that the RSE will not allow by itself the investigations of the interior properties deep into the object. Indeed, as it was demonstrated by the analysis of RS from the NEAR mission (Miller et al. 2002), there is no unique solution for the mass distribution. Radio reflection tomography or seismic experiments would be required to better discriminate between a rubble pile or a monolithic body, which would be of high scientific interest.

8.4.3.7 Heritage

The NEAR Shoemaker spacecraft performed a RSE campaign on the asteroid Eros and reached accuracies of 0.04% and 1% on Eros' mass and volume, respectively, with an X-band coherent communication system. The antenna was non-gimballed. The spacecraft orbited the asteroid during one year. Note that Eros's mean diameter is about 16 km (it is the second largest NEO after the 40 km-size Ganymed) so it is much larger (more massive) than potential future NEO targets.

The Rosetta satellite also carries a RSE and it may be suitable to fulfil the requirements. It is equipped with a dual X-band and S-band telecommunication system and has large flexibility through a steering antenna. It also has an Ultra Stable Oscillator for the accurate referencing of the one-way signal. Note that the target of Rosetta is an active comet, so that outgasing activities may occur during the campaign.

Bepi Colombo and the Don Quijotte concept are based on the same architecture as Cassini, i.e. carrying a dual X/Ka uplink/downlink RSE system. The results of the Cassini radio science experiments and the analysis carried out for the experiment MORE of the mission BepiColombo to Mercury clearly indicate that only a multifrequency link in its full configuration can provide the best observables (range and Doppler) over the long time scales of the experiment. Note that a potential target of the Don Quijotte concept was the D-type NEO 2002 AT4, whose size is below 1 km, and that the RSE was the main tool of the mission for the measurement of the mass and the deflection of the object by an artificial projectile. Building on the ongoing development of these two missions is certainly the best strategy. The X/Ka-band approach should then be adopted, as it is less sensitive than the S-band to plasma effects (but more sensitive to weather effects). However, the required level of accuracy does not need to have a Ka-band uplink and thus, a Ka/Ka transponder does not have to be considered.

Smart-1 also demonstrated in Europe the use of the Ka-band downlink through the experiment KaTe. This experiment can be reused in this frame and would be the most suitable for the considered application, with a total mass of 4.7 kg, consistent with the required mass budget. Ongoing development in the Bepi Colombo framework should also be taken into account to increase the performances. An X/Ka-band transponder (strictly similar as the one needed) has also been developed by Motorola and JPL and has flown onboard Deep Space 1 with a mass of 3 kg and a power consumption of 13 W.

Finally, the phase A of the Don Quijotte concept has provided detailed studies of RSE accompanied with theoretical exercises on the baseline targets. These studies have led to several documents and technical notes at ESA. Information given in this report have been inspired by these documents.

1.1.3.8. References

Abe, S., Mukai, T., Hirata, N., Barnouin-Jha, O.S., Cheng, A.F., Demura, H., Gaskell, R.W., Hashimoto, T., Hiraoka, K., Hona, T., Kubota, T., Matsuoka, M., Mizuno, T., Nakamura, R., Scheeres, D.J., Yoshikawa, M., 2006. Mass and local topography measurements of Itokawa by Hayabusa. Science 312, 1344-1347.

Miller, J. K., Konopliv, A. S., Antreasian, P. G., Bordi, J. J., Chesley, S., Helfrich, C. E., Owen, W. M., Wang, T. C., Williams, B. G., Yeomans, D. K. and Scheeres, D. J. 2002. Determination of Shape, Gravity, and Rotational State of Asteroid 433 Eros. Icarus 155, 3-17.

Yeomans, D. K., Barriot, J.-P., Dunham, D. W., Farquhar, R. W., Giorgini, J. D., Helfrich, C. E., Konopliv, A. S., McAdams, J. V., Miller, J. K., Owen, W. M., Jr. , Scheeres, D. J., Synnott, S. P. and Williams, B. G. 1997. Estimating the Mass of Asteroid 253 Mathilde from Tracking Data During the NEAR Flyby. Science 278, 2106.

Yeomans, D. K., Antreasian, P. G., J.-P., B., Chesley, S. R., Dunham, D. W., Farquhar, R. W., Giorgini, J.D., Helfrich, C. E., Konopliv, A. S., McAdams, J. V., Miller, J. K., Owen, W. M. J., Scheeres, D. J., Thomas, P. C., Veverka, J. and Williams, B. G. 2000. Radio science results during the NEAR- Shoemaker spacecraft rendezvous with Eros. Science 289, 2085-2088.

See also all relevant ESA technical reports and documents from the Don Quijotte study.

1.1.3.9. Summary Table

Table 14 Example of a summary table of technical features of the radio science experiment

PARAMETERS	Units	Value	Remarks
			Most of characteristics are TBC in the course of the study
GENERAL			
Instrument name		NEARSE	NEA-Radio Science Exp
Heritage		SMART-1, Bepi Colombo, Don Quijote	
Reference P/L		KaTe, BC/DQ RSE	
Type of instrument		Transponder	
Function mode		Range rate and rate measurements	
REQUIREMENTS			
Ranging tone frequency	MHz	25	
X uplink frequency	MHz	7200	
X downlink frequency	MHz	8400	
Ka downlink frequency	MHz	32500	
(Or S downlink frequency)	(MHz)	2300	
Instrumental Doppler shift $\sigma_v(t)$	m/s	1.10^{-7}	Over 10^4 s
Frequency readout interval	s	1	At ground station
Ranging accuracy	ns	TBD	
ALLAN VARIANCE			
Total	NA	$<10^{-15}$	At 10^3 -10^4 s integration time
Individual contributors	NA	TBD for all contributors (propagation media, ground system, spacecraft)	
DATA RATES/VOLUME			
Data rate	kbps	~0.1	Housekeeping only (Mostly taken into account in telecommunication budget)
OPERATIONS			
Operational time	weeks	mini. 6 weeks campaign	
Orbit	NA	Preferrably low altitude for better determination of gravitational field	
POINTING AND ALIGNMENT			
Pointing control	arcmin	0.1 times the 3dB beam	To limit losses in the Link budget
Pointing stability	arcsec/s	TBD	
THERMAL			
Operating temperature range	°C	-20 ; +60	
Non-operating temperature range	°C	-40 ; +75	
POWER			
Total average power	W	TBD	
Power peak	W	15	The power consumption of the Ka band downlink of Bepi Colombo is 9 W (Since highest powed peak is given by Ka band, it must be taken into account as payload power budget)
PHYSICAL			
Units	NA	1	Only X/Ka transponder considered as payload
Preferred location	NA	No specific requirement	
Mass, total	kg	1.5	This is the mass of the extra equipment needed to account for the Ka downlink. The mass of the regular X/X band transponder can be taken into account in the telecommunication budget as being 3 kg
Location	NA	Thermally stable location	For link stability
CLEANLINESS AND OTHERS			
EMC requirements		Standard	
Chemical		None	
Vibration	g	25 rms random	
Shock	g	100	
Mechanisms	NA	None	

8.5 Neutral Particle Analyser

8.5.1 INTRODUCTION

The surface properties of a NEO and its interactions with solar wind are the scientific targets through which important information about surface evolution and, finally, about the global evolution history of the body. In particular, this investigation will answer one of the main questions of the Marco Polo NEO Sample Return mission: "What processes can be identified as happening on the surface of these small airless bodies as a result of exposure to the space environment and collisions?"

The asteroid is eroded by different processes (such as solar wind, and solar and cosmic ray bombardment and by micrometeoroid impact vaporization) and its superficial composition is modified by this space weathering and gardening (Hapke, 2001). The particles released from the body's surface are essentially lost in space since the escape velocity is very low. The relevant surface release processes at these distances from the Sun are Photon Stimulated Desorption (PSD), Ion-Sputtering (IS) and Micrometeoroid Impact Vaporization (MIV). The mean surface temperature is low; hence, the surface erosion due to the thermal desorption (TD), relevant only at Sun distances lower than 1 AU (Plainaki et al., 2008), is negligible.

Observations of the gas expanding from the asteroids are of crucial importance to identify and to localize the physical processes acting onto the surface as well as to estimate their efficiencies. In particular the ion sputtering is one of the most important processes causing alteration and erosion of the surface.

The key questions of NPA are summarized as in the following:

1. What processes can be identified as happening on the surface of the NEO as a result of exposure to the space environment and collisions? What is the erosion and the space weathering significance at the NEO surface?
2. What is the efficiency of each process as a function of environment conditions?
3. Is the efficiency of particle release processes uniform in the NEO surface?
4. What is the composition of the escaping material and consequently, how it relates to the surface composition?
5. What is the role of the surface release processes in the body evolution?

8.5.2 SCIENTIFIC GOALS AND PERFORMANCE REQUIREMENTS

The NPA scientific objectives are:

1. To identify the particle release processes active on the NEO surface
2. To evaluate the efficiency of each process as a function of environment conditions
3. To evaluate the efficiency of each process as a function of surface properties
4. To determine the composition of the escaping material
5. To estimate the role of the surface release processes in the body evolution.

8.5.2.1 Estimated neutral atom signal

Ion-sputtering and other surface release processes at NEO

The expected signal needs to be carefully evaluated considering each surface release process

Ion-sputtering results from the impinging of an ion of mass m_1 onto a surface; if the impact energy (E_i) is high enough, a new particle (m_2) may be extracted. In most cases, the ejected particle is neutral (Hofer, 1991). The energy transmitted in the collision is:

$$T = T_m \cos^2(\alpha_r)$$
$$T_m = E_i \frac{4 m_1 m_2}{(m_1 + m_2)^2}, \quad (1)$$

where T is the transmitted energy, T_m is the maximum transmitted energy and α_r is the recoil angle of the ion. The distribution function (f_S) of the ejection energy has been empirically obtained (*Sigmund,* 1969; *Thompson* 1968); the results are reproduced by the following function:

$$f_S(E_e, E_i') = c_n \frac{E_e}{(E_e + E_b)^3} \left[1 - \left(\frac{E_e + E_b}{T_m} \right)^{\frac{1}{2}} \right], \quad (2)$$

where E_b is the surface binding energy of the atomic species extracted, E_e is the energy of emitted particles, c_n is a normalization constant.

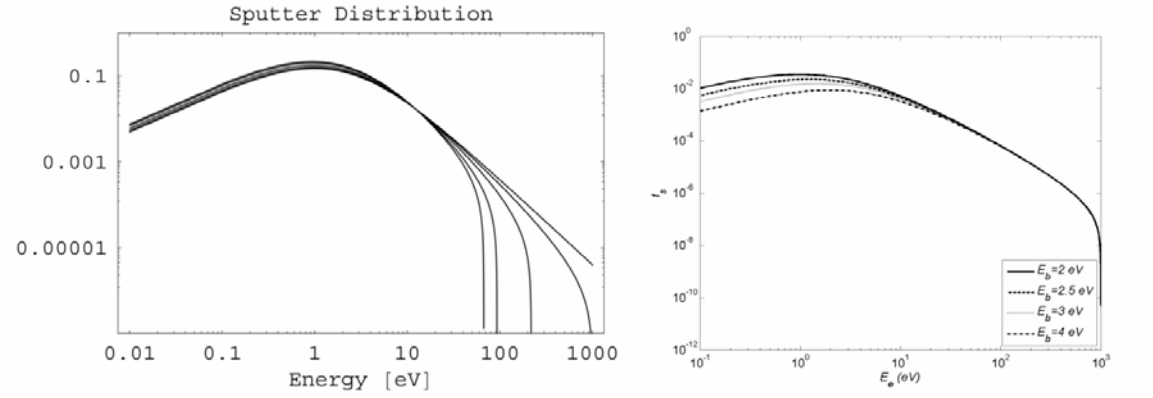

Figure 12. Solar wind sputtering normalized energy distribution function (left) for different species (Fe, Ca, Na, O, H) and (right) for different binding energies from a regolith.

The normalized energy distribution function for different species and different binding energies, assumes different profiles; anyway, generally it peaks at few eV but extends up to hundreds of eV (Figure 12).

The other surface release processes acting on the NEO are not able to eject particles at energies above few eVs; hence, the detection of particles above 10 eVs is a method to identify the action of the ion-sputtering process.

Plainaki et al. (2008) simulated the sputtered particles from a NEO. They considered a solar wind proton flux of $\varphi_{H+}=10^{12}$ m^{-2}s^{-1} as the total amount of the impinging particles. The NEO radius was assumed to be 0.5 km; its mass was taken as 10^{12} kg. Different kinds of NEO surfaces produce

some differences in the yield of the process and, hence, in the total released flux (Hapke and Cassidy, 1978). A similar study has been performed by Schläppi et al. (2008) for the asteroids (2867) Steins and (21) Lutetia in preparation of the upcoming Rosetta flybys. Plainaki et al. (2008) considered three different cases of carbonaceous chondrites comprising the actual body of the near Earth object: CI, CM, Tagish-Lake types. The bulk abundances of the main elements constituting each one of the above mentioned categories are presented in Table 15.

Table 15: Bulk element abundances for CI-chondrites, CM-chondrites and Tagish Lake type chondrites (adapted from *Brown et al.,* 2000).

Mass (amu)	Element	CI (atoms%)	CM (atoms%)	Tagish Lake (atoms%)
1	H	55	45	47
12/13	C	8	6	9
24/25/26	Mg	11	15	14
27	Al	1	1	1
28/29/30	Si	10	15	13
32/31	S	4	3	3
40/44	Ca	1	1	1
54/**56**/57	Fe	9	13	11
58/60/59	Ni	1	1	1
	Total	100	100	100

A summary of the input parameters used by Plainaki et al. (2008) is presented in Table 16.

Table 16: Input Parameters describing NEO environment

Parameter name	Symbol	Suggested Value
Solar-wind flux	φ_{H+}	10^{12} $m^{-2}s^{-1}$
Energy of the incident particle	E_i	1000 eV
Mass of the incident particle	m_1	1 AMU (proton)
NEO Radius	R_{NEO}	500 m
NEO Mass	M_{NEO}	10^{12} kg
Average sputtering yield	Y	0.05
Binding energy	E_b	2 eV

According to the simulations (Plainaki et al. 2008), for the case of a NEO surface consisting of CI type chondrites, significantly higher fluxes of neutral sputtered particles (up to 10^{11} particles m^{-2} s^{-1}) appear in a region extending from the NEO surface up to an altitude of about 1 km (Figure 13, left). Because MarcoPolo will perform a NEO a local characterization at a distance of about 1 km, the NPA instrument will have a good possibility of recording significant fluxes of sputtered particles. According to the right panel of Figure 13 the derived total emitted particle density is

sufficiently big, reaching the value of about $10^{6.5}$ particles m^{-3} near the NEO surface. This result is in good agreement with the calculations made by Scläppi et al. (2008) for asteroids Lutetia at a distance of about 2.72 A.U, and Steins at 2.14 AU.

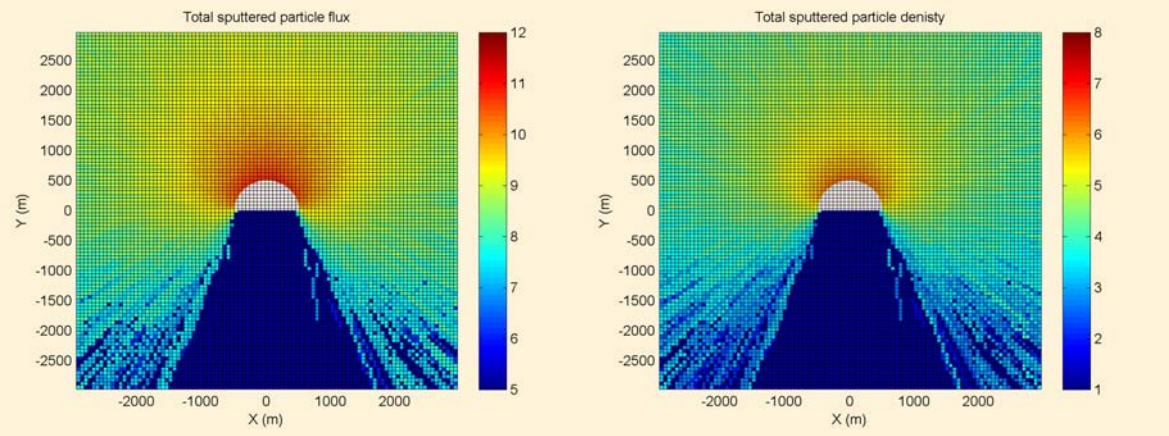

Figure 13: *Sputtered particle flux (in logarithm of particles m^{-2} s^{-1}, left) and density (in particles logarithm of m^{-3}, right) distributions for impinging particle of energy ~1000 eV. The NEO surface is assumed to be consisting of CI chondrites (Plainaki et al. 2008).*

PSD and TD contribute to the total released particle density emerging from the NEO surface. Especially for volatile elements like H and C, since it constitutes a process that regards exclusively volatile species. The results of Plainaki et al. (2008) simulations show that the total density of the volatiles emerging from the NEO surface, via the PSD process, is ~ $1 \cdot 10^8$ particles/m^3. Moreover, a rough estimation of the particles emerging via TD for different values of the surface temperature T results in values from ~10^4 particles/m^3 (for T=400K) to ~$5 \cdot 10^8$ particles/m^3 (for T=500K). Summarizing the results from simulating both PSD and TD, the total released particle density varies from ~ $1 \cdot 10^8$ particles/m^3 to ~ $6 \cdot 10^8$ particles/m^3. This value is in agreement to that calculated by Schläppi et al (2008) for asteroid Steins (~ $2 \cdot 10^8$ particles/m^3), at a distance of about 2.72 A.U. The fluxes emerging via the processes of PSD and TD are 1.5-2 orders of magnitude more intense than those emerging via solar-wind sputtering for volatiles at low energies. Other processes (like MIV) should be considered especially for refractories. Nevertheless, the higher energy released particles originate only via ion-sputtering (Milillo et al., 2005).The simulation considers an average solar wind condition. In the case of solar extreme event activity a major released flux is expected.

Plainaki et al. (2008) showed that the most important contribution to the total sputtered particle flux comes from the H particles emitted (about 90% of total flux). This is due to the big H relative atom composition, because of the low H atom mass.

The differences between the considered cases of CM and CI chondrite-type NEO surfaces are more distinguishable in the regions near the NEO surface.

The particles at energy E_e>10 eV (Sputtered High-Energy Atoms- SHEA) are about 1% of the total. If the orbiter will be at a distance of less than 1 km from a target with radius ~0.5 km, the estimated flux of high energy (above 10 eV) particles is $10^{8.5}$ $m^{-2}s^{-1}$.

8.5.2.2 Scientific requirements

The detection of released particles will provide a unique opportunity to estimate the loss rate from the NEO. The bulk of the surface released particles is in the illuminated side below the eV range and hence, the day-side measurement of the gas density will provide information about the intensity and the mass of emitted material. The identification of the mass of the released particles will give some hints on the NEO surface composition. It is likely that the radiation pressure action pushes some species toward the night side, forming a faint comet-like tail. Hence, the density measurements should be performed in the night side, as well

Nevertheless, different release processes are active on the NEO surface and, when only gas density is measured, it is difficult, if not impossible, to discriminate their different contributions or to reconstruct the emission regions on the surface (and derive areas with different release efficiencies). In fact, it is not possible to investigate whether the IS process is active without a measurement of the energy (or velocity) spectra, since this is the only process that releases particles at energies above 10 eV.

Moreover, a good angular resolution is important to identify the regions more active in releasing SHEA, thus evidencing possible anisotropies of solar-wind sputtering and/or of surface properties.

A comparison between simultaneous ion fluxes measured at the vicinity of the Earth and SHEA fluxes emitted from a NEO will provide an indication of the regolith efficiency in releasing material when exposed to solar wind.

Finally, in this way investigation of the alteration and erosion of the surface, in other words, space weathering activity, will be possible through remote sensing.

The ion sputtering and all the processes acting on the NEO surface will be even more investigated thanks to joint analysis of data from other payload instrumentation on board the Marco Polo mission that provides the remote-sensing of the surface properties (like V + NIR + MIR spectrometers and camera). In fact, additional information of the surface structure, mineralogy and composition will add constraints to model the release processes. Once the returned sample will be analyzed, even more detailed information will be achieved to be added to the RAMON data analysis. In fact Marco Polo will provide, for the first time, the opportunity to have in situ observations of the released particles together with detailed laboratory information on the mineralogy and composition of the emitting surface.

The following requirement is cited from the Science Requirements Document as reference for the expected scientific performance of this instrument;

GR-070: It shall be possible to measure the flux intensity, velocity, direction and mass of the particles escaped from the surface. This is needed to estimate the regolith efficiency in releasing material when exposed to solar wind sputtering. The discrimination of the major components of the escaping flux will provide an estimation of the loss rate and remote sensing of the upper surface composition. In order to detect the products of all active release processes, the energy range from 0.01 to 1 keV shall be covered, with an energy resolution of about 25% and the particles at energy <10 eV shall be measured with m/Δm of about 50.

LR-030: (As GR-070) It shall be possible to measure the flux intensity, velocity, direction and mass of the particles escaped from the surface. The energy range from 0.01 to 1 keV shall be

covered, with an energy resolution of about 25% and spatial resolution at surface about 10 m, the particles at energy <10 eV shall be measured with m/Δm of about 50.

In Table 17 the summary of NPA scientific performance requirements for each scientific objective is given:

Table 17: Summary of NPA scientific performance requirements. Red related to gas density measurements and blue related to SHEA detection.

Scientific Topic	Signal Intensity	Energy Energy resolution	Major Components	Angular FOV Angular resolution	Time resolution (s)	Observable region	Useful associated observations
1. particle release processes identification	10^2 cm^{-3}	< 1 eV Not req.	H, C, Mg, Si, S, Fe, others	- Not req.	60	Mainly dayside	
	10^4 cm^{-2} s^{-1} (for energy >10 eV)	>10 eV 25%	H, and refractories	5°x30° 5°x5°	60	dayside	
2. ion sputtering efficiency versus environment conditions	10^4 cm^{-2} s^{-1}	>10 eV Not req.	H, and refractories	5°x30° 5°x5°	60	dayside	Solar wind fluxes
3. ion sputtering efficiency versus surface properties	10^4 cm^{-2} s^{-1}	>10 eV 25%	H, and refractories	5°x30° 5°x2°	60	dayside	V+NIR+MIR+ camera observations
4.gas composition	10^2 cm^{-3}	< 1 eV Not req.	H, C, Mg, Si, S, Fe, others	- Not req.	300	Mainly dayside But also nigh side	
5. role of surface release processes in the evolution	10^2 cm^{-3}	< 1 eV Not req.	H, C, Mg, Si, S, Fe, others	- Not req.	300	Mainly dayside	
	10^4 cm^{-2} s^{-1} (for energy >10 eV)	>10 eV Not req.	H, and refractories	5°x30° Not req.	300	dayside	

8.5.3 INSTRUMENT DESCRIPTION

8.5.3.1 Neutral Particle Analyser required parameters

The estimation of the loss rate from NEO is accomplished by a Neutral Particle Analyser (NPA) able to resolve intensity, velocity and direction of the released particle flux. It is important to be able to cover the energy range up to hundreds of eV down to thermal energies in order to detect the products of all the active release processes.

In order to cover the whole energy range two sensors should be included in a single instrument design.

Required sensor characteristics

First sensor:

Energy range/resolution: <few eVs / no energy resolution

Mass resolution M/ΔM: about 50

Angular FOV/resolution: 5°x30°/ no angular resolution
Second sensor:
Energy range/resolution: 10-1000 eV / 25%
Angular FOV/resolution: 5°x30°/5°x5°
Mass resolution: no mass resolution
Time resolution: ~1 minute

8.5.3.2 Instrument concept

Detecting and characterizing neutral atoms in the energy range of interest, < 1 eV ÷ 1.0 keV, in an environment of photon, electron and ion fluxes, require 1) highly effective suppression of photons, electrons, ions and 2) two sensors for particles above and below 10 eV.

The incoming radiation made by neutrals, ions and photons impinges upon an aperture. The ions and electrons are deflected by electrostatic lens before the entrance. The neutral particles pass through an entrance of about 1 cm^2 divided for detecting low energies and higher energies.

For low-energy particles detection and mass analysis, the neutral particles pass through a carbon nanotube system (C1) that ionizes the particles (Modi et al., 2003). The ionized particles cross an electronic gate (C2) that provides the START of the ToF (example of such time tagging characterization is given in Brock et al. 2000). Then the particles are accelerated up to more than 1 keV and deflected by an electrostatic system (C3) and are detected by a STOP MCP detector (C4). Electrostatic analyzers are extensively studied in the frame of the CLUSTER/CIS instrument (Di Lellis et al. 1993; Rème et al., 1997). The ToF provides information about mass (since the spread in energy is assumed to be negligible).

For detecting particles between 0.02–1 keV, the neutrals pass through a double grating system (with slits of nanometric dimension) (D1) (Orsini et al. 2008b) that provides photon suppression. A shuttering system allows to move the two gratings one with respect to the other in order to permit the neutrals to enter in the sensor only when the slits are aligned (open gate), which defines the START time. Then the neutrals fly into a ToF chamber and are converted into ions by using the technique of neutral-ion conversion surface (D2) (Wurz, 2000). The ionization efficiency is sufficient at the lowest particle energies and even increases for higher energies. When particles impact at the conversion surface electrons are released, even at low impact energies (Wieser et al., 2005). An electrostatic system accelerates the released electrons keeping them well aligned to the original projection to the surface impacting point and pushing them toward the MCP detector, which also has position sensing capability (D3). The MCP will provide the STOP signal for the ToF measurement as well as the angular direction of the velocity of the registered neutral particle. The atom converted in ion by the conversion surface will be accelerated and detected by a MCP (D4) that will provide an additional STOP signal. Moreover, for increasing the geometrical factor, the detector can be used in open-gate mode. In this way the ToF can be identified using as START the first MCP signal. However, the energy resolution will be lower, due to the indetermination in the energy and recoil angle after the impact on the conversion surface.

The FOV of the two detection systems is 5°×30°. The higher energy distribution will be analyzed with an angular resolution of 5°x2.5° (high angular resolution mode) or 5°x5° (low angular resolution mode).

Taking into account the instrument elements, the estimate of the high energy detector geometrical factor is in the range 4 10^{-4}-2 10^{-5} cm^2 sr, and the mass spectrometer efficiency of about 0.14 (counts/s)/cm^{-3}.

These sensor characteristics permit a detection of the estimated particle release. In fact, if the estimated particle flux due to IS from NEO is 10^7 cm^{-2} s^{-1}, more than 1200 counts are estimated in the high energy sensor for 1 minute of integration time. The estimated gas density is, at least, of the order of 10^2 cm^{-3} close to the surface. In this case, for a 1-minute integration time, about 1000 counts in the low energy sensor are expected.

All the NPA operations will be controlled by an FPGA based microcontroller (Sensor Control Unit - SCU).

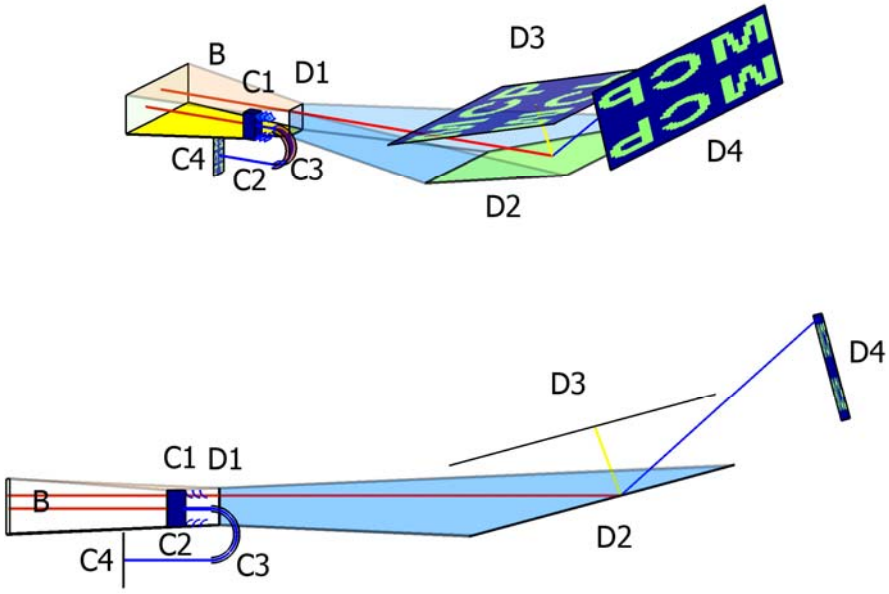

Figure 14. NPA basic concept

In summary the NPA sensor consists of the following subsystems:

A: Cover (not shown); B: Parallel plate collimator, balanced biased +5kV –5kV;

Mass spectrometer: C1: nanotube for ionizing lower energies particles, C2: electronic gate, C3: ESA, C4: MCP, C5: 2D Anode system (not shown).

The particle (red line) enters from the left side (B), gets ionized (blue line) passing through C1, accelerated by C2, deflected by C3, and finally detected by C4.

High energy detector: D1 two nanogrids and the shuttering system, D2: Conversion Surface; D3 MCP electron detector; D4: MCP ion detector; D5: 2D Anode system (not shown).

The particle (red line) enters from the left side (B), passes through D1, hits D2, releasing electrons (yellow line) detected by D3. The particle is deviated and ionized (blue line). Finally, the ion is detected by D4.

Table 18 Mass spectrometer geometrical factor

Element	Value	Unit
Cross section	$1.4\ 10^{-16}$	cm^2
Ionization lenght	2	cm
Electron current	$6.2\ 10^{15}$	e^-/s=1 mA
Collection efficiency	0.1	
TOTAL	**0.14**	**$(Cnt/s)/cm^{-3}$**

Table 19 High energy detector geometrical factor

Element	Value	Unit
FOV (5°x30°)	0.04	sr
Aperture	1	cm^2
Geometrical aperture ratio	0.2	
Shuttering grid	0.1	
Conversion surface efficiency (energy dependent)	0.001-0.1	
MCP electron efficiency	0.9	
MCP ion efficiency	0.5	
TOTAL	**$4\ 10^{-4}$-$2\ 10^{-5}$**	**cm^2 sr**

8.5.3.3 Orbit, operations and pointing requirements

The preferred satellite path is a 3D-axis-stabilized orbit at few kilometers above a NEO of radius less than 1 km. `

The pointing requirement is to have the object within the 30°x5° FOV of the instrument and to know the position and the orientation of the spacecraft with an accuracy of 10 mrad.

The orbit has not to be circular around the target as it may be inferred from the simulation parameters. Also during the close-approach phases the instrument should be active.

The instrument should be operated in survey mode during the first approaches to the target. Given the estimated signal, the first measurements should be performed at distances below 3 km from the object surface. While the mass spectrometer should be operated in the illuminated and not illuminated sides, the high energy detector needs to perform observation in the sun-illuminated side. Contemporaneous measurements of the two sensors are necessary. Crucial measurements are required during the closest approach phase.

Hence, according to the present mission scenario,

- calibration and survey operations are requested during phase “Far 1” (at least 10 hours);

- survey operations for high energy sensor (24 hours) and for mass spectrometer (at least 48 hours) are requested during phase "gravity field 2" ;
- nominal science operations are requested for achieving the primary scientific objectives during orbital phase "near 3", especially in the illuminated side. The average erosion rate can be evaluated with a statistics of 10 days of illuminated-side observations, but continuous day-side observations are requested for the study of erosion as a function of solar wind conditions especially for the high energy detector. Further observations time (at least 5 days) in survey mode is needed for the mass spectrometer in the night side.
- Nominal science operations in the descent phase, when the spacecraft is closer to the target.

A rough estimation of the total data volume during the mission is 7 Gbytes.

Table 20 Operation modes of the NPA (see next section)

	Calibration	survey		nominal	
Unit		Mass spectr.	SCU+High energy detector	Mass spectr.	SCU+High energy detector
Duration	10h	48h+120h	24h	240h+240h	>240h+240h
Power (peak and mean)	7 W	1.5 W	3+7 W	1.5 W	3+7 W
Pointing requirements		0.1 deg/s	0.1 deg/s	0.1 deg/s	0.1 deg/s
Telemetry (Data Rate & Volume)	770 Bytes/s	3 Bytes/s	3 Bytes/s	7 Bytes/s	51 Bytes/s
Operational constraints	Far from sources (cruise phase)		Illuminated side	Mainly illuminated side	Illuminated side
Number of occurrence of the operation					

8.5.3.4 Interfaces and physical resource requirements

The spacecraft resources for this instrument are not demanding. In fact, the dimension of the whole NPA instrument is about 20x20x10 cm^3, its mass will be about 2 kg and the total power requirement is about 11 W.

Table 21: Summary of NPA resources

	Mass (kg)	**Power (W)**	**Volume (cm^3)**	**Data rate (bytes/s)**
Mass spectormeter	1	1.5	15x10x10	7
High energy detector	1	7	20x10x10	51
SCU	0.2	3	16x1x10	N/A
NPA TOT	**2.2**	**11.5**	20x20x10	58

The required telemetry resources are not expensive. For the nominal science mode, if we consider 50 mass channels the mass spectrometer requires about 50x2 bytes/s, corresponding to 7 bytes/s for an integration time of 15 s. If we consider 32 TOF channels and 12 angular directions and 2 MCP signals the high-energy detection requires about 770 bytes/s, corresponding to 51 bytes/s for an integration time of 15 s.

In a survey mode, the foreseen telemetry rate is about half for the mass spectrometer (3 bytes/s) and 16 TOF x 3 angular dir. x 2 MCPs / 30s =3 bytes/s.

Data compression is provided by an included high reliability computation unit (factor 3 loss-less (Semi-log + HArtmann-Quad-tree loss less) and 4.5 lossy (Semi-log + HArtmann-Quad-tree lossy)). The SCU (System Control Unit) collects and processes all instrument data. The data inter face is CAN bus compatible.

The instrument design includes a DC/DC converter (28 V, regulated, from spacecraft) to feed the instrument with the required low voltage lines.

The instrument has no specific thermal control requirements.

There is no sun avoidance requirement.

The operational temperature is between -20°C to +40°C., non operational between -40°C to +50°C. The Switch-On-Temperature is min. -30°C and max +40°C.

8.5.3.5 Calibration

Far from sources, during cruise phase, it is requested a functional test of the instrument in order to verify the readout noise threshold.

8.5.3.6 Cleanliness, planetary protection and pre-launch activities

The instrument (MCPs) requires purging and humidity monitoring up to launch.

8.5.3.7 Critical points

The sensors are adequate for environments requiring strong radiation shielding like the BepiColombo mission to Mercury. The environment and mission duration of MarcoPolo is less constraining in comparison.

The UV and IR noise should be better evaluated. Anyway, the grids at the entrance prevents UV noise; an IR filter could be added in the case IR radiation will not be negligible.

8.5.3.8 Heritage

LENA sensors have been flown in the NASA IMAGE satellite and in MEX and VEX missions (ASPERA-3/4/ NPD). High energy detectors with characteristics similar to those proposed in the above description are being developed at INAF-IFSI for the BepiColombo payload (MPO/SERENA-ELENA; Orsini et al. 2008) and are proposed for the Solar Orbiter Mission (SCENARIO).

Many mass spectrometers have been flown in recent planetary missions. The mass spectrometer MPO/SERENA-Strofio has been developed and optimized for detection of very tenuous gas

environment. Presently a prototype is been tested at Southwest Research Institute for applications on the BepiColombo spacecraft to Mercury and the Ladee mission to the Moon.

8.5.3.9 References

Brock, A,. N. Rodriguez,and R.N. Zare, 2000. Characterization of a Hadamard Time-of-Fligth spectrometer, Rev. of Sci. Inst., 71, 1306-1318.

Brown et al.: *The Fall, Recovery, Orbit, and Composition of the Tagish Lake Meteorite: A New Type of Carbonaceous Chondrite*, Science, 290, 2000.

Di Lellis, A.M., P. Baldetti G. Chionchio, V. Formisano, 1993. The Hot ion analyzer instrument for the ESA Cluster mission; Il Nuovo Cimento -Vol16C, N. 6 10 Novembre-Dicembre.

Hapke, B., *Space weathering from Mercury to the asteroid belt*, J. Geophys. Res., 106, 10039-10074, 2001.

Hapke, B.W., Cassidy, W.A.: *Is the moon really as smooth as billiard ball/ remarks concerning recent models of sputtering on the lunar surface*, Geophys. Res. Lett. 5, 297-300, 1978.

Hofer, W. O.: Angular, Energy and Mass Distribution of Sputtered Particles, Sputtering by particle Bombardment III, Eds: R. Behrisch, K. Wittmaack, Springer-Verlag Berlin Heidemberg 1991

Jurac, S., Johnson, R.E., Richardson, J.D., Paranicas, C.: *Satellite sputtering in Saturn's magnetosphere*, Plan. And Sp. Sci., 49, 319-326, 2001.

Milillo, A., S. Orsini, P. Wurz, D. Delcourt, E. Kallio, R.M. Killen, H. Lammer, S. Massetti, A. Mura, S. Barabash, G. Cremonese, I.A. Daglis, E. De Angelis, A.M. Di Lellis, S. Livi, V. Mangano, K. Torkar, *Surface-Exosphere-Magnetosphere System of Mercury,* Space Science Reviews, **117**, issue 3, 397-444, 2005.

Modi A., N. Koratkar, E. Lass, B. Wei and P. M. Ajayan, 2003. Miniaturized gas ionization sensors using carbon nanotubes, Nature 424, 171-174, doi:10.1038/nature01777.

Mura, A., S. Orsini, A. Milillo, D. Delcourt S. Massetti and E. De Angelis, *Dayside H+ circulation at Mercury and neutral particle emission*, Icarus, 175, 305, 2005

Orsini, S., S. Livi, K. Torkar, S. Barabash, A. Milillo, P. Wurz, A. M. Di Lellis, E. Kallio and the SERENA team, *SERENA:a suite of four instruments (ELENA, STROFIO, PICAM and MIPA) on board BepiColombo-MPO for particle detection in the Hermean Environment*, BepiColombo Special Issue on Planetary and Space Science, in press, 2008a

Orsini, S., A.M. Di Lellis, A. Milillo, E. De Angelis, A. Mura, S. Selci, R. Leoni, F. Mattioli, S. Massetti, R. Orfei, I. Dandouras, P. Cerulli-Irelli, N. Vertolli, *Low energy high angular resolution neutral atom detection by means of micro-shuttering techniques: the BepiColombo SERENA/ELENA sensor*, proceeding of the meeting "Future perspective of space plasma and instrumentation and international collaboration" (Rikkyo University, Tokyo, Japan, November 1-3 2006) in press, 2008b (arXiv: 0811.4722)

Plainaki, C., A. Milillo, S. Orsini, A. Mura, E. De Angelis, A. M. Di Lellis, E. Dotto, S. Livi, V. Mangano, S. Massetti, M. E. Palumbo, *Space Weathering on Near Earth Objects based on neutral particle detection*, Planetary and Space Science, in press, 2009 (arXiv: 0811.4727)

Rème, H., J.-M. Bosqued and J.A. Sauvaud *et al.*, 1997. The cluster ion spectrometry (CIS) experiment, *Space Sci. Rev.* **79**, 303–350.

Sigmund, P. (1969) *Theory of sputtering. I. Sputtering yield of amorphous and polycrystalline targets*. ***Phys. Rev.* 184**, 383–416.

Sieveka, E.M., R.E. Johnson, (1984) *Ejection of atoms and molecules from Io by plasma-ion impact*, ***Astrophys. Journal,* 287**, 418-426.

Wieser, M., P. Wurz, R.J. Nemanich, and S.A. Fuselier., 2005. Secondary electron emission of CVD diamond by impact of slow H+, D+, H2+, C+, O+, and O2+ ions, Jou. Appl. Phys. 98, 034906-1 - 034906-4.

8.5.3.10 Summary table

Table 22 Summary data sheet of the NPA

Parameter	Units	Value/Description	Remarks
Reference P/L	N/A	Serena on BepiC	
Type of Ion supressor		electrostatic lens	
Type of ionisation		Carbon nanotubes	
Type of detector		MCP	
Type of positioning system			
Geometrical Factory mass spectrometer			
Equivalent aperture	mm^2	50	
FOV	°x°	5x30 deg	
Angular resolution	°x°		
Number of mass channels	#	50	
Dynamic range	$(Cnt/s)/cm^{-3}$	0.14	
Energy range	eV	<10	
Mass resolution	AMU	50	
Sensitivity			
Geometrical Factory			
Equivalent aperture	mm^2	100	
FOV	°x°	5x30 deg	
Angular resolution	°x°	5x2.5	
Number of channels	#	12	
Overall geom. factor	cm^2*sr	$4\ 10^{-4}$-$2\ 10^{-5}$	
Energy range	eV	<10-1000	
Spectral or energy resolution		32 TOF	
Sensitivity			
Detector			
Active area			
Acquisition time			
Orbit			

Pointing	n/a	Toward target	
Type of orbit	n/a	Below few km distance from NEO	
PHYSICAL			
Mass, total	kg	2.2	
Dimension	cm^3	20x20x10	
No. of units	#	1	
Footprint	mm		
POWER			
Total average power	W	11	
Peak power	W	11	
Data rate / volume			
data rate	kbs	0.06	
Compression	n/a	yes	internally done
Total data	Gbit	7 Gbit	
Thermal			
Operating temperature	°C	-20 to +40	
Non ops temperature	°C	-40 to +50	
Contamination			
Particulate/chemical	n/a		requires purging and humidity monitoring up to launch.

9 ADDITIONAL (TOUCH-DOWN) INSTRUMENTS

This chapter summarizes scientific instruments forming an additional payload suite that may be included in the overall payload complement if resources are available. These instruments will be operated during the sampling period once the spacecraft is attached to asteroid's surface. However, the operation of these instruments shall not interfere with the sampling process at any given time.

9.1 Alpha Particle X-ray Spectrometer

9.1.1 INTRODUCTION

tbw

9.1.2 SCIENTIFIC GOALS AND PERFORMANCE REQUIREMENTS

The following requirements are cited from the Science Requirements Document as reference for the expected scientific performance of this instrument;

SC-030: The bulk chemical composition of the sampling area should be determined.

SC-040: An additional "local characterisation" shall be performed after the sample collection (i.e. fulfil LR-010 and LR-020 again).

The scientific goal of an APXS-type instrument is the measurement of the elemental composition of solid material. Typical APXS is very suitable to measure the composition of planetary surfaces. The experiment requires to measure in-situ, i.e. at the surface of the body, and in close distance (few cm) with the surface material. APXS systems are complementary to instrument that assess the chemical (i.e. molecular) and mineralogical composition (molecular) of surface material, since it provides elemental concentrations in particular of the heavier elements (in particular from sodium to nickel). Lighter elements (C, N, O) are also detectable.

9.1.3 DESCRIPTION

An APXS instrument usually consists of a sensor head, a deployment device, and instrument electronics. In the case of the Rosetta APXS, used here as reference, the sensor head contains Curium-244 alpha sources that bombard the sample with alpha particles of an energy of about 5.5 MeV and x-rays of about 14 keV (emitted by the Plutonium-240 daughter). As a result, alpha particles are backscattered and x-ray radiation is emitted by the sample. The back-scattered alpha particles are measured by six alpha detectors and the x-ray radiation by one high-resolution x-ray detector. Energy dispersive alpha and x-ray spectra are recorded. The x-ray mode detects most elements from sodium to nickel depending on their concentration (usually about 0.1 to 1 weight per cent), while the alpha mode is sensitive to elements with low atomic weight, such as carbon and oxygen (concentration levels above ~1 weight %). The x-ray mode makes use of two excitation processes simultaneously: alpha-particle induced x-ray spectroscopy or particle induced

x-ray emission (PIXE) and x-ray induced x-ray spectroscopy or x-ray fluorescence (XRF). This permits to determine elements with low and high atomic weight with rather comparable sensitivities. X-ray lines of low-Z elements (Na, Mg, Al, Si, P, S, Cl, and K) are mainly the result of PIXE, while lines of high-Z elements (Mn, Fe, Ni and higher Z) are mainly the result of XRF; the elements Ca, Ti, and Cr benefit from both excitation processes.

In the laboratory, the instrument is calibrated in vacuum, usually measuring a geological sample, called SSK-1 with known composition in a standard geometry (distance between sample surface and detector). The data from this sample are used to compare the performance and sensitivity of the APXS instrument in-flight. This cross calibration mainly determines the response function of the x-ray detector, namely efficiency versus x-ray energy and in addition energy resolution and line shape.

Provided a flawless docking on the surface of the target body will occur, the surface material data can be directly compared with concentrations derived from laboratory samples measured in the same standard geometry. If a different geometry will be encountered, which will be probably the case due to irregular surface morphology, then, element ratios can be determined, first hand. A larger distance than the standard one reduces the amount of received radiation because of the inverse distance law of radiation and hence, results in a seemingly lower concentration of all detected elements (fake dilution). If all elements of a sample could be determined then the so-called closure to 100 percent can be calculated (the weight percent concentration of all elements must sum up to 100%).

9.1.3.1 Instrument concept

The Rosetta-Philae APXS system is described here as a typical instrument concept. The arrangement of the Rosetta detectors and alpha sources is strictly concentric (Figure 15). The x-ray detector is in the center of the front side. Six alpha sources (total of ca. 30 mCi = 1.1 GBq of Curium-244) are placed on a circle around the centre of the sensor head at a movable holding device. On the outer periphery of the aperture, six alpha detectors are located concentrically to the alpha sources. The alpha detectors have a thickness of 300 µm, which makes them also sensitive to charged background particles. Therefore, they are operated with lower than usual voltages so that they are not fully depleted (volume reduction). This decreases the sensitivity to cosmic or solar energetic particles.

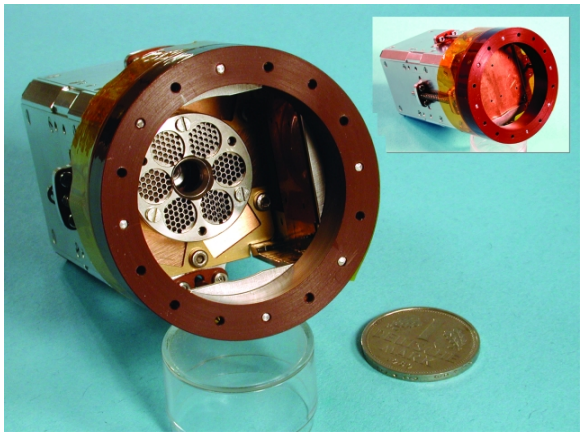

Figure 15 The APXS sensor head mounted on Philae, the Rosetta lander.

The sensor head is located on the outside of the lander, mounted in an opening of the balcony's floor. To bring the APXS in contact with the comet surface, it is moved by the deployment device that can lower and raise the sensor head. The nominal working distance between detectors and sample is ~30 mm (standard geometry) and is defined by a cylindrical apron (Figure 16). The end is surrounded by a ring that moves inward when it is brought in contact with the surface and opens two protective doors. The backside of the doors serves as a calibration target when in closed position. The backside material consists of a copper-beryllium alloy (Cu98Be2). The nominal diameter of the surface sample is 25 mm. The sensor head and the deployment device are fully exposed to the environmental conditions of the comet. The instrument was tested in a wide temperature range (down to -150ºC) and the overall signal gain was found to be stable.

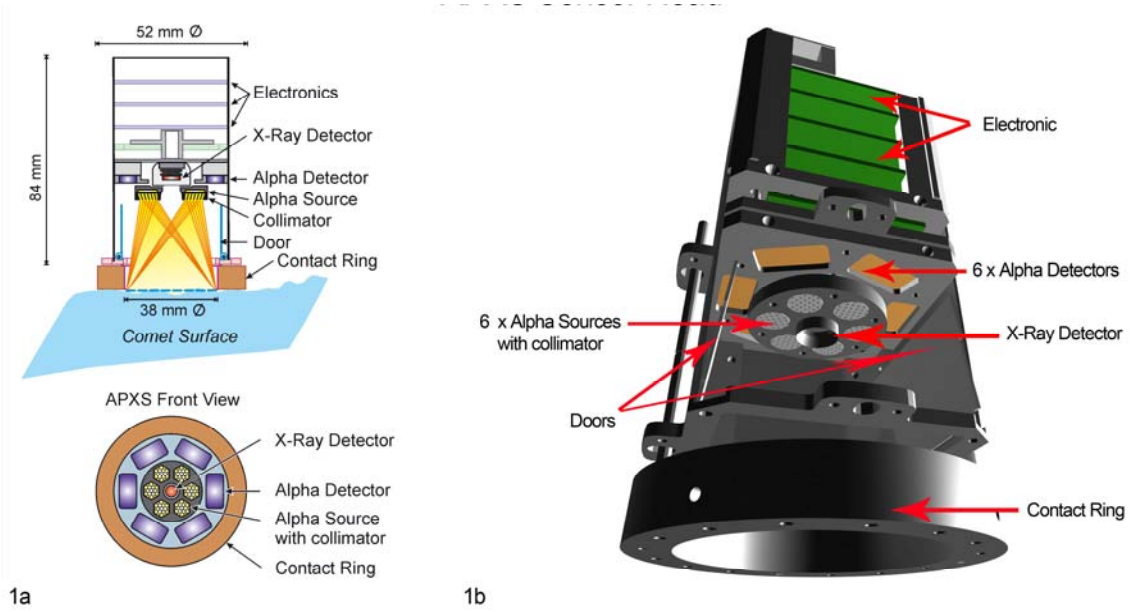

Figure 16 A new design for a compact APXS instrument

9.1.3.2 Operation requirements

Lab calibration requirements are described in section 1.1.3. In-flight calibration requirements are provided in the text above and below

9.1.3.3 Interfaces and physical resource requirements

Depending on the science goals (i.e. whether to measure the actual sampling area or its surrounding), the deployment of the APXS may be different. The key point is to bring the APXS in contact to the surface. In the most simplified approach an APXS might be installed in the feed of the landing unit.

9.1.3.4 Calibration

Lab calibration requirements are described in section 1.1.3. In-flight calibration requirements are briefly addressed in section 1.1.3.1: The calibration is done through measurements of the backside material (copper-beryllium alloy Cu98Be2 in the case of the Rosetta APXS) of the front cover of the instrument.

9.1.3.5 Cleanliness, planetary protection and pre-launch activities

APXS contain radioactive material (e.g. Curium-244) that emits alpha particles and γ radiation of a few to about 15KeV. Cleanliness and planetary protection is TBD.

9.1.3.6 Critical points

tbd

9.1.3.7 Heritage

Various APXS instruments were developed for space missions and have been or are flown onboard Mars96 (4 APXS), Mars Pathfinder (1 APXS), Mars Exploration Rovers (2 APXS) and Rosetta (1 APXS). The Mars Pathfinder and Mars Exploration Rover devices have proven records for successful operations and for very interesting science return. The Mars96 devices never arrived at the planet since the spacecraft got lost after launch. The Rosetta APXS is successfully commissioned and awaits scientific usage at comet 67P/Churyumov-Gerasimenko onboard the Philae lander in 2014.

9.1.3.8 Summary table

. The Rosetta APXS device used as a reference in the table below has a 5mm^2 x-ray detector. Detectors with sensitive areas of up to 100 mm^2 are feasible in the meanwhile which has immediate impact (linear) on the measurement time for the surface sample.
On the MER mission X-ray spectra with sufficient quality (allowing determination of elemental abundances with high accuracy) have been recorded within 20-30 minutes with a 7 mm^2 SDD

detector. With a 80-100 mm^2 SDD detector system, and with an measurement geometry optimized for the X-ray detection (which is not the case for the APXS on MER), **X-ray spectra with sufficient quality can be obtained within several minutes (2-5 min.) !!**

Table 23 Summary table of the APXS instrument

Parameter	Unit	Value/Description	Remarks
Reference P/L	n/a	**Rosetta APXS onboard Philae Mars-Exploration-Rover APXS**	Both instruments are very similar in design and sensitivity
CHARACTERISTICS			
Type of detector	n/a	alpha particle detectors **x-ray detector**	Si-PIN detector or Si-Surface barrier; SDD (Silicon-Drift-Detector) system ; Sensitive area up to 100 mm^2
Spectrum range	keV	1-16	
FOV (degrees)	°	~45	
FOV (diameter / mm)	mm	35-40	circular field of view (irradiated area)
Measuring time	min.	2 - 5	X-ray channel; optimized geometry; 80-100 mm^2 SDD system
Energy Resolution	eV	160-180	Depending on temperature
Number of samples	#	>/=1	
CONFIGURATION/ LAYOUT			
Units	#	1	
Preferred location for sensor	n/a	at front end towards surface of surface sampling head	
Preferred location for electr.	n/a	attached to sensor and source device	
Excitation sources	#	6	
Strength of sources	mCi	30	total for six sources
PHYSICAL			
Mass, total	g	350	Not including deployment device; design and mass of deployment device depends on lander design and mission requirements
Dimensions (detector + electronics)	mm	52 x 84 160 x 80 x 10	diameter x length of sensor head length x width x hight of electronics board (not including DC/DC power converters (depends on mission/ lander configuration)
Sample area	mm	35 - 40	diameter
POWER			
Average	W	1.5	
Peak	W	(a) 1.5 (b) TBD	Electronics board + sensor head (short peak (milli-sec) in power when switched on) Deployment device; power profile depends on design etc.
DATA RATE/VOLUME			
Average tm rate	kbits	13.3kbits/sec	
Data volume per sample	kbyte	21 kbyte (science data) + 3Kbyte pro transmitted housekeeping packet.	
Data volume total	Mbit		

POINTING				
Pointing	n/a	on surface sample		
Pointing accuracy	°	~20		half of field of view
THERMAL				
Temperature ranges op. Sensor Head and electronics board	°C	-150	+50	for sufficiently good signal/noise ratio a temperature of the SDD detector below ~0°C is needed. On the MER and Rosetta APXS no active cooling is performed, but can be performed because the SDD can be cooled by Peltier device (part of the SDD design). This would require additional power (1-2 W).
Temp. ranges op. Deployment-device		-150	50	Valid for the Rosetta design; may be different for different design.
Temperature ranges Non-op	°C			
Sensor Head / electronics board		-150 / +100		
Temp. ranges Non-op. Deployment-device		-150	100	
Temperature stability	°C	-150	50	temperature dependent variation of gain of detectorsystem is corrected for by software. n.a. for deployment device (Rosetta design). May be different for different design.
CONTAMINATION				
EMC requirements	power supply	"clean" Supply voltage with max voltage ripple of xx mV (TBD)		The limits on max voltage ripple are frequency dependent. Compatibilty with simultaneously operated other devices needs to be verified
DC magnetic	n/a	Not sensitive		
Chemical requirements	n/a	No sepecial requirements		Contamination of detector window by gases / dust etc. is prevented first order by doors at frontside of sensor head
SUPPORT ITEMS				
Deployment system	n/a	yes		
Covers, Shutters	n/a	front shutter		also used for in-flight calibration

9.2 Thermal sensor

9.2.1 INTRODUCTION

During the landing on the surface the temperature can be measured with a high degree of accuracy. Depending on the actual accommodation of the sensors a temperature profile or gradient can be measured.

9.2.2 SCIENTIFIC GOALS AND PERFORMANCE REQUIREMENTS

The temperature measurements will be used as "ground truth" data to be compared with measurements from orbit by remote sensing instruments and also precursor temperature models.

9.2.3 DESCRIPTION

9.2.3.1 Instrument concept

A suite of thermal sensors can be mounted in the feet of the spacecraft. It can be envisaged to mount some sensors on a thin needle like structure penetrating the first few centimetre of the regolith. The current design comprises 2 units per feet

Another mounting location is the sampling tool. The actual accommodation has to be explored during the development of that facility. The temperature measurements also support to monitor the working condition of the sampling head. It is planned to place 3 sensors at this location.

Platinum Resistance Thermometers cover the temperature range from -200 to +600 °C. For example the “PT100” sensor would be a good candidate for an application on an asteroid.

9.2.3.2 Orbit, operations and pointing requirements

The instrument is passively deployed during landing on the surface.

9.2.3.3 Interfaces and physical resource requirements

The total weight including sensors, cabling and electronic box is 240 g. While the sensors itself have a size of a few mm only the electronic box will be in the order of 20x20x40 mm. The location of this electronic box is tbd.

9.2.3.4 Calibration

tbd

9.2.3.5 Cleanliness, planetary protection and pre-launch activities

not applicable

9.2.3.6 Critical points

Beside the accommodation there are no critical points.

9.2.3.7 Heritage

Various space missions.

9.2.3.8 Summary table

tbd

9.3 ACE – Asteroid Charge Experiment

9.3.1 INTRODUCTION

The asteroid's electrical environment and interactions between it and the spacecraft will play a key role in the sample collection process. The asteroid will be in the supersonic solar wind, and photoemission on the sunlit side will ensure a positive potential there, while the shaded side will charge negatively within the plasma wake (Lee, 1996). Depending on the location of the surface sample collected, material that has been electrostatically transported may form a significant proportion of the material returned to Earth. In addition the spacecraft itself will charge positively, and during the sample collection process it is possible that electrostatic effects may disturb or otherwise affect the sample. There are no direct observations of asteroid electrostatics, but on Eros, the "ponds", craters filled with smooth deposits, are thought to have been formed by the motion of charged dust (Fujuwara et al, 2008; Hughes et al, 2006). These effects can only be quantified by a combination of electron and electric field instruments.

An additional motivation for the ACE instrument relates to "space weathering", modulation of the optical reflectivity of asteroid surfaces from micrometeorite impacts and/or irradiation from energetic particles or cosmic rays (Chapman, 2004). This process provided the explanation for the apparent discrepancy between the most common stony meteorites and S-type (weathered) asteroids, as the differing space weathering rates of the asteroids and meteorites lowered the reflectance and suppressed mineral absorption features. However, space weathering effects on primitive objects, such as the asteroid to be visited by Marco Polo, are less clear due to their already dark, neutral spectra.

An integrated approach to characterisation of the electrical environment at the asteroid through electric field and electron flux measurements, and assessment of electrostatic effects at the time of sample collection would be highly novel. In addition we propose and to characterise the radiation environment, particularly solar energetic particles, during sample collection. These measurements will be significant in terms of both sample characterisation and scientific understanding of processes affecting transport of material at asteroid surfaces.

9.3.2 SCIENTIFIC GOALS AND PERFORMANCE REQUIREMENTS

The proposed instrument has three parts

- An electric field detector with two concepts currently under investigation
    1. based on the ExoMars ARES instrument to measure the fields, and local conductivity, generated by the charged dust (EField) (Berthelier et al, 2000). The proposed instrument will measure vertical (and perhaps horizontal) electric fields on the surface of the asteroid in the range 0-500 ± 1 kV m-1 (low gain mode), with a maximum resolution of 0.1 Vm-1 (high gain mode: expected range 0-500 ± 1 kV m-1).

2. displacement current sensor, to detect the entire charge on the asteroid during approach. This could be determined by mounting two small metal plates on the outside of the spacecraft, facing the asteroid, and measuring the Maxwell displacement current generated at the plate by the change in electric field (e.g. Bennett and Harrison, 2006).

- To measure the solar wind and asteroid charging electron environment, we propose a miniaturised top hat electron spectrometer, based on the Improved Plasma Analyser (IPA) developed at UCL/MSSL (see Figure) under the STFC Rolling Grant. This is known as the Charged Particle Environment Monitor (CPEM), with Cassini heritage (Young et al, 2004).
- A radiation detector, integrated into the CPEM housing, for measurement of the penetrating radiation dose on the return journey (PenRad).

9.3.3 DESCRIPTION

9.3.3.1 Instrument concepts

9.3.3.1.1 Electric field measurement

There are two instrument concepts under study for electric field measurement.

A. *E field sensor* will consist of conducting cylindrical electrodes mounted at different heights and with horizontal displacement, for two-dimensional E field detection. The electrodes could be made of wrapped conducting tape to reduce the mass loading. The electric field is measured from the differential potential acquired by the electrodes. Local conductivity can also be measured by the rate of decay of a small bias voltage initially applied to the electrodes. This concept is the same as that used on the Atmospheric Relaxation and Electric field Sensor (ARES) on the Exomars mission. The ARES instrument will be deployed on a boom, to make the measurements away from the geometrical field distortion of the spacecraft. For 2-D electric field measurements, a two axis boom would be required to cover the variety of conditions expected at the dayside, night side and terminator. However, as a boom seems unlikely for Marco Polo, the possibility of mounting the electrodes on the spacecraft legs will be studied, Figure 1.
B. The *displacement current sensor* is simply two small conducting plates connected to a logarithmic current amplifier, Figure 2. The displacement current, proportional to the asteroid electric field, is proportional to the detector surface area, whereas local plasma currents will only be related to the cross-sectional area. Two sensors of differing geometry, but identical horizonal cross-sectional area, can therefore be used to to remove the effects of local plasma currents and measure the displacement current only. The displacement current sensor will be studied in parallel to the cylindrical electrodes as a complementary technique for asteroid electric field measurement.

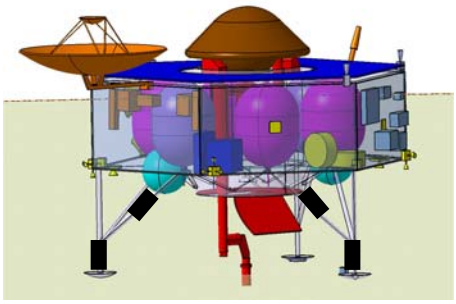

Figure 17 Diagram of spacecraft showing suggested locations for E field electrodes (A) to measure horizontal and vertical electric fields (not to scale).

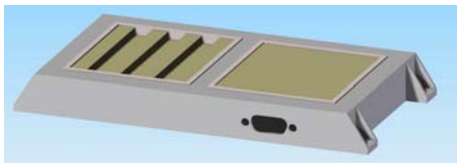

Figure 18 Displacement current sensor concept (B), showing two isolated metallic plates of differing geometry.

9.3.3.1.2 CPEM

The CPEM instrument, based on the Improved Plasma Analyser (IPA) developed at UCL/MSSL (see Figure 3), will consist of a top hat electron spectrometer measuring in the energy range 3 - 5000 eV with electrostatic deflector plates to increase its field of view to ±45º. The analyser will have a wide field of view (360ºx45º) to enable simultaneous sampling of both the solar wind as well as the asteroid.

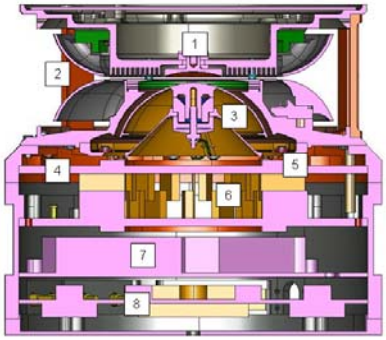

Figure 19 Schematic of the CPEM. (1) Analyzer top cap and UV rejection baffles, (2) Entrance aperture and deflection system, (3) Electrostatic Analyzer, (4) Anode and grid, (5) Annular Micro Channel Plate and radiation absorbers, (6) 16 charge amplifiers mounted on the reverse of the anode, (7). High Voltage power supplies and sweep modulation circuits, (8). CPEM control functions implemented in an Field Programmable Gate Array (FPGA) and interface circuits may be required around the parts of the sensor away from the aperture.

9.3.3.1.3 PenRad

To assess the radiation dose to the collected sample, particularly at the time of collection of the exposed sample, but also during the return phase, a simple radiation sensor is proposed. Figure shows a prototype built at MSSL to study highly energetic electrons using an MCP. The proposed sensor will be a simplified low resource miniaturized system based on penetrating radiation seen by the MCP and a solid state detector, measuring both electrons and ions in the energy range 1-50 MeV.

9.3.3.2 Electrical Design

The CPEM requires primary power and a SpaceWire connection for command and data transmission to the spacecraft electronics. The CPEM control functions are implemented in an FPGA based processor. The CPEM electronics consists of three circuit boards housed in the base of the sensor as shown in figure 3.

1. The top board doubles as the MCP mount and readout system anode as well as holding the 16 pre-amplifier channels. It also includes embedded HV coupling capacitors, providing a low resource and a low noise signal readout configuration.
2. The third board provides the main HV generator based on a standard MSSL flyback converter design using a Cockroft-Walton multiplier. The unit will generate two rails: 2.5kV for the MCP bias and 1.5kV to supply the sweep modulators. Also included are the HV sweep modulation circuits based on the Amptek HV601 opto-coupler devices.
3. The fourth board will accommodate a hybrid DC-DC converter with input filter, an Actel FPGA that contains all the EAS digital functionality and the LVDS interface circuits for the SpaceWire link, and the PenRad detector electronics.

The CPEM unit will also provide support to the E-field and Displacement current sensors.

- Secondary power

- Bi-directional UART interface for command and data communications

9.3.3.3 Orbit, operations and pointing requirements

A high time-resolution, high data rate, low gain mode will be required for terminator crossings when the electric field is expected to be at its highest and most rapidly changing. On the dayside, electrostatic levitation of dust is expected even though the electric fields are lower, which is likely to require a high-resolution, high gain mode. Actual data rates are TBC pending calculations of the time of asteroid terminator crossing and dust charging.

Independently switchable gain, resolution and data rate for both electric field sensor concepts would be controlled by the instrument processor.

The E field electrodes will only be operated when the spacecraft is at, or very close to, the asteroid surface. The displacement current sensor can be used for remote sensing of E field changes on approach or during orbit. The sensing range of the flat plate electrodes is TBC.

The CPEM instrument requires an outgassing period (~3 weeks from launch) before turn on.

9.3.3.4 Interfaces and physical resource requirements

The E field electrodes are likely to be very similar to the ARES electrodes which are $2x10^4$ mm^2 each in surface area, elliptical in shape, 140 mm long with semi-major and major axes of 15 and 30 mm. The initial assumptions for the ACE electrodes are that they are cylindrical, 140mm long and mounted on the spacecraft legs.

The preliminary design of the flat plate electrode unit is 136mm long x 70mm wide x 15mm high, including the mounting feet. This could be reduced following a study of expected signal levels and how they scale with detector surface area.

9.3.3.5 Calibration

Electric field instruments: Calibration on the ground will be required before and after integration. No in orbit calibration required.

CPEM: Both ground and in-flight calibrations will be required for the CPEM instrument. In-flight calibration will ideally be required before arrival at the asteroid.

9.3.3.6 Cleanliness, planetary protection and pre-launch activities

The CPEM instrument is EMC and magnetically sensitive, see specification in table. The electric field instrumentations are also EMC sensitive, but should not generate any electric or magnetic field issues.

On ARES, solar cells are a potentially significant source of electromagnetic interference, in particular for DC electric field measurements. According to the ARES ICD, the optimal solution is to use solar arrays that are coated with a very thin transparent conductive layer of vacuum deposited indium or tin oxide that is grounded to the electronics ground. This is a well known technique that has been commonly used on many ionospheric or magnetospheric spacecraft in the last 20 years. This issue should be considered at an early stage for the Marco Polo electric field instrument.

9.3.3.7 Critical points

The most critical point is the geometric location of the E field sensors, for which an orthogonal boom arrangement would be ideal. However, we realise that this is unlikely for the Marco Polo mission and our baseline assumption is that there is no boom. A key part of the study is to confirm that the measurements can be made without a boom.

The preferred accommodation option for the E field instrument is for the electrodes to be mounted on two of the legs of the lander. This would involve geometric screening of the electric field by the spacecraft, but this would be constant, and could be modelled and measured. This screening could have some effect on the instrument specification (sensitivity, resolution). An accommodation study would be required to compare these options.

There is a need to know exactly where the terminator is with respect to the instrument, and it is assumed that a camera will provide this information.

The specification for the displacement current sensor will be defined in parallel. The scientific advantages of using both types of sensor will also be traded against their mass and power.

CPEM will require accommodation such that its undeflected field of view plane is ideally within +/- 45º of both the asteroid and the sunward direction in order to be able to effectively measure the asteroid's charge environment.

9.3.3.8 Heritage

MSSL has significant heritage (e.g. Cluster, Double Star, Cassini, and Venus Express) with undeflected top-hat analysers. A prototype analyzer head has already been built and is undergoing testing.

The cylindrical E field sensor is closely based on the Exomars ARES electric field instrument for which K Aplin (PI) is Deputy PI. The ARES PI (Franck Montmessin) is a Co-I on this instrument. The flat plate E field sensor has no space heritage but is a miniaturised version of an instrument that has been successfully operated in the terrestrial atmosphere, where the measurement is expected to be more difficult (Bennett and Harrison, 2008).

9.3.3.9 Summary table

Table 24 Summary table for the ACE instrument

Parameter	Unit	Value/Description	Remarks
Reference P/L	n/a	**E field: ARES Exomars** **Electron environment (CPEM): Cluster, Double Star, Cassini, Mars Express, Venus Express**	A prototype CPEM analyzer head has already been built and is undergoing testing at UCL/MSSL.
INSTR. CHARACTERISTICS			
Type of detector	n/a	E field: Conducting electrodes CPEM: Electrostatic particle detector with aperture deflection system;	Two measurement principles under consideration A. allowing electrodes to acquire a voltage related to horizontal/vertical E field B. measurement of displacement current due to electric field changes with two plate detectors of differing geometry (1 flat, 1 corrugated) Electrons from a chosen azimuth are deflected into the hemispherical analyser section (which has

			360° acceptance in elevation) of each sensor. Electrons of the selected energy then pass around the hemisphere and are recorded by the MCP or CEM detectors. Sweeping of the ADS and hemispherical voltages allows electron fluxes of the full angular and energy range for each sensor to be obtained.
No. of detectors	#	2 pairs of electrodes on S/C legs 1 unit 1 unit	A B CPEM
Temperature range	K	70 - 350	
Duration of measurement	s	E field: Measurements only needed close to the asteroid. Continual low frequency, (TBC) high frequency during terminator crossing. CPEM: Continual (TBC)	(1) Cylindrical electrodes need to be close to asteroid surface (whether actually landed or not TBC) (2) Displacement current detector can sense electric field changes remotely on approach and also after landing
Number of measurements per sample	#	E field: Hi / low sampling res mode depending on position of terminator and high res also needed on landing CPEM:1 energy spectrum per 2s	CPEM: 32 energies X 16 anodes x 8 bits/2s = 2kbps. In practice an on board reduction by a factor 4 (angle) and 5 (compression) should be possible giving 100 bits/sec Penrad: 5 (energy)x 8 (bits)/2s=20bps.
MEASURED PARAMETER			
Parameter 1	V	Quasi-DC voltage 0 – 500 kV (low gain) 0-500 V (high gain)	Differential measurement from which electric field can be calculated (E field electrodes)
Parameter 2	S/m	Conductivity	Range TBC. Measured through voltage changes on one E field electrode. Measurement at two or more electrodes could give a conductivity profile
Parameter 3	A	Current	Range TBC but likely to be pA-nA. Measured at each of the displacement current sensors (the E field is related to the difference between the two sensors).
Parameter 4	eV	Electron energy spectrum	60 energy bins, 2-4 elevation bins, 16 azimuthal bins $\Delta E/E \sim 15\%$ if 30 energy bins are used to cover full range; Elevation resolution is 4-7º and 16 azimuth bins implies angular resolution of 22.5º
Frequency range	Hz	E field: DC – 2 kHz?	TBC. Higher frequency measurements needed on landing and at the terminator for E field measurements
dynamic range instantaneous	kV	1/ 10	16 bits
dynamic range total	kV eV	E field: 0 – 10 CPEM 3-5000	
CONFIGURATION/ LAYOUT			
Displacement current sensor	#	1 unit, facing asteroid	Flat plate detectors need to face asteroid wherever possible, ideally on bottom of S/C
Electric field sensor	#	4 electrodes, provisionally on S/C legs	ARES electrodes ≥ 60cm apart. Spacing/screening compromises to be studied. Separation of horiz/vertical E field detectors is required. Orthogonal sensors preferred.
CPEM/PenRad	#	1 unit	Needs to be accommodated such that its undeflected field of view ≤ 45º along the asteroid or the sunward direction
PHYSICAL			
Mass, total	g	~1700	
Mass, sensor head + cables	g	60 180 1400	E field sensor (horizontal + vertical) (concept A) Displacement current sensor mass includes preamps (concept B) CPEM +PenRad (includes electronics)

Mass, electronics	g	124		Only if a separate spacecraft interface is needed for the Efield instrument (mass estimate based on Exomars ARES)
Dimensions (detector)	mm	E field sensors: Volume: $7.7x10^4$ mm^3 Surface Area:2 electrodes $1.4x10^4$ mm^2 Displacement current unit: 136mm long x 70mm wide x 15mm high CPEM 116mm high x 137mm diam		Assumes 2-D electric field measurements (=4 electrodes)
Dimension (electronics)	mm	E field: 110 x 95 x 115		CPEM includes integrated electronics
POWER				
Average	W	1.5		E field 0.15W, CPEM+PenRad 1.3W
Peak	W	1.7		
DATA RATE/VOLUME				
data rate	KB / sec	CPEM: 100bps PenRad: 20bps E Field (A+B): 50 bps TBC		
Volume per sample	KB	TBC		
Volume total	KB	E field: 1.5-5.5 Mb		Dependent on rotation rate, and orbit. Highest resolution needed around day/night terminator.
THERMAL				
Temperature ranges op.	K	253?	298	Upper limit is imposed by the CPEM to avoid thermal runaway of the detectors. Ideally the CPEM will operate in the range 278-298K. Electric field sensors could operate in a wider temperature range
Temperature ranges Non-op	K	253	323	
CONTAMINATION				
EMC requirements		CPEM requirements: Minimise any exposed voltages; i.e. care must be taken to ensure that the spacecraft surfaces are all at spacecraft ground potential, particularly in the vicinity of the sensor apertures. Eliminate non-conductive areas on the spacecraft surface, particularly close to the sensor apertures. Spacecraft surfaces exposed to the plasma environment need to be conductive and grounded to minimise differential charging potential to less than 1 V(design goal) between any two points of the spacecraft external surfaces. Ideally, the potential of the exposed surfaces of the sensors should always be within 10% of the average potential of the whole spacecraft.		The E field instrument requirements are TBC but are likely to be similar to the CPEM. Consider coating solar cells with a transparent conducting layer to reduce potential EM interference (as on ExoMars).
DC magnetic		CPEM requirements: The magnetic field due to the spacecraft and payload (with the solar panels in sunlight) measured along the line of sight of a sensors should be less than 25 nTm. Some electronic components inside the instrument may be magnetic, but magnetostatic emission will be less than 1 nT at 1m.		The B field instrument requirements are TBC but likely to be less stringent than the CPEM
SUPPORT ITEMS				

9.4 Volatile Sensor and Regolith Microscope

9.4.1 INTRODUCTION

The volatile sensor and regolith microscope described here is based on WatSen. The WatSen sensor is a combined miniaturized ATR (Attenuated Total Reflectance) spectrometer, humidity sensor, and optical microscope. It is currently being developed as a compact breadboard prototype designed to be suitable for carrying as part of a suite of instruments onboard a mole on a planetary lander similar to ExoMars. It is capable of investigating the presence of water and also silicate mineralogy. The ATR sensor operates by measuring the changes that occur to the totally internally reflected infrared beam upon contact with the sample. Surface properties alter the spectral reflectance in a mineral grain, thus the ATR has a flat surface for intimate contact with the sampling surface. The optics are built by Norsk Elektro Optikk (NEO) and the electronic and software by NavSys (both based in Norway). The humidity sensor was tested and validated at the Open University, UK. The principle testing for the complete WatSen prototype will be done at the Open University.

Infrared (IR) spectroscopy is a rapid and non-destructive technique used for the analysis of minerals. It allows identification of major mineral species present, including secondary products such as carbonates and sulphates, and is a sensitive indicator of the presence of water (either as liquid or bound in mineral grains). IR spectroscopy can also yield mineral chemistry, distinguishing between iron-rich and iron-poor silicates and different species of carbonate. When combined with a microscope, IR spectroscopy can map variations in mineralogy with texture and zoning.

The ATR diamond window is employed as a part of the optical system for a microscope that can image the area being studied with the spectrometer, i.e. in contact with the diamond window. This can be used to measure grain size distribution and regolith features.

9.4.2 SCIENTIFIC GOALS AND PERFORMANCE REQUIREMENTS

The volatile sensor should be capable of identifying volatiles, specifically water-ice, on the asteroid near-surface (first few 10s of centimetres) within pore spaces and as films around mineral grains. This could be achieved by placing the sensor on a mole or penetrator. Additionally, the optical microscope will be capable of measuring grain size distribution and other regolithic features, down to a resolution of 18 microns, in colour. A secondary goal will be to determine mineralogy and mineral chemistry of the near-surface using the ATR sensor. For example, a difference of 40 mol% Mg in silicate composition (both pyroxene and olivine) would correspond to a band shift of ~0.2 um. The WatSen instrument is sufficiently miniaturised, even at the current breadboard stage, to fit into a mole of compact dimensions equivalent to ExoMars (cylinder diameter 26 mm, length 158 mm. Used in this context, the volatile sensor and regolith microscope combined will be able to preview potential sample material within reach of the lander, and thereby allow selection of the appropriate sampling technique.

Ideally, the specific wavelength range should be from 2.5µm up to 11µm, to allow detection (and thus identification) of features from the silicate minerals expected to be present within the regolith. However, for WatSen, trade-offs were made in order that the final sensor could fit into the mole on ExoMars, resulting in a range from 5.5µm to 10.8 µm. This wavelength range is a trade off

between technical boundaries and scientific capability; H_2O absorption is stronger at 3 μm, but strong and distinct absorption peaks for minerals occur in the mid infrared spectrum (5 - 11 μm). An example is carbonate minerals, which display a unique spectral shape between 6.3 - 7.4 μm. Water IR spectral features are displayed between 6-7 μm, but major features of anhydrous silicates occur at wavelengths greater than 9 μm. Furthermore hydrated minerals such as clays display combined features of water and silicate. The ATR spectrometer has a resolution $\Delta\lambda/\lambda = 0.015$. This resolution is sufficient to resolve distinct spectral features for water and minerals.

9.4.3 DESCRIPTION

9.4.3.1 Instrument concept

ATR Spectrometer

One effective method for determining the presence, or absence, of water is infrared spectroscopy. This technique utilizes energy changes during stretching, bending and vibration of intra-molecular bonds. The ATR sensor utilises the effect that the reflectance properties of a mineral grain are altered when the grain is coated with a thin layer of water. Because spectral reflectance features are almost always dependent on surface properties (flat or uneven, rough or smooth, etc), the signal generated must be from a representative grain surface. This is best achieved by placing the sensor in direct contact with the surface of the grain; the most appropriate sensor type to achieve this measurement is an ATR sensor.

Attenuated total reflection (ATR) spectroscopy is a powerful technique for studying the absorption IR spectra of a variety of materials. It is based on the phenomenon of total internal reflection, occurring when electromagnetic waves in a transparent dielectric medium impinge onto the surface of an absorbing medium with a lower index of refraction and with an angle of incidence above the critical angle. An evanescent wave is excited which propagates a certain distance (penetration depth) into the sample. Some of the energy of the evanescent wave is absorbed by the sample at particular wavelengths and this affects the signal received be the detector. In addition to a light source and the ATR probe itself, a spectral separation technique (spectrometer) is needed to obtain a useful spectrum.

The optical design of the ATR sensor comprises the following components:

- An infrared light source (electrically heated thermoresistive carbon film)
- An optical system that collects the light and couples it into the ATR crystal (germanium lenses)
- An ATR crystal exposed to the material to be probed (diamond window)
- An optical system that collects the light from the exit of the ATR crystal (germanium lenses)
- A wavelength-selective element that spatially separates the wavelengths of light (LVF filter)
- A detector (currently a pyroelectric 128 element linear array, but an electrically compatible 256 element sensor is becoming available for future development)

In addition the following components are included to prevent unwanted light from the source from reaching the detector:

- A band pass filter that removes light emitted outside the selected spectral region
- Mechanical structures that block light which is not coupled into the ATR crystal (apertures or masks).

The light source used (Intex) has an emitter that is a thermoresistive film of conducting amorphous carbon heated electrically to temperatures up to 750 ºC. The film emits radiation with a black body spectrum with an emissivity of 0.8. The source is electrically chopped with 100 % modulation depth up to 10 Hz. The emitting area is less than 2 x 2 mm. For the WatSen breadboard a mask was used that shapes the beam from the source optics. This is to get an optimised beam shape for the best possible ATR spectrometer performance.

The optical system for the ATR sensor contains two lens assemblies, a collimator system in front of the source and a focusing lens assembly in front of the detector. The lenses are made from AR-coated germanium. The LVF Filter, which is integrated into the package as the detector window, has an effective wavelength range of 5.5-10.8 μm and a resolution $\Delta\lambda/\lambda = 0.015$.

The detector is a custom version of the DIAS Infrared 128LTI SP1.0. The sensor is an uncooled pyroelectric 128-element linear array with integrated CMOS multiplexer including amplifiers. The size of the responsive elements is 90 μm × 1000 μm with a pitch of 100 μm (array size 1 mm × 12.8 mm). The sensor responds to chopped radiation, with maximum responsivity at 10 Hz. The effective resolution of the sensor is in general less than 128 spatial channels as a result of thermal diffusion into neighbour pixels.

An ATR spectroscopy system based on a linear variable filter spectrometer and a linear sensor array is very competitive with regards to robustness, physical size, power consumption and performance. In particular it is possible to implement this concept with no moving parts. It is also possible to use a sensor technology that has no or very moderate requirements for cooling (thermoelectric), further reducing the complexity and power consumption of the system.

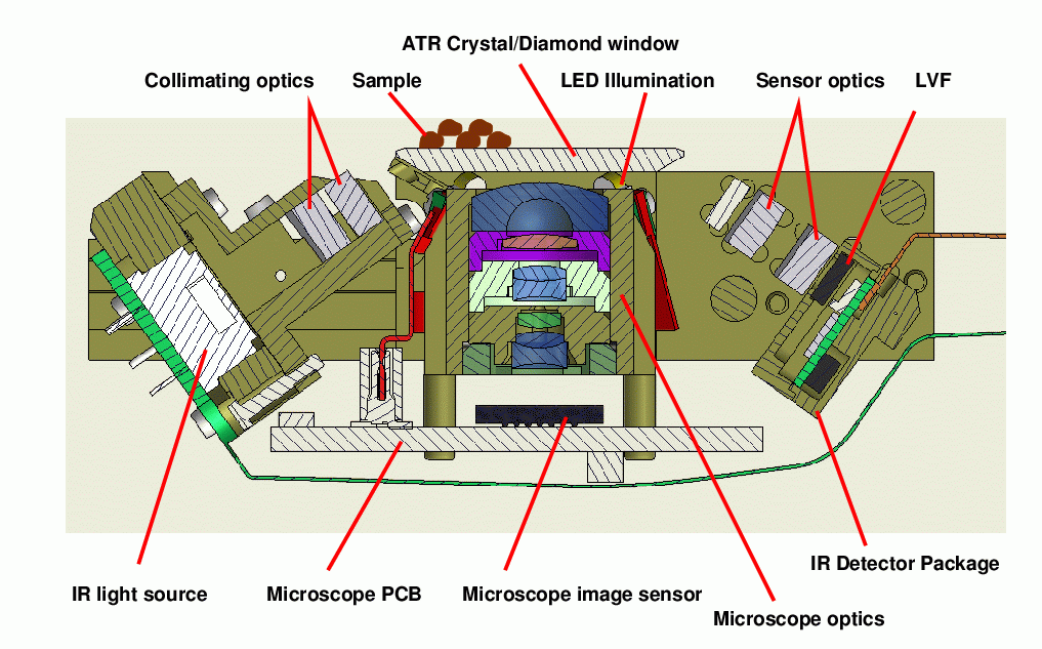

Figure 20 Cross-section of optical design of WatSen ATR Spectrometer

Mechanical Design and Housing

All mechanical parts are made of titanium. The outer shell is mainly made of two halves with o-ring seals. The two halves form a cylindrical housing and this housing has two compartments, one for the optics, IR source and detector and the other for the general electronics.

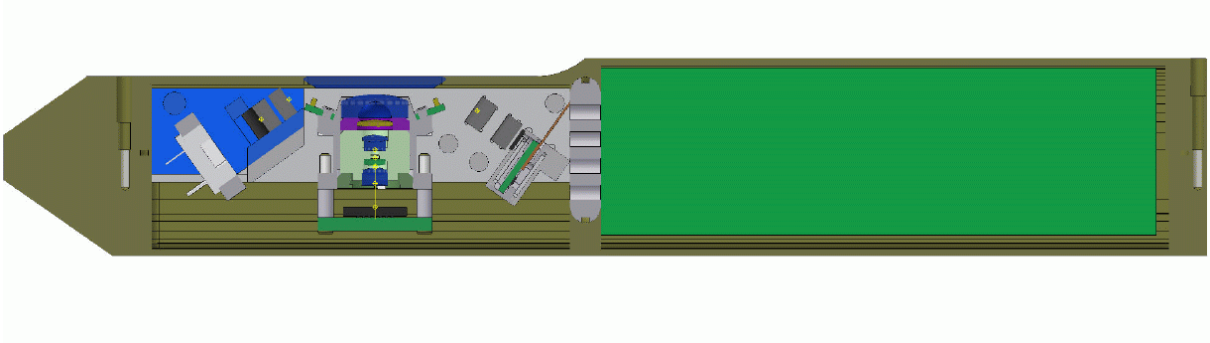

Figure 21 Section through the probe and in particular the optical parts and its mounting frame. Only selected optical components are shown for clarity. PCBs for the general electronics are shown to the right. The microscope is shown in the centre of the optical part.

Microscope

The microscope system utilises a CMOS colour sensor 1/3" from Micron Imaging MT9M111STC and a light source based on four white LEDs SMB mount (Everlight). The system

has a sensor resolution 1280X1024 and no focussing mechanics. Table 1.1 gives the resulting specifications:

Table 25 ***Specifications of WatSen Microscope***

Specification	
Paraxial magnification	-0.5x
Pixel size on the object (centre)	7.2x7.2µm
Pixel size on the object (edge)	approx 11x11µm
Diagonal field of view	23mm
Field of view (Horizontal, Vertical)	14.5x8.5mm
Depth of field (MTF 30% at 70 lp/mm)	0.6 - 1.7 mm

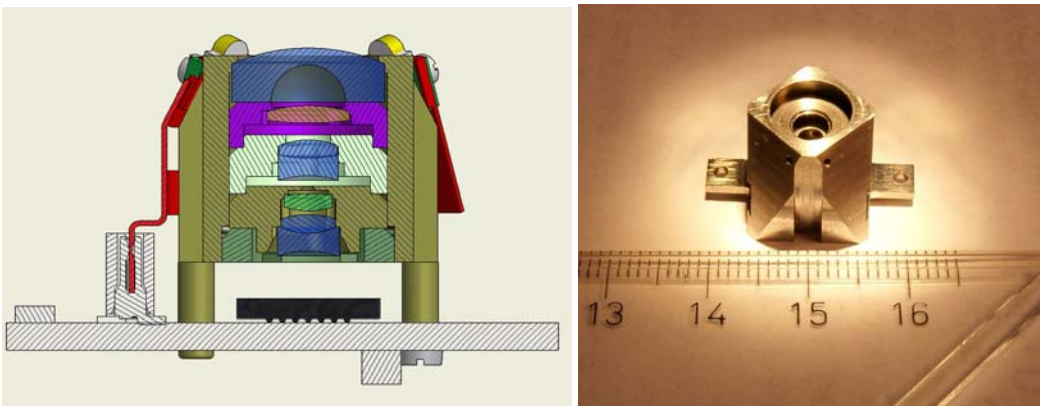

Figure 22 Cross-section of the microscope (left). The yellow notches on the top left and the top right are the LEDs. The image sensor is the dark device on top of the PCB (bottom). The different lens elements can also be seen. To the right are the machined titanium parts for the lens barrel.

9.4.3.2 Operation requirements

ATR Spectrometer

Sensor spatial (spectral) resolution vs. chopping frequency

The spectral resolution of the ATR sensor depends on the spatial resolution of the IR sensor, which is characterized by the detector modulation transfer function (MTF). The MTF depends on the chopping frequency, and is a result of thermal crosstalk between neighbouring pixels. Defining the effective spatial resolution of the detector as the resolution (linepairs per mm) where the MTF assumes the value 0.5, the spatial resolution increases roughly with the square root of the chopping frequency. The optimum chopping frequency has been found to be 10 Hz giving best signal to noise ratio and a sufficiently high spectral resolution.

Signal to noise ratio

The detection limit of the ATR sensor depends on the absorption strength of the material to be detected and the capability of the sensor to detect absorption which is limited by the system noise. The estimated signal to noise ration (S/N) is in the range 10 to 60 depending on averaging and binning and assuming 10 Hz chopping frequency.

Spatial/Spectral Sensitivity Interrelation

A multiple bounce ATR crystal design normally has bands that are sensitive to the sample and bands that are more or less blind to the sample (Figure 1.4). Depending on the optical design the spectral sensitivity could also be different depending on where on the window the sample is located. There is a parallel beam in and a parallel beam out. Due to the parallel beam, rays from one side of the diamond window will be focused on one end of the sensor while beams from the other side of the window will be focused onto the other end of the sensor. Since the LVF is placed in front of the sensor, light with wavelength 5.5 um will reach the detector in one end and 11 um will reach the detector in the other end. This leads to different spectral sensitivity for different spatial positions on the window.

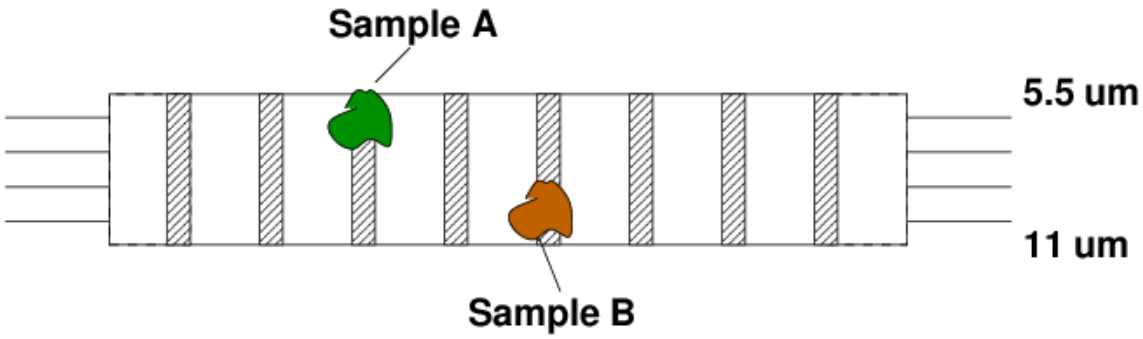

Figure 23 Two different materials on the ATR diamond window. Sample A will contribute to the acquired spectrum from around 5.5 um to around 7 um. The spectral properties of sample A in the range 7-11 um are lost. Sample B contributes to the spectrum from around 9 um to 11 um while all spectral features of sample B in the range 5.5-9 um are lost.

The resulting spectrum from sample A and B in Figure 1.4 is useless if the full spectrum is required to discriminate sample A and B from other substances or from each other. This measurement concept will work well if the sample is well mixed and well distributed over the ATR crystal window.

Thermal management

The thermal management is controlled by the WatSen general electronics. The IR source will heat itself while the analogue detector amplifiers, the detector itself and the general electronics will be heated to -55 ºC using heat films on the printed circuit boards. A similar approach is used for the microscope and illumination LEDs.

Microscope

The performance of the microscope is given in Table 26.

Table 26 WatSen microscope performance

Parameter	Centre	Edge
Field of view, mm	14.5 x 8.5	
Magnification	0.5x	0.33x
Spatial frequency (image) lp/mm	110	95
Spatial frequency (object) lp/mm	55	31
Resolution (object) (μm)	18	32
Contrast, %	30	30

Field of view is the depicted area on the diamond window. Spatial frequency on the image sensor is given in line pairs per mm where one line pair is one white and one black line. The system has a very large field of view and great depth of focus. However the FoV is so wide it is not possible to correct for distortion, hence the different performance at the centre and the edge. However, the distortion should be constant, and therefore can be corrected in post-processing.

9.4.3.3 Interfaces and physical resource requirements

The total mass is estimated to be 180 g. Dimensions are a cylinder of diameter 26 mm and length 158 mm. Total average power is 1.2 W (peak < 3 W).

The WatSen interfaces:

- The Front-end I/F interfaces to the Lander, which provides power, data communication, temperature sensors interfaces and heaters control through a flat, flexible tether cable
- The Mole I/F interfaces to the Mole/Penetrator, providing it with regulated power for its internal heaters through a short, reinforced, round cable

Table 27 shows a summary of voltage and power requirements for the most significant circuitry.

Table 27 Power Supply Requirements (TBC)

Description	Device	Voltage [V]	Max. Active Power [mW]
SVGA Image sensor	MT9M111	1.7-3.1 (digital & I/O) 2.5 – 3.1 (analog)	76 @1.8V, 30 fps
FPGA 500.000 gates	Spartan-3A	1.2 (core) nom. 2.5 (aux.) nom. 1.2 – 3.3	111 (idle) + dynamic (design dependent)

		(I/O) nom.	
IR Source	Intex	5 – 10	1000
IR Detector Array	DIAS128LTI-1.0 (custom)		40 (approx.)
TOTAL			1.2 W

Data rate are dominated by the microscope images. if the Micron MT9M111 image "System On Chip" (SOC) sensor is selected, each uncompressed, raw image will contain 1280 x 1024 x 2 bytes = ~21 Mbits. WatSen uses the SpaceWire Data Handling System I/F (ESA SpWb VHDL "IP" used). SpaceWire links are serial, high-speed (2 Mbit/s to 400 Mbits/s), bi-directional, full-duplex, differential point-to-point data links. A data strobe signal is included for each data transfer direction. Alternatively, the electrical interface could support redundant LVDS or RS422 serial asynchronous communication.

9.4.3.4 Calibration

A reference database is being constructed of minerals saturated with water using ATR Fourier Transform infrared spectroscopy (FTIR). The minerals are also frozen with and without water to ~268 K and ~77 K and spectra taken (Figure 1.5).

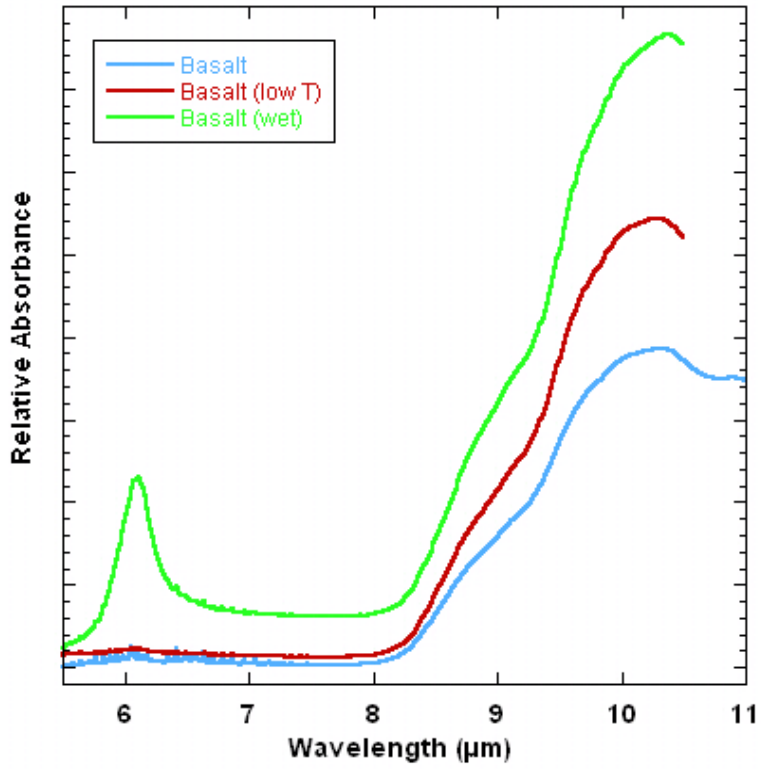

Figure 24 IR spectra of powdered dry basalt taken at 295 K and 268 K, and of water-saturated basalt, also at 268 K.

When the WatSen prototype is completed it will be tested using the Environmental Chambers at the Open University (UK) using a variety of substrates, a range of water/rock ratios, and a range of temperatures.

9.4.3.5 Cleanliness, planetary protection and pre-launch activities

The completion of the testing of the WatSen breadboard prototype (Summer 2008) will bring this sensor to Technology Readiness Level (TRL) 5 (Component and/or breadboard validation in relevant environment). Since the prototype goes some way beyond a breadboard model it would be close to reaching TRL 6 [System/subsystem model or prototype demonstration in a relevant environment (ground or space)]. Pre-launch activities would include a re-design of WatSen for NEO activities, especially the investigation of integration into a mole that could operate in low-g environments, then the construction of a new prototype, followed by a construction of actual system and flight qualification through test and demonstration.

9.4.3.6 Critical points

Can a mole be designed to work on NEO surface gravity conditions? Or can WatSen be adapted for use in a penetrator?

Design is currently constrained to fit on the ExoMars mole, resulting in small volume. If this constraint was relaxed, optics could be redesigned to allow larger spectral range for ATR spectrometer and less distortion for microscope. The overall performance and sensitivity could also be improved given a larger physical volume.

9.4.3.7 Heritage

The heritage for the volatile detector and regolith microscope is the WatSen ("Water Sensors for Mars Exploration") instrument breadboard, which is being built under ESA contract (Statement of Work ID: TECMMG/2005/916).

9.4.3.8 Summary table

Table 28 Summary data sheet on the Volatile Sensor and Regolith Microscope.

Parameter	Unit	Value/Description	Remarks
Reference P/L	n/a	**WatSen: Water Sensor (ATR Spectrometer), Humidity Sensor and Regolith Microscope**	
INSTR. CHARACTERISTICS			
Type of detector	**n/a**	**ATR spectrometer**	
Wavelength Range	um	5.5- 10.8	
wavelength resolution	Δλ/λ	0.015	LVF filter only
S/N		10-60	depending on binning, integrating several spectra, assuming 10 Hz chopping frequency

Type of detector	**n/a**	**Regolith Microscope**		
magnification (centre, edge)		0.5x, 0.33x		
Pixel size (centre, edge)	µm	7.2x7.2, ~ 11x11		
Diagonal field of view	mm	23		
Field of view (Horizontal, Vertical)	mm	14.5x8.5		
Depth of field (MTF 30% at 70 lp/mm)	mm	0.6 - 1.7		
Resolution (centre, edge)	µm	18, 32		
CONFIGURATION/ LAYOUT				
Units	#	2		
Preferred location for sensor	n/a	In mole or penetrator		
Preferred location for electr.	n/a	Integrated within mole or penetrator		
PHYSICAL				
Mass, total	g	180		
Dimensions (detector)	mm	cylinder diameter 26 mm, length 158 mm		
POWER				
Average	W	1.2 W (3 W)		Value in parenthesis is if include power for DC motor for a mole or instrument heaters operation
Peak	W	1.2 W (3 W)		
DATA RATE/VOLUME				
data rate	MBits / sec	1-100		Capability of SpaceWire, data rate probably will not have to be so high
Volume per sample	MBits/ image	21		for microscope, spectra TBD but should be much lower
Volume total	KB	TBD		
THERMAL				
Temperature ranges op.	K	130	320	Humidity sensor 210 – 410 K
Temperature ranges Non-op	K	130	320	
CONTAMINATION				
EMC requirements		TBD		
DC magnetic		TBD		
SUPPORT ITEMS				
Deployment system	n/a	mole or penetrator		

10 PAYLOAD SUPPORT ELEMENTS (PSE)

The APXS instrument requires a deployment device. The contact ring of the instrument has to come into contact with the asteroidal surface in order to assure defined measurement geometry.

The Volatile Sensor/Microscope requires close contact to the surface. In principle this can be achieved by a variety of deployment systems. One could be similar to a simple device used for the APXS. Others may include a deployment by a Mole system or other penetrator type device.

The option to mount both instruments on the landing gear especially feet of the spacecraft needs to be explored.